THE INNER MAGNETOSPHERE OF JUPITER AND THE IO PLASMA TORUS

by

FRANCES BAGENAL

B.Sc., University of Lancaster, England
(1976)

SUBMITTED IN PARTIAL FULFILLMENT
OF THE REQUIREMENTS FOR THE
DEGREE OF

DOCTOR OF PHILOSOPHY

at the

MASSACHUSETTS INSTITUTE OF TECHNOLOGY

June 1981

Signature of Author _____
Department of Earth and Planetary Sciences
May 13, 1981

Certified by _____
John W. Belcher
Thesis Supervisor

Accepted by _____
Theodore R. Madden
Chairman, Department Examination Committee

Abstract

When Voyager 1 passed through the inner magnetosphere of Jupiter on March 5, 1979, the plasma instrument on the spacecraft measured the characteristics of the Io plasma torus between 5 and 9 R_J (1 R_J corresponds to the equatorial radius of Jupiter, ~71,400 km). Energy per charge spectra for positive ions in the range of 10 eV to 6 keV have been analysed for the three main plasma sensors to determine the properties of the plasma. In the innermost region, where the plasma is cold, the energy per charge spectra define composition, density, temmperature and bulk motion of the positive ions. Further away from Jupiter the plasma is warmer and the spectral peaks corresponding to ions with different A/Z^* ratios overlap. Therefore the characteristics of the plasma in warmer regions cannot be uniquely determined, and it is necessary to make assumptions about the bulk motion and thermal state of the ions.

A sharp gradient in plasma temperature of -7×10^5K R_J^{-1} at 5.7 R_J divides the torus into two parts, a cold inner region where the ions are closely confined to the centrifugal equator and a warm outer region which includes the orbit of Io and has a thickness scale height of ~1 R_J. The outer edge of the warm torus is defined by a drop in plasma density near 7.5 R_J. In the cold inner region the bulk motion of the plasma is within 1% of the value expected on the basis of strict corotation with Jupiter. The ions in this inner region appear to have the same cold temperature (< 1 eV) and are of low ionisation state, predominately S^+ with some O^+, which is consistant with the ground-based observations of optical emission at the forbidden spectral lines for these ions. In the outer region of the torus, the ions appear to be warmer (~50 eV) and of higher ionisation states (predominately S^{2+}, with S^{3+} and O^{2+} as well as O^+ and S^+), which is consistant with the spectrum of the ultraviolet radiation that is emitted from the torus. The measurements of the density and temperature of the plasma along the spacecraft trajectory have been combined with the assumption of azimuthal symmetry and theoretical expressions for the distributions of

plasma along a magnetic field line to construct a two-dimensional map of plasma density.

The ions of sulphur and oxygen are presumably the products of the dissociation and ionisation of volcanic gases such as SO_2 which are ejected from the volcanoes on Io. About 1 tonne per second of new plasma is produced near the orbit of Io. Most of the plasma diffuses rapidly away from Jupiter under the influence of a strong centrifugal force. Since the time the plasma takes to diffuse away from the inner magnetospere (10 to 50 days) is smaller than the characteristic time for cooling by radiation, the plasma outside the orbit of Io remains quite warm. The remaining ~10% of the plasma that slowly diffuses inwards has plenty of time to radiate most of its energy and to collapse onto the centrifugal equator to form the cold inner torus.

Finally, perturbations of plasma fluxes and the magnetic field during Voyager 1's passage close beneath Io suggest that Alfvén waves are generated in the interaction between Io and the magnetospheric plasma. If the field aligned currents that are carried by the Alfvén wave trigger plasma instabilities in Jupiter's ionosphere, then variations in the characteristics of Alfvén wave propagation with the position of Io in the torus may explain how Io modulates the emission of decametric radio bursts.

Thesis supervisor : Dr. John Belcher
Title : Associate Professor of Physics

Table of Contents

List of Figures

List of Tables

Chapter 1

Introduction

a) Overview

The interaction of the planet Jupiter with its satellite Io is one of the most interesting phenomena in the solar system. Caught in the gravitational coupling between Jupiter and Europa, Io is heated until its interior is molten and explosive volcanism overturns its surface layers. Some of the volatile material that is ejected from the volcanoes escapes Io's gravity and forms a large exospheric nebula along the satellite's orbit around Jupiter. Moreover, the interaction between Io and Jupiter is not confined to gravitational forces. The satellite is electrically conducting and electric currents, induced in the body, perturb the strong magnetic field in which Io is immersed. The disturbances propagate along the magnetic field to the ionosphere of Jupiter where they trigger powerful bursts of radiation. The volcanic gases from Io are bombarded by the charged particles that are trapped in the strong, rotating magnetic field of Jupiter and become collisionally ionised. The resulting ions are picked up by the magnetic field and accelerated until they too rotate with Jupiter, drawing rotational energy from the planet. The ionised material from Io forms a dense ring of plasma near the satellite's orbit and ultimately spreads into a vast region surrounding Jupiter.

This thesis is concerned with the measurements made by the Voyager 1 plasma experiment when the spacecraft traversed the region of Io's

orbit and the implications of these measurements about the interaction between the satellite and the magnetosphere of Jupiter.

This first chapter begins with a brief description of the structure of Jupiter's magnetosphere and a comparison with a more familiar magnetosphere, that of the Earth. There then follows a review of ground-based observations of radio and optical emissions from the vicinity of Jupiter as well as some of the theoretical models which these observations inspired. Chapter 1 concludes with a list of the experiments on the Voyager spacecraft which made measurements pertaining to the inner magnetosphere.

Chapter 2 is concerned with instrumentation and describes the spacecraft trajectory, the plasma instrument and the procedure for deriving macroscopic plasma properties from the measurements. A more detailed description of the instrument and data analysis is given in Appendix I while Appendix II is a discussion of the physical assumptions made in the analysis.

In Chapter 3 the Voyager plasma measurements are presented. Firstly, variations in the macroscopic properties of the plasma with radial distance are discussed. Secondly, these measurements (which were made along the curved line of the spacecraft trajectory) are combined with a theoretical distribution for plasma along the magnetic field (described in Appendix III) to construct a two-dimensional model. Thirdly, the discussion returns to original spectral measurements to point out some small-scale features which may have important implications.

Chapter 4 includes a comparison of the plasma measurements with the plasma properties inferred from other experiments. There then follows

in Chapter 5, a discussion of what the measurements imply about the role of Io in the Jovian magnetosphere. Io is considered as the main source of the plasma which initially populates the dense toroidal region near Io's orbit and ultimately diffuses throughout the magnetosphere. The actual interaction of Io with the magnetospheric plasma is probably a very complex process but the Voyager plasma and magnetic field measurements may provide some clues of what was happening when the Voyager spacecraft passed near Io. Chapter 5 concludes with a possible explanation of how the emission of decametric radio bursts is modulated according to the position of Io in its orbit. Finally, the main conclusions of the thesis are summarized in Chapter 6.

b) The magnetosphere of Jupiter

A magnetosphere may be thought of as the "sphere of influence" in the solar plasma of a planet which has a strong internal magnetic field. The solar wind compresses the magnetic field upstream of the planet and draws out a "magnetotail" downstream, in the planet's wake (Figure 1). The extent of the planetary field in the solar direction is determined by a balance between magnetic field pressure and solar wind pressure (at the "magnetopause"). For a dipole magnetic field the sub-solar "stand-off" distance is

$$R_S = R_P \left(\frac{2 B_o^2}{\mu_o n m V^2} \right)^{1/6}$$

(where R_p is the planetary radius; B_0 is the magnitude of the magnetic field on the surface of the planet at the equator; n, m, and V the

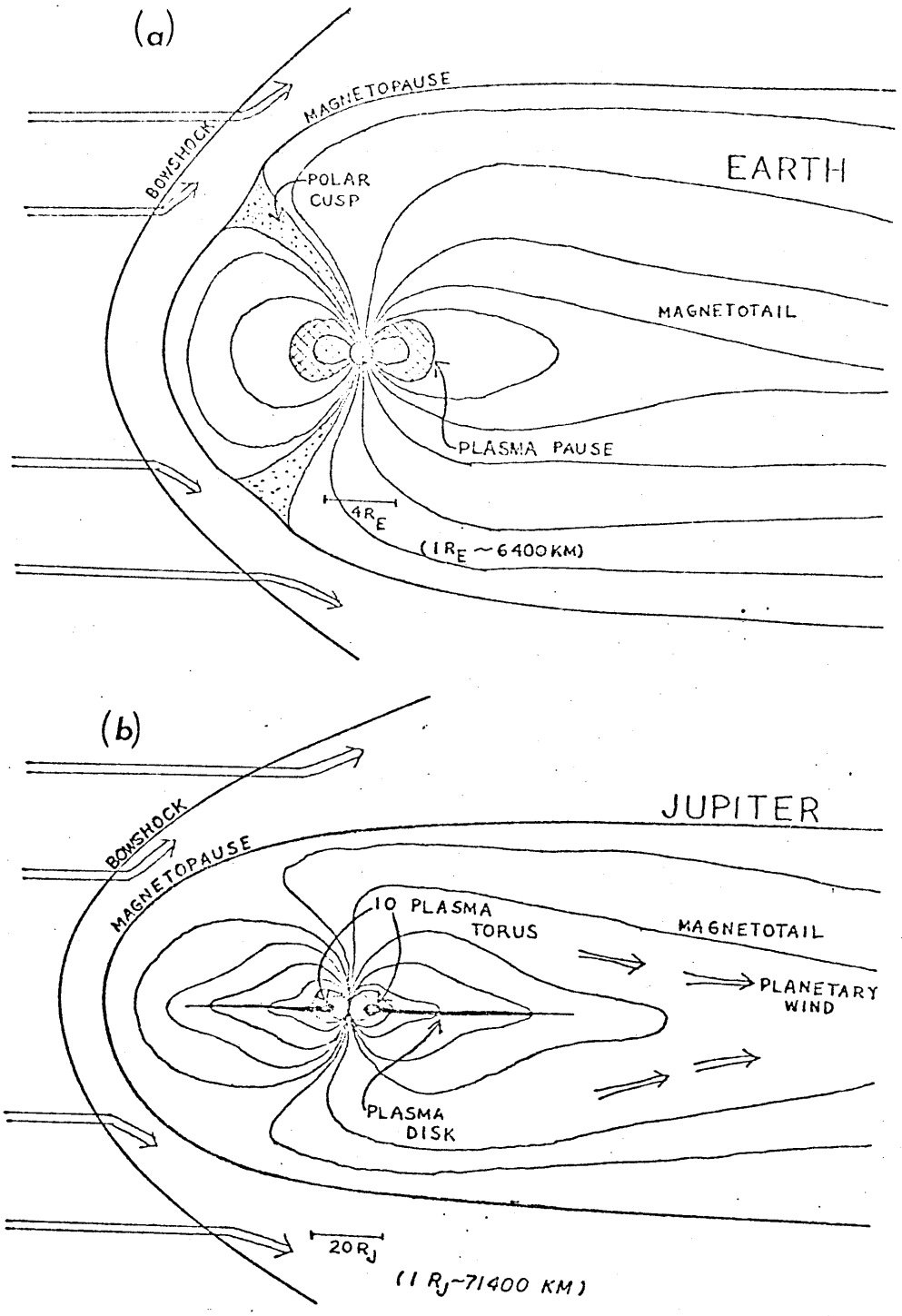

Figure 1. Comparison of the magnetospheres of Earth and Jupiter. For each planet a cross-section from noon to midnight (in a plane parallel to the rotation axis) has been sketched. The tilt of the magnetic dipole with respect to the rotation axis has been ignored for simplicity.

number density, mass and speed of the solar wind particles; and μ_o is the permeability of free space). At Jupiter the value of B_o is 29 times the value for Earth while the solar wind density is reduced by a factor of ~25. Therefore this simple pressure balance gives a much larger value of R_s for Jupiter, ~50 R_J, compared with 10 R_E for the Earth.

In addition to the different sizes of the magnetospheres there are also major dissimilarities in structure, which are partly due to the unique nature of Io as a large source of plasma but mainly due to Jupiter's larger radius (R_J ~71,400 km) and rapid rotation ($\frac{2\pi}{\Omega}$ = 10 hours). In the Earth's magnetosphere there is a boundary, the plasmapause, at about 4-5 R_E which separates a region where the plasma generally corotates with the planet from a region where the plasma motion is controlled by the electric fields generated in the interaction between the solar wind and the planetary magnetic field (Brice, 1967). At Jupiter the effects of the solar wind are weaker and this factor combined with Jupiter's larger magnetic field and rotation rate put the Jovian plasmapause at a radial distance roughly the same as the distance of the magnetopause. Therefore the solar-wind-induced flow of the magnetospheric plasma should be smaller than the corotational flow essentially throughout the Jovian magnetosphere.

The ratios of Jupiter's centrifugal to gravitational accelerations $b=\frac{\Omega^2 R}{g}$ is five times larger than for Earth so that the point where the accelerations are equal and opposite (at the distance of synchronous orbit, $R_s=b^{-1/3}$) is much closer to the planet (2.3 R_J). The Earth's synchronous orbit is at 6.5 R_E which is outside the plasmapause. Therefore the Earth's plasmasphere is populated with particles that have diffused along the magnetic field against the Earth's gravity with

little help from centrifugal forces.

In contrast, Jupiter's gravitational potential is relatively easily escaped and the centrifugal force pulls the plasma out along the magnetic field to the furthest point from the planet. With a large density of plasma near the equatorial plane, the magnetic field becomes distorted. The plasma forms a thin disc around Jupiter and the whole magnetosphere is flattened and radially extended (Melrose, 1967; Gledhill, 1967; Brice and Ioannidis, 1970). The confinement of the magnetospheric plasma to the equatorial plasmadisc is enhanced by the fact that the plasma largely originates from the equatorial region near the orbit of Io and the ions are of sulphur and oxygen which are much heavier than the protons that dominate the Earth's magnetospheric plasma.

When the Earth's moon briefly enters the distant magnetotail for a few days each month, the magnetosphere is little disturbed. In contrast, the Galilean satellites of Jupiter are deeply embedded in the Jovian magnetosphere and strongly interact with the plasma.

This brief description of the "global" structure of Jupiter's magnetosphere has been given to set the scene for a more detailed discussion of the inner magnetosphere region. The review articles by Goertz (1976), Kennel and Coroniti (1977), and Scarf et al. (1981) are recommended for a more complete description.

c) Ground-based and Pioneer observations of the inner magnetosphere

Before any spacecraft reached the Jovian system considerable knowledge of Jupiter's inner magnetosphere had been gleaned from ground-based observations. Burke and Franklin's serendipitous discovery

of radio bursts from Jupiter in 1955 gave the first indication that the planet was highly magnetised and surrounded by energetic particles (Burke and Franklin, 1955). The wavelength at which emission was first observed is in the decametric range and since its discovery the Jovian decametric emission has exhibited a complex structure both in its sporadic occurrence and emission properties (e.g., frequency, polarisation, duration, etc.) (Carr and Desch, 1976). As yet the origin of these energetic decametric bursts is unknown. A more useful tool for investigating the radiation environment around Jupiter was found at shorter wavelengths, in the decimetric range of radio emission (Berge and Gulkis, 1976). The decimetric radiation is weaker but steady and its regular 10 hour sinusoidal variation suggested a dipolar magnetic field with the magnetic symmetry axis tilted at an angle of ~10° to the rotation axis of the planet. The emission was assumed to be synchrotron radiation from electrons with energies of ~10 MeV that gyrate around dipolar magnetic field lines at a radial distance of a few times the radius of Jupiter. A rough estimate of the rate at which these relativistic electrons radiate their energy indicated a half-life of less than a year. This interpretation implies that there must be a considerable source of ionised particles and a mechanism by which they can obtain such high energies. At this time, the Earth's radiation belts had only recently been explored and there was evidence that the radiation belt particles originally came from the solar wind which provoked the suggestion that a similar process might also be taking place at Jupiter. However doubts were raised about a solar wind source for the Jovian radiation belts when no correlation could be found between the decimetric emission intensity and solar activity (Klein,

1976).

Although the decametric emission did not provide very much information about the particle population in Jupiter's magnetosphere, Bigg's discovery that the occurrence probability of the bursts is strongly modulated by the position of Io raised many questions about the interaction between the Galilean satellites and magnetospheric plasma (Bigg, 1964). It was concluded that the radiation was generated in the ionosphere of Jupiter approximately at the "feet" of the field lines that intersect the position of Io in its orbit, but what processes could be going on at Io to trigger a release of energy of the order of 10^8 Watts in a burst of radio emission? Why is the emission sporadic? Why is Io and none of the other satellites so important? Several theories were developed over the pre-Voyager years but they were limited by the complete lack of information about the density and energy of the magnetospheric plasma (Piddington and Drake, 1968;Goldrich and Lynden-Bell, 1969; Gurnett, 1972; Goertz and Deift, 1973).

The first clue that Io might actually be a source of plasma particles was the discovery by Brown (1974) of optical emission from a cloud of neutral sodium atoms in the vicinity of Io. This sodium D-line emission has been monitored at several observatories since its discovery and the cloud shape and emission intensity appear to be fairly constant (Bergstrahl, 1977). The "banana-shaped" cloud is about 3 R_J by 1.5 R_J with Io towards one end and the other end preceding Io in its orbit, tilted by ~30-40° towards Jupiter. The most probable source of the neutral atoms seems to be sputtering of the surface of Io by energetic charged particles from the magnetosphere (Matson et al., 1974) while the optical emission is produced by resonant scattering of sunlight (Trafton

et al., 1974). Even with quite moderate densities of ambient plasma the dominant loss process for the neutral sodium atoms is probably electron impact ionisation (Carlson et al., 1975 and Eviatar et al., 1977). Variations in the cloud shape and emission strength then indicate changes in the source or the local plasma conditions. Trafton and Macy (1977) noticed the sodium emission weakened when Io crossed the magnetic equator. They suggested that this was evidence of enhanced ionisation of the neutral sodium atoms due to enhanced plasma densities near the magnetic equator.

The first direct information about the properties of the Jovian magnetosphere came from experiments on the Pioneer 10 and 11 spacecraft which flew past Jupiter in 1973 and 1975 respectively (reviewed by Goertz, 1976). The magnetosphere was found to be inflated to as much as twice the size expected from a simple scaling of the Earth's magnetosphere. The outer magnetosphere appeared to be flattened into a disc-like structure in the magnetic equatorial region. The inner magnetosphere was subsequently defined as the region closer than ten Jupiter radii to the planet where the magnetometers showed the magnetic field to be largely dipolar. The four detectors on each spacecraft that were designed to measure fluxes of energetic charged particles ($> 10^5$ eV) detected intense radiation belts in this region. These high energy particles appeared to be well-ordered by the symmetric configuration of the magnetic field. The particle fluxes were significantly depleted at the radial distances corresponding to the orbits of the inner satellites which suggests that the particles are swept up and absorbed by the satellites.

There were no measurements made of charged particles with energies

below ~100 eV. The Pioneer 10 plasma instrument did detect positive ions near Io's orbit which were interpreted as protons with a temperature of ~100 eV and a density of ~100 cm^{-3} (Frank et al., 1976). It has subsequently been shown that these ions could not have been protons but were probably heavy ions coming from Io (Neugebauer and Eviatar 1976; Goertz and Thompsen 1979; Mekler and Eviatar 1980). However the experiment did not provide hard evidence concerning the plasma environment near the orbit of Io. Similarly, the Pioneer 10 observations of ultraviolet radiation from the inner magnetosphere were interpreted in terms of relatively weak emission from atomic hydrogen (Carlson and Judge 1974) and the strong emission from ionised sulphur and oxygen seen by the ultraviolet spectrometer on the Voyager spacecraft was not observed by Pioneer 10.

Soon after the Pioneer encounters with Jupiter the first direct evidence of the presence of ionised material near Jupiter at low energies came with the discovery by Kupo et al. (1976) of optical emission at wavelengths corresponding to the forbidden lines of S^+ ions. The radiation observed by Kupo et al. came from a region inside the orbit of Io (5.95 R_J) and they put an upper limit of 10^4 cm^{-3} on the local density of electrons. Brown (1976) borrowed techniques from studies of more remote astronomical gaseous nebulae and by comparing the emission intensity at different lines he concluded that the S^+ emission came from a dense ring of cold plasma. Although this conclusion provoked some debate at the time and was not fully appreciated by the energetic particle community, it marks the discovery of the plasma torus at Io. Under the assumption of local thermodynamic equilibrium, Brown (1976) determined the electron temperature to be 5.4 to 8.6 eV and the

electron density 1600 to 6300 cm^{-3}. Under less stringent assumptions, Mekler et al. (1977) estimated the electron density to be ~500 cm^{-3} and the temperature T_e ~10 eV. Mekler and Eviatar (1978) assembled the data from many observations of the sodium and S^+ emissions and concluded that the intensities of the two emissions were anti-correlated and inferred that there were episodic variations in the electron density between 50 and 900 cm^{-3} between 1974 and 1977. From a similar catalogue of observations of the sulphur emission Nash (1979) concluded that the torus was oriented closer to the magnetic equator than the rotational equator and had a wedge-shaped cross-section with height of the emission region decreasing radially inwards from a value of ± 1 R_J at the orbit of Io to ± 0.2 R_J at a radial distance of 5 R_J.

Since the Voyager encounter Pilcher (1980) has published images of the S^+ emission and Pilcher and Morgan (1979) have discovered emission from O^+ ions. Line emissions from S^{2+} ions have been observed at various wavelengths (Trauger et al., 1979; Brown, 1980; Oliversen et al., 1980), and Brown (1980) has recently discovered an emission feature near Io, which indicates the presence of neutral oxygen atoms. However, to retain some semblance of chronological order a discussion of these observations is postponed until Chapter 4, after the Voyager plasma results have been presented.

d) Theoretical Considerations

Concurrent with the experimental observations of the Jovian magnetosphere there have been extensive theoretical investigations aimed to explain or predict magnetospheric phenomena. Some pertinent theoretical considerations are briefly described here so that the

Voyager observations can be regarded in their theoretical context. The first question to be addressed concerns the bulk motion of the plasma in the inner magnetosphere. The second question is what are the main sources of plasma particles. Thirdly, what are the properties of the plasma and how do these characteristics change as the plasma diffuses through the magnetosphere.

The question of the plasma dynamics around a rotating magnetized body was first considered for magnetic stars (Ferraro, 1937), then applied to the planets Earth and Jupiter (Gold, 1959; Brice and Ioannidis, 1970). The simplest approach is to work from the central body outwards. Momentum is transferred from the rotating surface via the neutral atmosphere to the ionized layer above (ionosphere) by collisions between the neutral atoms and ionised particles. This frictional drag on the ionosphere is generally sufficient to make the ionosphere corotate with the planet. Under steady state conditions, magnetic field lines emanating from the planet may be regarded as electrostatic equipotentials because of the high mobility of charged particles moving along a magnetic field (i.e. $\sigma_{\parallel} \rightarrow \infty$). This means all ions on particular field lines that are connected to the ionosphere must have the same bulk angular motion as the ionospheric particles, i.e., the magnetospheric plasma must also corotate with the planet.

As the influence of any body is inherently limited, corotation cannot extend to unlimited radial distances. At some point the plasma motion must deviate from strict corotation due to the effects of either external forces or the plasma's own inertia. Models of pulsars suggest relativistic inertial effects limit corotation at distances where the speed of rotation approaches the speed of light. With the Earth's much

weaker magnetic field external forces due to the interaction between the solar wind and the magnetosphere dominate the plasma motion outside a boundary, the plasmapause, at about 5 Earth radii. Inside the plasmapause the plasma corotates with the planet. At Jupiter the solar wind effects are weaker and the planetary magnetic field stronger so that a simple scaling of the Earth's magnetosphere to Jupiter puts the Jovian plasmapause at distances of 50 R_J or greater (Brice and Ioannidis, 1970).

Hill (1979) has shown that if there is a source of plasma in the magnetosphere (with accompanying radial transport under steady state conditions) then the atmosphere must exert a viscous torque on the ionosphere to balance the inertial loading due to the production and transport of magnetospheric plasma. To provide the torque on the ionosphere there must be some differential motion between the atmosphere and the ionosphere. Because all particles in a magnetic L-shell have the same angular motion, the resulting lag of the ionospheric plasma motion behind corotation is shared by all the magnetospheric plasma along corresponding L-shells. The magnitude of the corotational lag depends on rate of production (and transport) of plasma mass in the magnetosphere as well as the degree of collisional coupling between the ionospheric ions and the atmospheric neutral atoms. As the increase of angular momentum due to a given mass loading is larger at greater radial distances then the deviation from corotation will also increase with larger L values. The Voyager plasma measurements showed that the large source of plasma at Io results in a ~25% lag behind co-rotation by L=20 (McNutt et al., 1979) which confirmed Hill's hypothesis (Hill, 1979). Inside this distance the deviation of the bulk plasma motion from

corotation is therefore expected to be much less, maybe a few percent towards the outer boundary of the inner magnetosphere at 8 R_J.

The obvious association of the region of the magnetosphere containing the densest plasma with Io implies that the plasma must come from the satellite. However, the exact nature of the production mechanism is not clear. Two theories have been proposed:

i) The plasma is produced by the ionisation of clouds of neutral atoms (or molecules) similar to the observed neutral sodium cloud, which are essentially extended atmospheres of Io, spread along the satellite's orbit.

ii) The plasma is produced in the immediate vicinity of Io during the complex interaction between the magnetospheric plasma and the satellite.

In each case the characteristics of the freshly ionised plasma may be very different. When neutrals are ionised they experience a Lorentz force due to their motion relative to the local magnetic field; this force causes the ions to gyrate about the magnetic field at a speed equal to the magnitude of the component of the neutral's initial velocity perpendicular to the field in the rest frame of the surrounding plasma and also accelerates the particles until their guiding centers are fixed in the rest frame of the plasma. In the inner magnetosphere the rest frame is usually the one corotating with Jupiter. If the ions are indeed picked up in this way then they would initially have an unusual distribution in velocity space. Siscoe (1977) has considered the pick-up process in detail and predicted a "tin-can" velocity space distribution for each ionic species produced in this way (Figure 2).

The major difference between the two source mechanisms for ions at

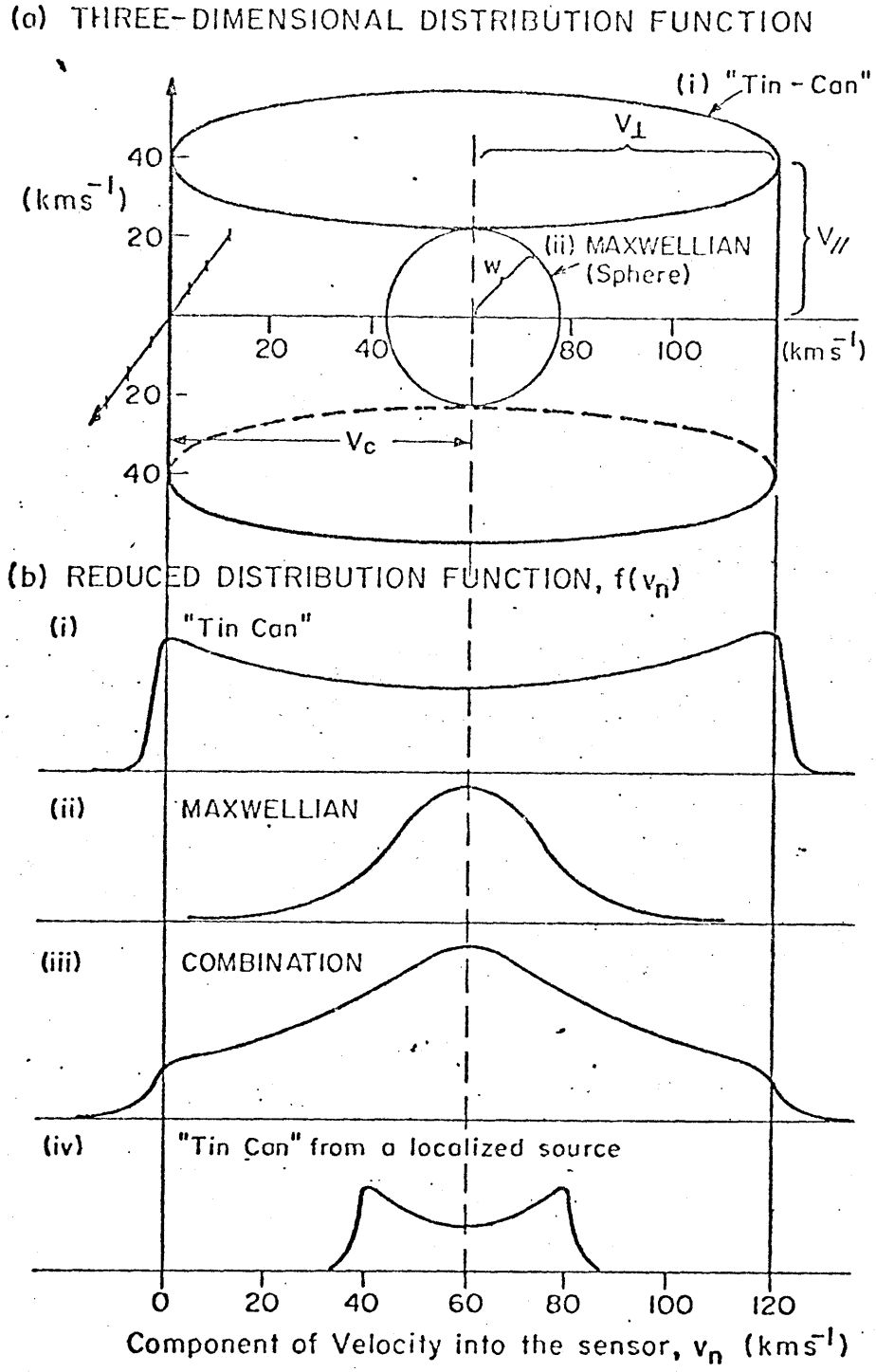

Figure 2. In (a) the three-dimensional distribution of particles in velocity space has been sketched for (i) a "tin-can" distribution of ions which have been recently ionised and (ii) for a Maxwellian distribution of ions which are in thermal equilibrium.
In (b) the three-dimensional distributions have been integrated in two directions to give a reduced, one-dimensional distribution function (see Appendix I).

Io is the nature of this initial distribution function. In the first case the ions come from an extensive neutral cloud and the local magnetic field may be taken to be that of a dipole tilted by 10° from the rotation axis. The rest frame of the plasma is then simply the corotating frame. The new ions therefore have a gyro-speed equal to the difference between Io's orbital speed and the local corotation speed. At Io's orbit (5.95 R_J) this produces a tin-can distribution in velocity space of radius 57 km s^{-1}. The height of the tin-can is due to injection of particles when Io is not on the magnetic equator. At longitudes where the magnetic equator does not coincide with the orbit of Io the new ions will gain a bounce motion parallel to the magnetic field so that the ions may have aligned motion of up to -40 km s^{-1} at the magnetic equator. Ions produced where Io's orbit intersects the magnetic equator will have essentially no initial field aligned motion. The thickness of the tin-can is due to the spread in original orbital velocities of the neutral atoms before being ionised. Observations of the sodium neutral cloud suggest the spread is small, on the order of 2.5 km s^{-1} (Murcray and Goody, 1978).

The rest frame is the same for all ionic species so assuming the different neutral species started with similar orbital motion, the corresponding ionic species will share the same gyrospeed. This means the tin-can velocity distributions should have the same dimensions for sulphur and oxygen ions. However the energy of the ions is scaled by their atomic mass so that sulphur and oxygen ions have energies due to their gyromotion of 540 eV and 270 eV respectively.

In the second theory, where ions are produced in the localised interaction region near Io, the local plasma rest frame at the point of

ionisation is no longer simply the corotating frame. In the satellite/ magnetosphere interaction the local magnetic field is perturbed and the electric currents which flow in the plasma, the ionosphere and solid body of Io effectively reduce the local electric field from the full corotational value. This means the gyromotion of the new ion is correspondingly reduced in magnitude. As the freshly ionised material moves away from the perturbed region near Io the ions are then accelerated by the corotational electric field until their guiding centers acquire the full corotation speed. However the gyro-motion retains the initial reduced magnitude so that resulting velocity distribution of freshly ionised material in the torus is a tin-can of reduced radius (Figure 2). Goertz (1980) suggests that the electric field in the vicinity of Io is reduced to about one third of the corotational value so that the initial gyro-energies of sulphur and oxygen ions are 66 eV and 33 eV respectively.

Ions with a tin-can velocity distribution are not in thermodynamic equilibrium. Coulomb collisions between ions or with electrons will change the distribution to a more stable one. The observed torus densities are much larger than those initially considered by Siscoe in his early work on this problem (Siscoe, 1977) so that collisions are consequently much more important. However, except in the cold inner torus, complete thermal equilibrium cannot be assumed even for the bulk of the plasma because the timescales for collisions are of the same order as the time scale for diffusion (i.e., days). The situation is further complicated because the evolution of a distribution from a tin-can to Maxwellian function is not understood even for a single ionic species let alone a multi-component plasma. The effects of collisions

over increasing time scales are, firstly, to make the velocity distribution of each ionic species isotropic; secondly, to produce equipartition of energy for each species; and eventually to produce equipartition of energy between ions of different mass so that the plasma becomes isothermal. A simplistic model of a distribution function found in an intermediate stage in this thermalization process has been made in the analysis of the plasma measurements by giving the different ionic species a common "thermal" speed.

In conclusion, many aspects of the structure of the Jovian magnetosphere, the special role of Io as a source of plasma and the characteristics of the plasma produced by Io were anticipated long before the Voyager spacecraft arrived at Jupiter.

(e) Voyager magnetospheric experiments

Eight of the eleven scientific experiments on the Voyager spacecraft made direct measurements of the magnetospere of Jupiter. These eight experiments and some of their major observations are listed in Table 1. Two of the remaining three experiments contributed the discovery of Io's volcanic plumes (Imaging Science experiment) and provided the evidence of "hot spots" and gaseous SO_2 on Io (Infrared Radiation experiment). These observations are vital clues of how the volcanic processes on Io produce the materials which ultimately, become ionised and populate the magnetosphere. For summaries of the primary results from the Voyager encounters with Jupiter, see the special issues of Science (Vol. 204, No. 4396, 1979, and Vol. 206, No. 4421, 1979) and Nature (Vol. 280, No. 5725, 1979).

This thesis is primarily concerned with the positive ion

Table 1 Magnetospheric Experiments on the Voyager Spacecraft

Investigation (Principal Investigator)	Abbreviation	Measurement	Observations in the Inner Magnetosphere
Plasma Science (H. S. Bridge)	PLS	Electrons and ions with energy per charge of 10eV to 6 keV	Velocity distribution of electrons and ions of sulphur and oxygen at different ionization states.
Radio Science (V. R. Eshleman)	RSS	Phase of coherent radio signal at wavelengths of 13 and 3.6 cm	Dispersion of the radio signal transmitted from the spacecraft as it propagates through the plasma torus.
Ultraviolet Spectroscopy (A. L. Broadfoot)	UVS	Ultraviolet emission between 500 and 1700 Å	Line emission from ions in the warm region of the plasma torus. Auroral emission from the polar regions of Jupiter's magnetosphere.
Magnetic Fields (N. F. Ness)	MAG	Magnetic field	Planetary magnetic field, magnetospheric structure and the current system near Io.
Plasma Waves (F. L. Scarf)	PWS	Electric field fluctuations between 10Hz and 56KHz	Resonant electrostatic waves, whistler mode turbulence and discrete whistlers.
Planetary Radio Astronomy (J. W. Warwick)	PRA	Radio emissions between 1.2 KHz and 40.5 MHz	Electrostatic resonant emission at various characteristic plasma frequencies, bursts of decametric and kilometric radio emission.
Low Energy Charged Particles (S. M. Krimigis)	LECP	Electrons with energies $\geq$ 15 keV ions with energies $\geq$ 30 keV	Fluxes of energetic particles: their depletion and change in pitch angle near the L-shells of the Galilean satellites and the outer boundary of the torus.
Cosmic Ray Particles (R. E. Vogt)	CRS	Electrons with energies 3 to 110 MeV ions with energies 0.4 to 500 MeV per nucleon.	Distribution, composition and flow of high-energy trapped nuclei and electrons.

measurements obtained by the Plasma Science experiment during the seven-hour period preceeding Voyager 1's closest approach to Jupiter with only a cursory comparison of the results with other measurements. The next step is to integrate the measurements made throughout the magnetosphere by all magnetospheric experiments on both Voyager spacecraft (as well as with ground-based experiments) to draw a more complete picture of the magnetosphere.

Chapter 2

The Voyager Plasma Experiment: Spacecraft trajectory, plasma instrumentation and analysis technique

a) Voyager Trajectory

On March 5, 1979 the Voyager 1 spacecraft passed through the inner magnetosphere of Jupiter and within 4.9 Jovian radii (R_J) of the planet (Figure 3). The trajectory was within ~5° of Jupiter's equatorial plane (as well as the ecliptic) but because of the 9.6° tilt of Jupiter's dipolar magnetic field, the spacecraft's magnetic latitude varied between +4 and -16° as the planet rotated with a period of ~10 hours. Similarly, the magnetic longitude (System III (1965)) of the spacecraft changed rapidly because of the planet's rotation. In the period illustrated in Figure 3, Jupiter made just over one complete rotation while Io made nearly half an orbit from mid-afternoon to after midnight.

On the inbound leg of the trajectory Voyager crossed Io's L-shell considerably behind Io in its orbit and upstream in the magnetospheric plasma flow. On the outbound leg Voyager caught up with Io and passed directly below (~26,000 km) the satellite at about 1500 UT, traversing the region where the local magnetic field lines were connected to the vicinity of Io. It was hoped that during Voyager's close approach to Io, measurements of magnetic field, plasma and energetic particle fluxes would ellucidate the nature of the satellite's interaction with the magnetosphere.

For an hour or so before the closest approach to Io and for a short while afterwards the spacecraft moved through the region of Io's neutral

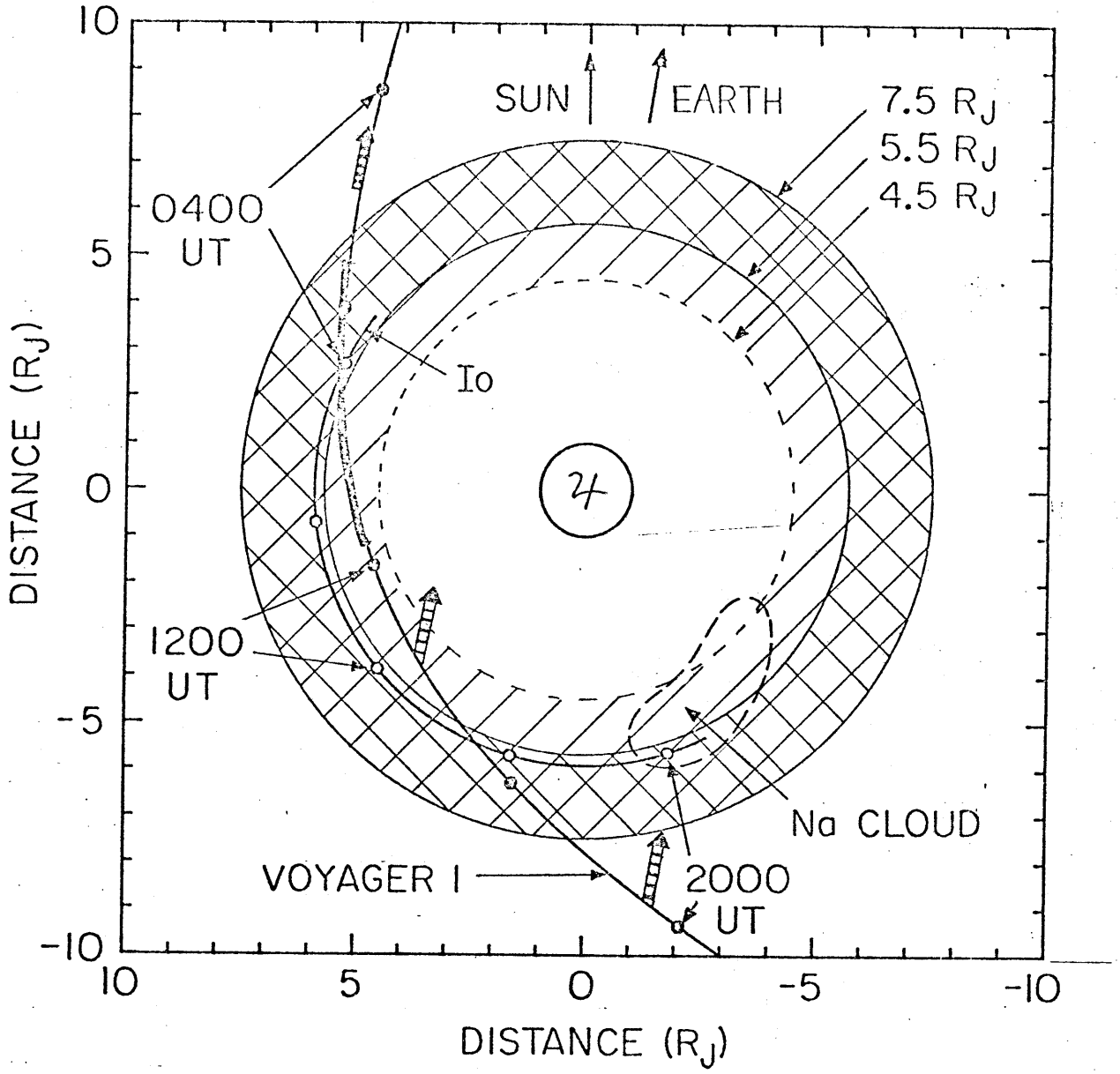

Figure 3. Trajectory of the Voyager 1 spacecraft through the inner magnetosphere projected onto the plane of the ecliptic. Voyager 1 traversed the outer (warm) torus (double hatched) in the mid-afternoon inbound and late evening outbound. The spacecraft moved through the inner (cold) torus (single hatched) near closest approach. The projection of the instrument symmetry axis onto the plane is shown by the hatched arrows. The extent of the cloud of neutral sodium atoms around Io is illustrated for 2000 UT. All the times are Universal Time (UT) on March 5, 1979. The orbital motion of Io during this period is also illustrated.

sodium cloud. Although the cloud appeared from the ground to be emitting visible light as usual (Goldberg et al. 1980) none of the Voyager instruments were designed to measure such emission.

b) Plasma instrument

The Voyager plasma science instrument consists of a main sensor of three cups (A, B, C) symmetrically positioned about an axis anti-parallel to the spacecraft Z-axis which generally points away from the Earth and a fourth cup (the side sensor, D) pointed at right angles to the Z-axis. The normals to the A, B and C cups each point 20° from the symmetry axis ($-\hat{Z}$). These cups are modulated-grid Faraday cups with apertures that are irregular pentagons with effective areas (including grid transparencies) of roughly 64 cm^2. The D-cup aperture is circular and smaller. Because the cups are shallow they have a wide field of view. The fields of view of the three cups of the main sensor together cover nearly a full hemisphere with a common field of view covering a cone of ~45° half-angle about the symmetry axis. Figure 4 includes an illustration of the detector while a full description of the instrument is given in Bridge et al. (1977). Throughout most of the inbound leg of the trajectory, before 0500 UT on March 5, 1979, the side sensor was pointed into the azimuthal flow of plasma around Jupiter. As the spacecraft approached the planet, the viewing geometry changed rapidly so that after 0500 UT the main sensor was swept into the direction of corotational flow and then rapidly away after closest approach at 1204 UT (Figure 3).

The response of the sensors to high sonic Mach number plasma flow at angles $\lesssim$60° into the cups is very close to a constant factor which is easily calculated (See Appendix II). For flow at more oblique angles, the response is more complex and analysis of the data on the outbound leg

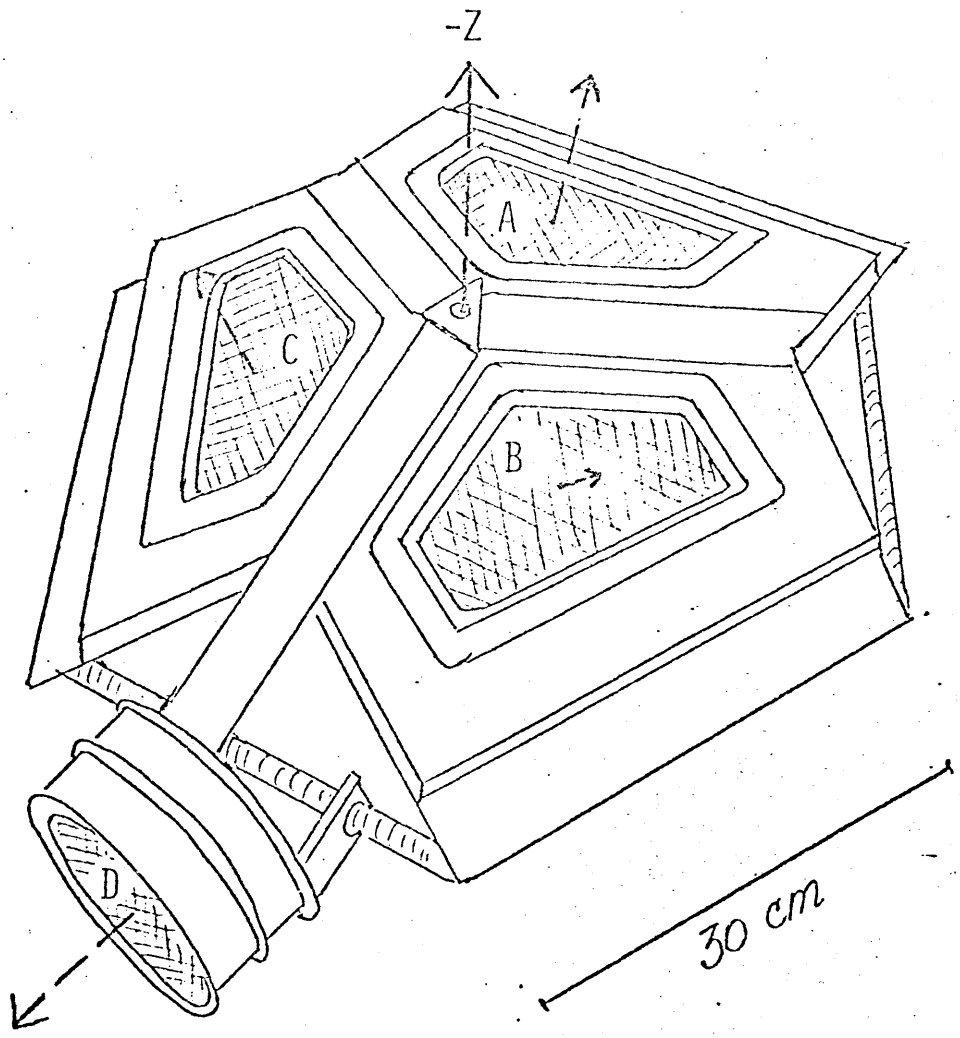

Figure 4. This diagram of the Voyager plasma detector shows the three cups (A, B and C) of the main sensor clustered around the symmetry axis the -Z axis of the spacecraft, which usually points towards Earth. The side sensor (D-cup) points at right angles to the Z axis.

through the torus is as yet incomplete. The analysis presented here has been confined to the inbound leg of the trajectory.

Positive ion measurements are made with each cup in an energy per charge range spanning nearly 6 kilovolts. Under typical plasma conditions, when the spacecraft is at the same electrostatic potential as its surroundings this voltage range is from 10 to 5950 volts. In the event that the spacecraft becomes charged, which may be the case in the warm torus, the voltages will be correspondingly shifted. However, the spacecraft will be assumed to be at zero potential in the initial analysis. In the high resolution mode the voltage range is scanned in 128 steps with an energy resolution of ~ 3.6%. The 128 steps are measured in 30.72 seconds with 96 seconds between adjacent scans. However, during the Jupiter encounter period, only 72 of the 128 steps were transmitted for any given 96 second measurement sequence. The two voltage ranges 10 to 750 volts (steps 1 through 72) and 400 to 5950 volts (steps 57 to 128) are transmitted alternately each 96 seconds. Hence, it took 192 seconds to obtain a complete high resolution spectrum. Any differences in the fluxes measured in the 16 overlapping channels indicate variations in the ambient plasma within 96 seconds.

c) Derivation of plasma parameters

The details of the analysis of the positive ion data in the inner magnetosphere are given in Appendix I and only an overview of the general principles involved will be discussed here. The electric currents measured by a Faraday cup are velocity space integrals of the product of the ion distribution function $f(\vec{v})$, the component of ion velocity into the cup and the response of the sensor. The present data analysis procedure is limited to situations where it can sensibly be assumed that

the response function is near unity over the region of velocity space in which $f(\vec{v})$ is appreciable. Under this assumption a simple analytic relation between the measured currents and the plasma parameters that describe $f(\vec{v})$ can be obtained (equation 9 in Appendix I). With such an analytic relation, a least squares determination of the plasma parameters from the measured currents is straightforward, although complicated by the fact that the plasma consists of a mixture of many ionic species.

Although the Voyager plasma detectors separate ions according to energy per charge, the addition of a velocity selector converts the instrument into one which differentiates ions by their mass per charge, A/Z^*. In much of the inner Jovian magnetosphere the velocity selection is found by observation to be inherent: all ions corotate with the planetary magnetic field and have a common bulk velocity perpendicular to the field (but not necessarily along the field). In this circumstance cold ions with different values of A/Z^* appear as separate peaks in the energy per charge scan of the instrument, with the peaks at values of energy per charge equal to A/Z^* times the energy per charge of H^+. The derivation of plasma parameters in this case is particularly straightforward.

A typical well resolved spectrum from the C sensor at 5.3 R_J is shown in Figure 5. The measured currents have been converted to a "reduced" (one dimensional) distribution function, F_p, assuming all the particles are protons (see Appendix I). If one assumes that all ions represented by the peaks in Figure 2 are corotating with Jupiter, i.e., they have a common flow velocity $\bar{v} = \bar{\Omega} \times \bar{r}$, then the values of A/Z^* are uniquely determined. Assuming corotation, the dominant peaks in Figure 2

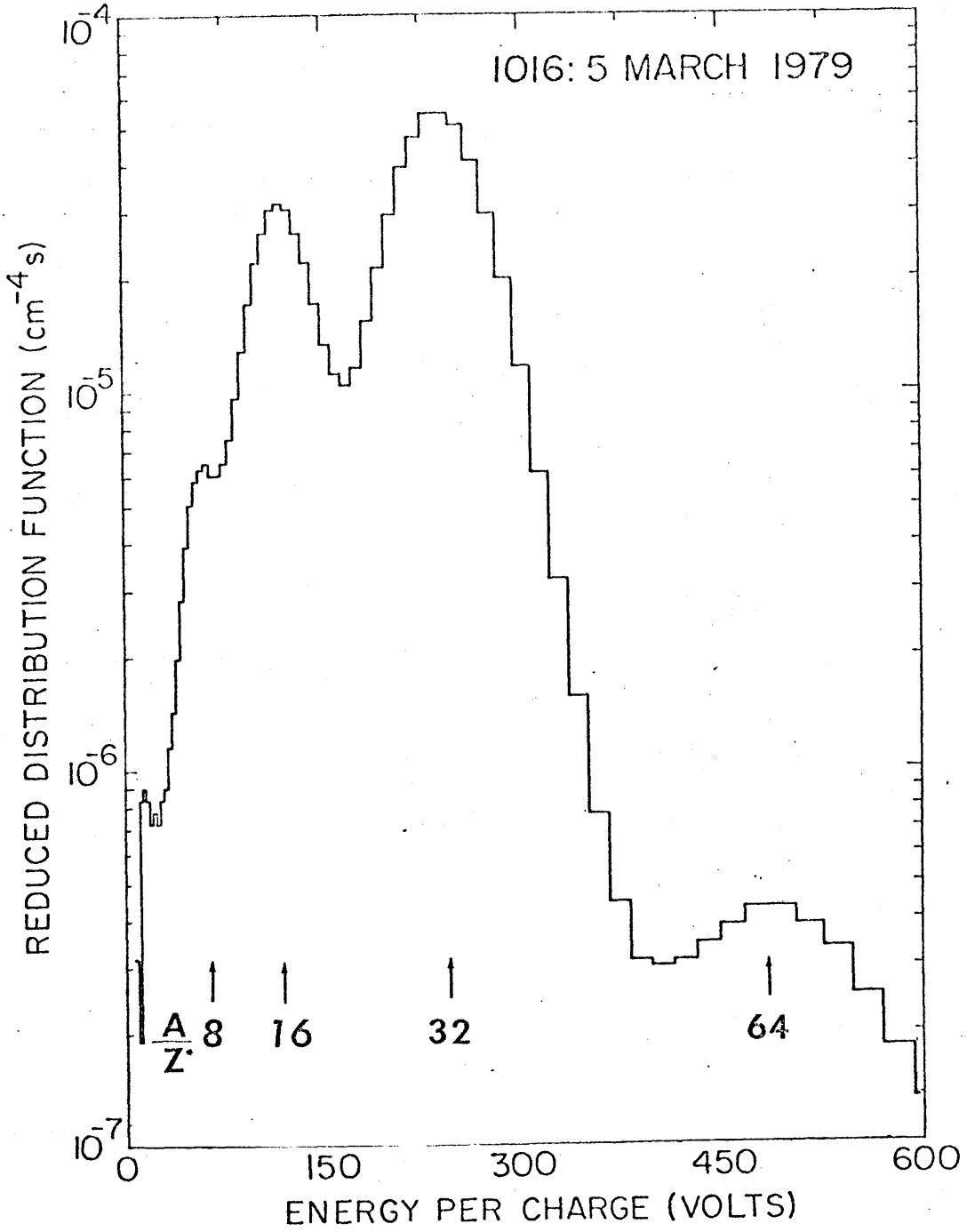

Figure 5. An example of part of a high resolution energy per charge spectrum from the inner (cold) torus showing peaks corresponding to ions with mass to charge ratios (A/Z^*) of 8, 16, 32 and 64. Corotating protons would have an energy per charge of 7.5 volts which is below the voltage threshold of the instrument (10 volts).

correspond to O^{2+}, O^{+} or S^{2+} and SO_2^{+} which have values of A/Z^* of 8, 16, 32, and 64 respectively. A different assumption concerning the velocity would, of course, give different values of A/Z^* which are, in general, impossible or implausible on physical grounds; thus, the conclusion that the plasma in the cold region of the torus moves with the velocity of corotation rests on the physical plausibility of the identifications of the spectral peaks in the spectrum of Figure 5 and in many similar spectra.

The resolved spectra in the cold region of the torus were analysed as follows. Each energy per charge spectrum was converted to the corresponding velocity distribution function and was analyzed using a simultaneous fit to a sum of convected isotropic Maxwellian distribution functions with the sum over the assumed values of A/Z^*. It is assumed that all species have a common bulk velocity. Spectra with well resolved peaks (such as that shown in Figure 5) are well fit by this procedure assuming the peaks are at values of $A/Z^* = 8, 16, 32,$ and 64. For each ionic species the fit determines the number density and thermal speed; it also determines for all species a common component of velocity in the direction normal to each plasma sensor. For those cases where simultaneous spectra are available from the A, B, and C sensors, this procedure yields three components of the plasma velocity vector. In these cases, when the spectra from the three cups are fitted separately they also provide three independent measurements of density and thermal speed for each ionic species. The three spectra can also be fitted simultaneously, which reduces the number of free parameters and provides a better single determination of each density and thermal speed. Although such simultaneous three cup fits have been made in some isolated

cases most of the results presented here have been derived using data from a single cup, the cup chosen being the one whose look direction is closest towards the corotating flow.

Unfortunately, single peaks do not always correspond to a single ionic species and the determination of kinetic temperatures is complicated for this reason. The most troublesome example in the Io torus and throughout the magnetosphere is at $A/Z^* = 16$, the common ratio for both S^{2+} and O^+ ions. It is possible to distinguish between these two to some extent by considering the thermal spread of the $A/Z^* = 16$ peak. The width of a peak at a known value of A/Z^* is a direct and unambiguous measure of the thermal speed of the ionic species (assuming only one species with that value of A/Z^* contributes to the peak). However a determination of the temperature from the measured thermal speed requires the additional knowledge of the mass number A of the species. Conversely, if one has an estimate of the temperature from some independent source, the observed thermal width of a given A/Z^* peak can be used to deduce the mass number A. Fortunately in most cases the identification of the specific species corresponding to a given A/Z^* value is unambiguous. For example, the peaks at A/Z^* equal to 8 and 32 are presumably dominated by O^{2+} and S^+ ions (through there could in principle be contributions from S^{4+} and O_2^+ or SO_2^{2+} respectively). The temperature determination from such unambiguous peaks, coupled with the assumption that the different ionic species have the same temperature, can be used to deduce the probable mass number of the ambiguous peaks. For example, under the assumption that the ions are isothermal, the width of the O^+ peak is larger than that of the S^{2+} peak and the experimental data can be fitted by suitable

proportions of the two ions. For the spectrum in Figure 5, this procedure yields the fit shown in Figure 6. In the inner region of the torus where the A/Z^* peaks at 8 and 32 are well-resolved, independent fits to each peak suggest that the O^{2+} and S^+ ions have equal temperatures. Therefore, the data in the cold region of the torus have been analysed under the assumption that all the ions have the same temperature so that S^{2+} and O^+ ions can be separated.

Outside about 5.5 R_J the ions are warmer. For a given selection of ionic species the resolution of their spectral peaks depends on the sonic Mach

number. For the spectrum shown in Figure 6 the Mach numbers are between 18 and 25. In the warm torus however, the Mach numbers drop to ~3 or less, whereas the overlap between peaks becomes significant for Mach numbers greater than ~6 (discussed in more detail by McNutt et al. 1981). Individual peaks are usually not resolved and there is no direct evidence that the plasma is isothermal or that it moves with the corotational velocity. Thus, in the warm region of the torus the results of the fitting procedure depend critically on assumptions concerning the a) composition, b) temperature, and c) bulk motion of the plasma. There is also evidence from comparing the electron and positive ion measurements that the spacecraft is slightly negatively charged in the warm region of the torus which further complicates the situation. Luckily all three of the main sensors were pointed into the corotating flow around this time so that the information from all three cups can be used to constrain some of the variables. The range of uncertainty in these parameters is, of course, limited by arguments of physical plausibility. Results of the fitting procedure in the warm torus and the possible range of parameters

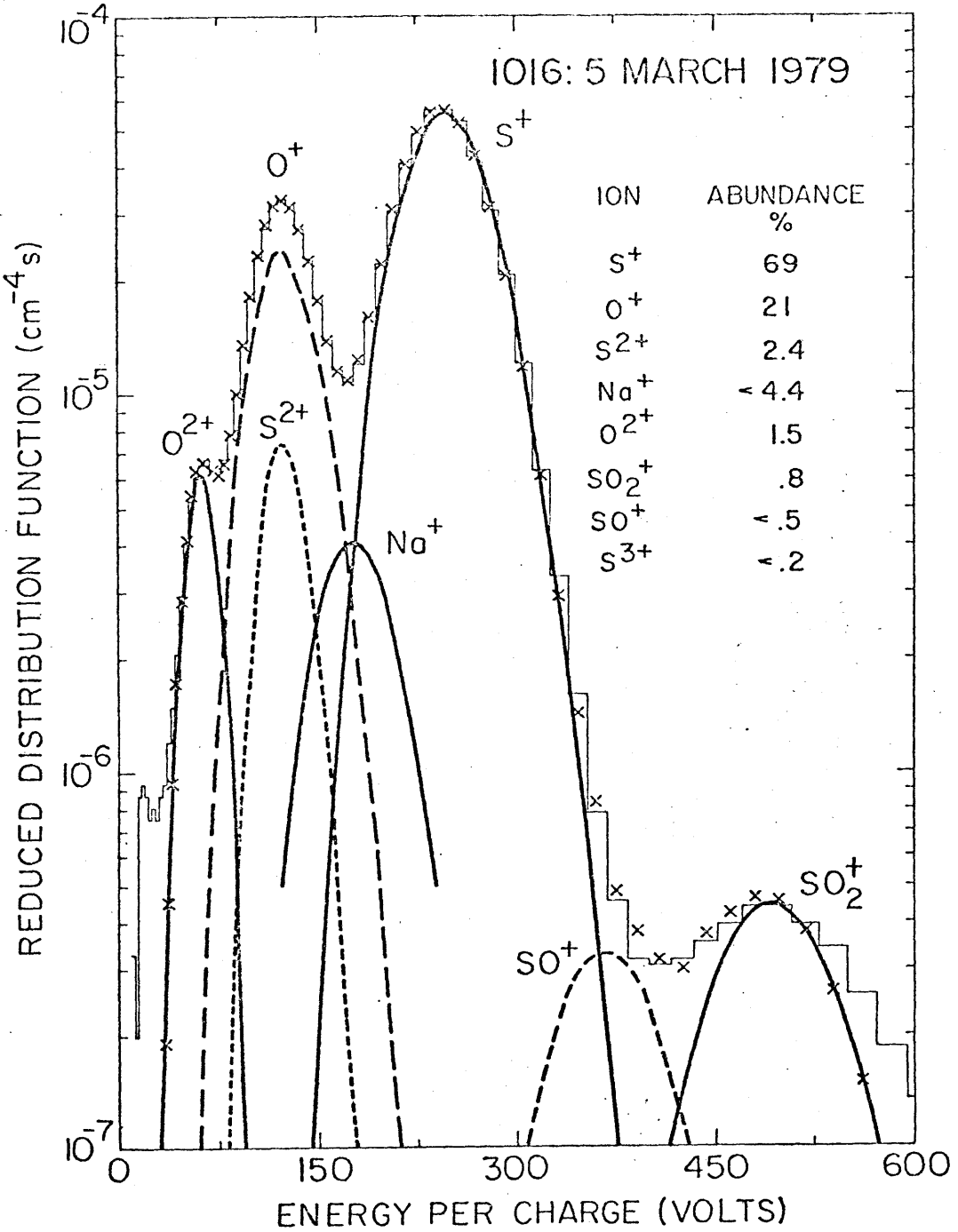

Figure 6. The energy per charge spectrum made in the C-cup of the main sensor at 1016 UT, (5.3 R_J) 5 March 1979. The data are shown as a histogram and the fit to the current in each measurement channel is shown by x's. The individual Maxwellian distributions of each ion that make up the reduced proton distribution function of the fit are shown by the curved lines.

which are consistent with the data are discussed in detail in subsequent sections. An example of the fit to a single spectrum in this region is shown in Figure 7 for two thermal models; for both cases it was assumed that the composition was represented by the five species shown in the figure and that the bulk motion was fully corotational. The results illustrate the sensitivity of the relative abundances of S^{3+} and O^{2+} to the thermal model used in the fit.

Finally, it should be emphasized that the volume density of charge and the volume density of mass associated with a resolved spectral peak at some value of A/Z^* can be estimated directly from the analysis without assumptions of ionic composition or charge state of the ions in the peak (McNutt et al., 1981; and see Appendix I).

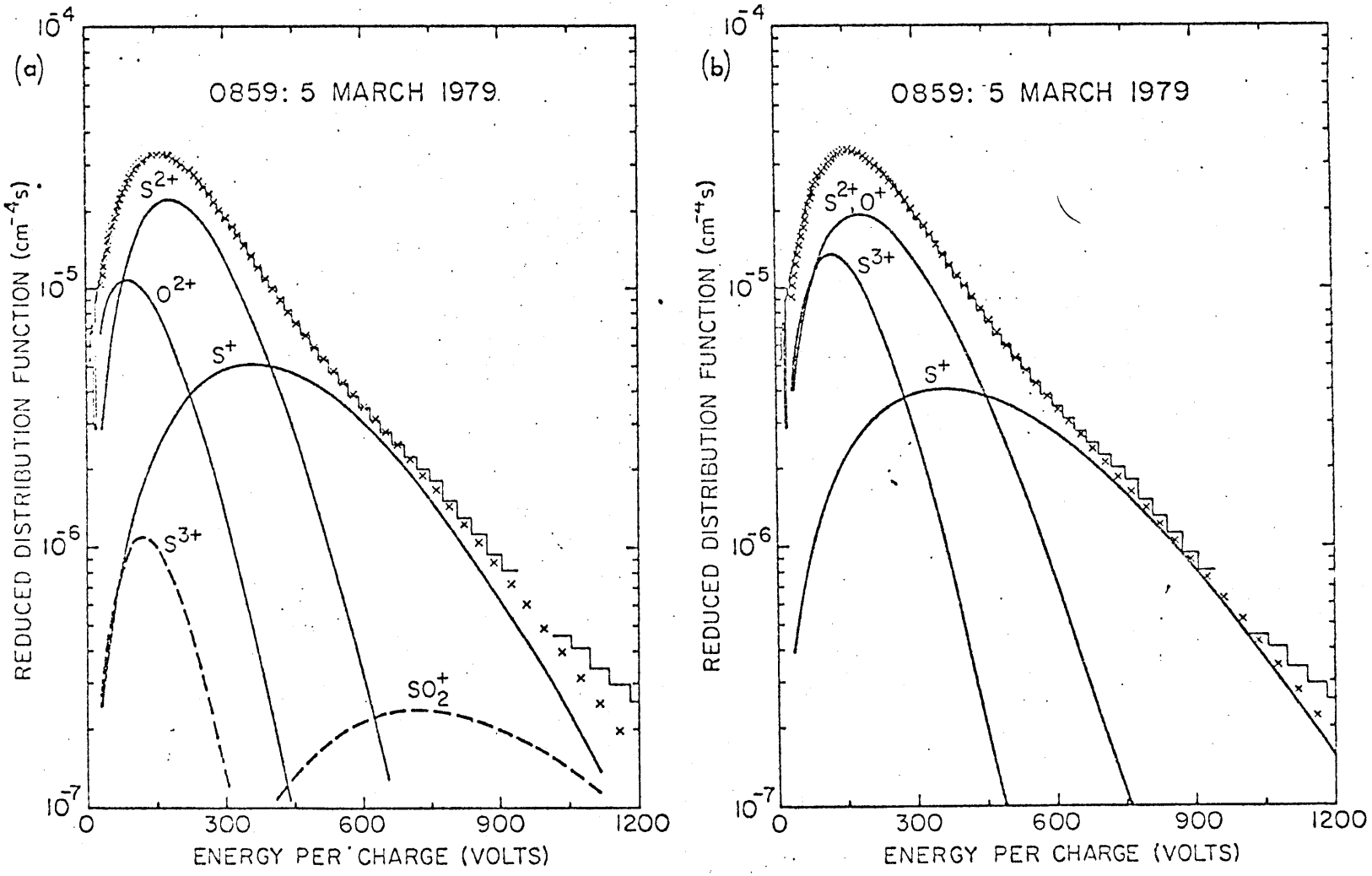

Figure 7(a)-The C-cup energy per charge spectrum for 0859 UT on 5 March 1979 (5.9 R_J) which has been fitted under the assumption that all the ions are corotating with Jupiter and have the same temperature. The data are shown as a histogram and the fit to the current in each measurement channel is shown by x's. The individual Maxwellian distributions of each ion that make up the reduced proton distribution function of the fit are shown by the curved lines. (b) The same spectrum with the fit made under the assumption that all the ions are corotating but have a common thermal speed instead of being isothermal.

Chapter 3

The Voyager Plasma Measurements in the Inner Magnetosphere

a) General Survey of the Data

A comprehensive display of plasma data obtained in the torus between 7 and 5 R_J (corresponding to the portion of the trajectory shown by the thickened line in Figure 3) is shown in the three-dimensional plot of Figure 8 where the reduced distribution function F_p is plotted against time (spacecraft event time) and energy per charge. All of the 80 spectra obtained in this period are included in the plot. After ~1000 UT in the cold inner torus, three peaks stand out in the energy per charge spectra at A/Z^*=32, 16 and 8; the relative amplitudes of these peaks vary systematically; maximum values for the individual ionic species occurred at 1030, 1050 and 1130 UT, respectively. Before ~0930 UT in the outer torus, the spectra are characterized by a single broad peak in F_p at about A/Z^* = 16. There is no dramatic change in spectral shape at the outer boundary of the torus. A similar broad peak is characteristic of spectra at radial distances of up to ~10 R_J where the plasma flow first came into the main sensors' field of view. Noise due to interference from another instrument on the spacecraft causes the notch near ~20 volts in many of the spectra displayed. The back panel shows, as a function of time, the positive charge density determined from fits to each spectrum assuming only ions with A/Z^* between 8 and 64 are present. The local maxima in the charge density profile at 0902, 0924 and 1016 UT are labeled as points 1, 2 and 3, respectively.

There are a few spectral features which are of minor importance with respect to the gross properties of the plasma but may indicate some

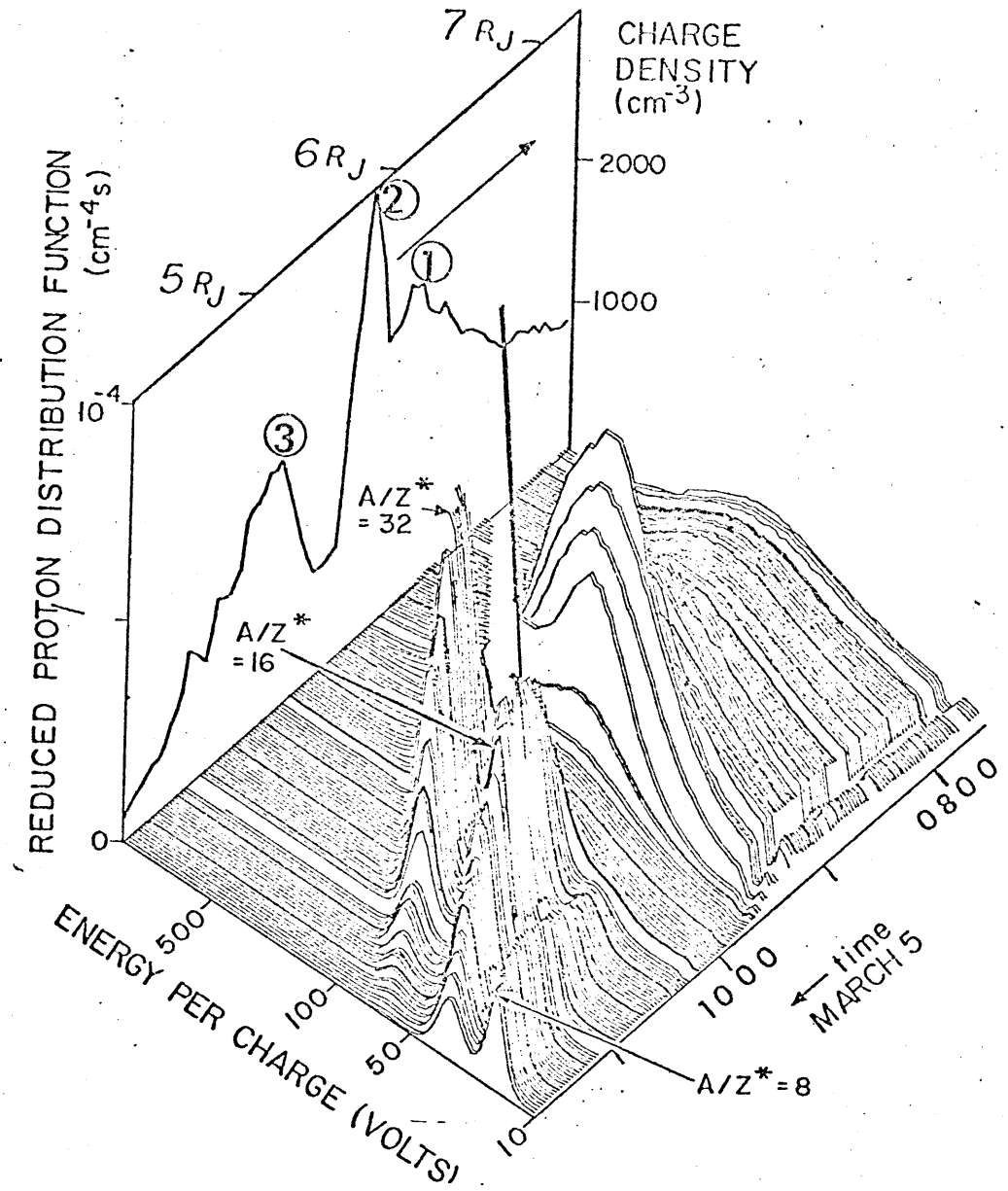

Figure 8. A three-dimensional plot of reduced proton distribution function against energy per charge for spectral measurements made in the C-cup of the main sensor between 0730 UT (7 R_J) and 1145 UT (4.9 R_J) on 5 March 1979. A total of 80 separate spectra are shown (Each spectrum is shown by a double line). Two spectra are omitted every 48 minutes as the instrument was in a different measurement mode. Every tenth spectrum is emphasized with a darker line. The back panel shows the total positive charge density as a function of time determined from fits to the corresponding spectra.

interesting phenomena. For example, the currents measured by the detector reached the saturation level for one spectrum in all 3 cups of the main sensor at 0937 UT and there is a significant particle flux that was detected throughout the inner magnetosphere at energies well above the energy of the bulk of the plasma. These and other non-Maxwellian spectral features will be discussed at the end of the chapter.

b) Radial profiles of plasma properties

Each full spectrum obtained in one of the main sensors (C-cup) between 0515 and 1200 UT (9 to 5 R_J) has been fitted with a sum of Maxwellian functions as described in Appendix I. The plasma properties derived from the fits (i.e., charge density, temperature, ionic composition and bulk motion) all varied during this period. Assuming these variations are spatial rather than temporal, radial profiles of the plasma properties can easily be constructed because the spacecraft's radial distance from Jupiter decreased monotonically in this period.

(bi) Charge Density

To preserve local charge neutrality the total positive charge density must equal the electron density; thus measurements of the positive charge density should equal the total electron number density assuming that the contribution of ions with $A/Z^* < 8$ (i.e., ions below the 10 Volt energy per charge threshold of the instrument) is negligible. A radial profile out to 9 R_J of the electron density determined from fits to the positive ion spectra is shown in Figure 9. Indirect estimates of the local electron density were made by the Planetary Radio Astronomy (PRA) experiment on Voyager 1 from the cutoff frequency of upper hybrid resonance emission (Birmingham et al., 1981). Their measurements are also shown in Figure 9. There is close agreement between the two measurements over the entire

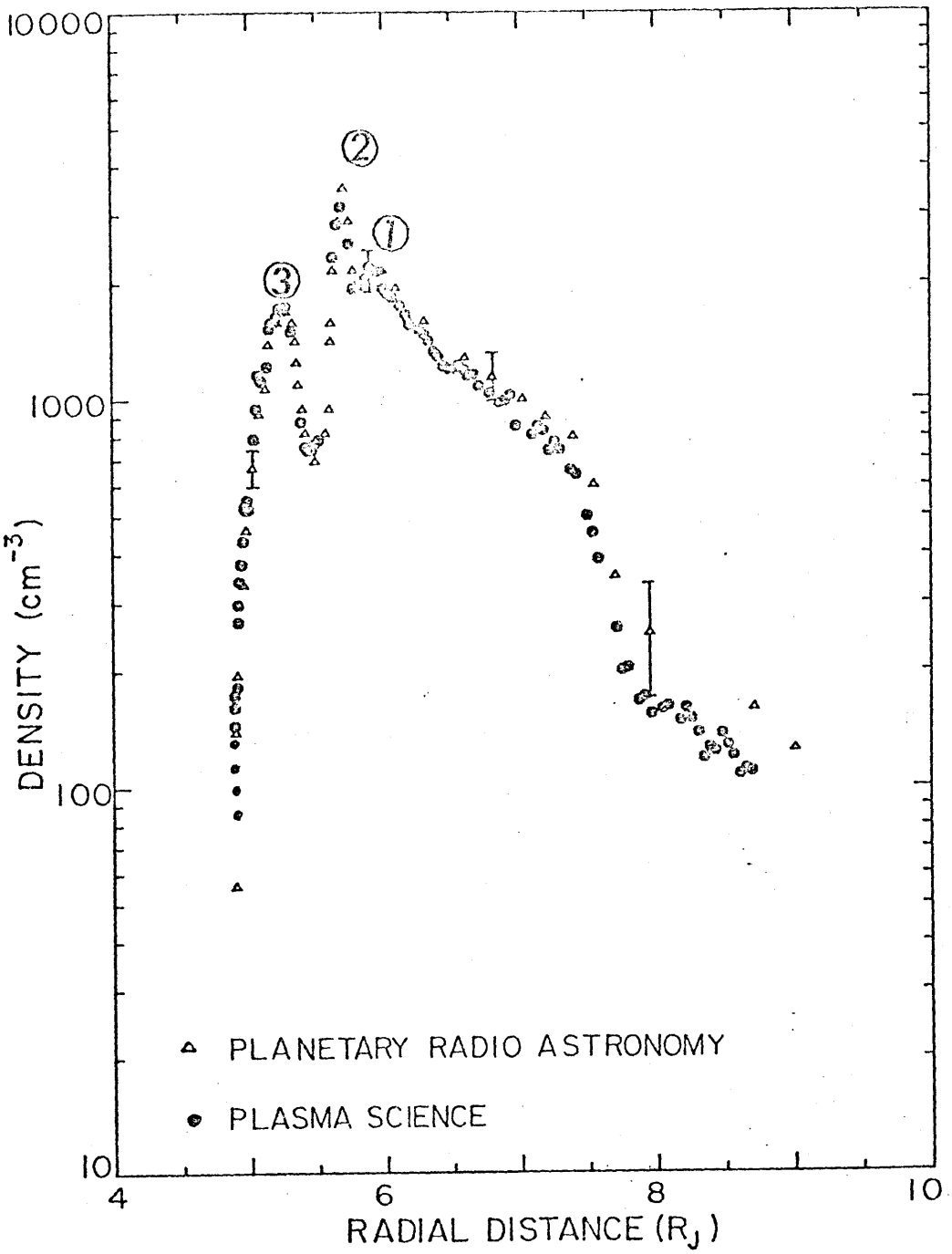

Figure 9. Radial profile of in situ measurements of charge density. The plasma science measurements (●) are of the positive charge derived from fits to positive ion energy per charge spectra. The Planetary Radio Astronomy data (Δ) from Birmingham et al. (1981) are electron density determined from the cut off frequency of plasma wave modes (typical uncertainties in the PRA determinations are shown by vertical bars).

region indicating that most of the ions have $A/Z^* \geq 8$. The slightly larger values obtained by PRA outside the torus (>7.5 R_J) may be due to electrons required to balance the charge density contributed by heavier ions with energies above 6 keV of protons with energies below 10 eV.

The outer edge of the Io plasma torus is indicated by the rapid increase in density measured by both instruments as the spacecraft moved inside ~7.5 R_J. The density built up to a broad maximum around the orbit of Io at 5.95 R_J (marked by (1) in Figure 9). The density then sharply rose to a value of ~3100 cm^{-3} at ~5.7 R_J marked by (2) well inside Io's L-shell; PRA recorded a maximum density of 3500 cm^{-3} around this time. However, the PRA measurements have a much higher time resolution and there were few measurements of such large values, all measured near 5.75 R_J. The bulk of the core of the torus had a charge density from 1000 to 2000 cm^{-3}. Radially inward of 5.7 R_J, the charge density dropped rapidly by a factor of ~5 to a value of ~740 cm^{-3}. As the spacecraft moved through the cold inner part of the torus, the charge density reached a second maximum of 1740 cm^{-3} at 5.3 R_J (indicated by (3) in Figure 9) before rapidly decreasing by an order of magnitude as the spacecraft made its closest approach to Jupiter at 4.89 R_J.

Outside the torus (> 7.5 R_J), the values of charge density determined from the positive ion measurements closely match electron densities directly measured by the plasma instrument (Scudder et al. 1981). The agreement is not as good in the warm torus (5.7 to 7.5 R_J), where the spacecraft probably had a small negative charge which introduces uncertainties in the determination of the electron density from the PLS electron data. No direct electron measurements were made in the cold inner torus where the energy per charge of the bulk of the electrons was below

the 10 Volt threshold of the plasma instrument.

(bii) Temperature

In the inner torus, independent determinations of the thermal speed for each ionic species from the well-resolved peaks in the spectra from all three cups of the main sensor indicate that the positively charged component of the plasma is predominantly isothermal at temperatures of a few eV or less. Fitting the three peaks separately for the spectrum at 1120 UT suggested the A/Z^* = 8 and A/Z^* = 32 peaks had very similar temperatures (0.44 and 0.46 eV respectively) if they correspond to O^{2+} and S^+. The fit to the A/Z^* = 16 peak produced a thermal speed of 2.2 km s^{-1} which corresponds to temperatures of .80 or .40 eV if the peak is entirely due to S^{2+} or O^+ respectively. A rough estimate of the time scales for coulomb collisions to produce equipartition of energy between ionic species in a plasma of T ~ 0.6 eV and n_e ~ 850 cm^{-3} is 20 minutes. This is a relatively short time compared with time scales for diffusion (τ_{diff}~ days, to be discussed in Chapter 4) so that the plasma observed at 1120 (4.96 R_J) was probably fairly close to thermodynamic equilibrium.

To interpret the spectra obtained in the outer part of the torus where the spectral peaks overlap it is necessary to assume something about the thermal state of the plasma. As discussed in part (d) of Chapter 1, two extreme assumptions were used: the different ionic species were assumed to either have the same temperature or have a common thermal speed. Figure 10 shows the radial temperature profile determined from fitting the data to the two models. In the case of the common thermal speed model, the temperature plotted in Figure 10 is the average temperature of all the ions when the A/Z^*=16 peak is taken to be either all S^{2+} or all O^+ ions. The

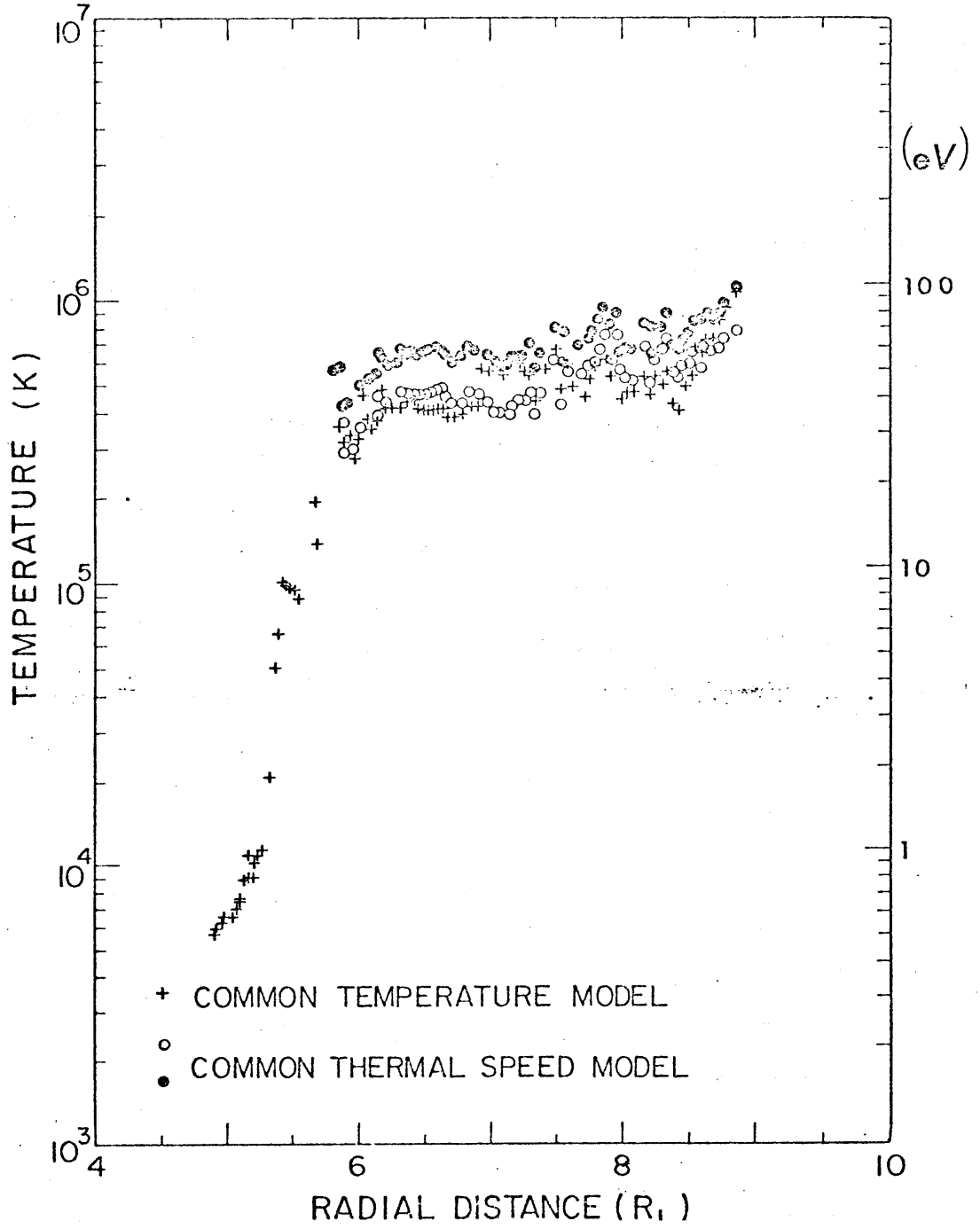

Figure 10. Radial profile of ion temperature derived from fits to the positive ion energy per charge spectra. The +'s are from the fits where the ions are assumed to have the same temperature. With the common thermal speed model the average ion temperature has been calculated assuming the $A/Z^+ = 16$ spectral peak to be all S^{2+} (o) or all O^+ (●).

different thermal models produce only 50% range in temperature which does not significantly affect the conclusions.

The outer torus had a fairly constant temperature of (6 ± 1.5) x 10^5 K (~50 eV), considerably less than what would be expected if the initial gyro-speed of the ions was equal to the full corotational value (e.g., sulphur and oxygen ions at 6 R_J would pick up initial gyro-energies of 540 and 270 eV respectively which, if there were no losses, would result in a plasma with a temperature of 180 to 360 eV after sufficient collisions. The temperature slowly increased with distance from Jupiter in the inner magnetosphere to a value of 8x10^5 K at 9 R_J. Further out in the middle magnetosphere the temperature at mid latitudes (> 10°) continued to gradually increase with radial distance. However in the equatorial plasma disc the temperature dropped to values of ~10 eV which are less than the temperatures in the outer torus (McNutt et al., 1981).

As the spacecraft moved inward through the torus, the temperature decreased sharply inside 5.7 R_J dropping by a factor of ~50 to less than an eV. This sharp transition is the division between the inner (cold) torus and the outer (warm) torus and occurs in the same region that the local plasma density decreased by a factor of 5.

(biii) Bulk Motion

In fitting the positive ion spectra, it is necessary to assume either a bulk flow or a particular composition. In the cold inner torus, assigning the three main peaks A/Z^* ratios of 8, 16, and 32 suggests the ions had the same average component of velocity into each sensor to ~1% and that value was within 1% of the value expected for corotation (cf. Fig. 6). Since all three cups of the main sensor collected large fluxes at this

time, the components of the bulk velocity of the plasma into each cup can be combined to construct the velocity vector of the plasma flow.

First of all the velocity components derived for each peak separately are compared so that any spacecraft charging effects can be removed. These effects are very small and are discussed in Appendix I. The three velocity components derived from a simultaneous fit to the spectra in the 3 main sensors (A, B and C) are then transformed into the corotating reference frame by subtracting the velocity of the spacecraft in that frame. This velocity vector can then be compared with the local magnetic field direction as measured by the magnetometer on Voyager (Ness et al., 1979). Table 2 shows the parallel and perpendicular components of the residual velocity with respect to the magnetic field for two measurement times in the inner torus.

Figure 11 shows simultaneous fits to spectra from the three main sensors at (a) 1120 UT (4.95 R_J) and (b) 1016 UT (5.28 R_J). The spectra at 1016 UT were the first to show well-resolved peaks and the value of -0.059 km s^{-1} for $V_{\perp 2}$ shows that the plasma was corotating to better than one percent. In this corotating frame there was a small field aligned southward flow of ~1.4 km s^{-1} and a smaller flow radially inward of ~0.9 km s^{-1}. Very similar velocity components were found at 1120 UT when the spacecraft was well inside the cold inner torus. The two values for the radial flow suggest the plasma takes 22 to 30 hours to move 1 R_J. This is consistent with the inward diffusion rates derived by Richardson et al. (1980) which are discussed in Chapter 4.

In contrast to the corotating cold inner torus inside of 5.7 R_J, there are several well resolved peaks in the energy per charge spectra observed outside the torus at radial distances greater than ~12 R_J, which could not

Table 2

Time UT	Distance R_J	V_c (Corotation) km s^{-1}	Velocities in the corotation frame of reference					
			$V_{\parallel}$ km s^{-1}	$V_{\parallel}/V_c$	$V_{\perp 1}$ km s^{-1} (~radial)	$V_{\perp 1}/V_c$	$V_{\perp 2}$ km s^{-1} (~azimuthal)	$V_{\perp 2}/V_c$
1016	5.28	66.3	1.388	2.1%	-0.913	-1.3%	-0.059	-0.09%
			±0.041		±0.011		±0.009	
			2.9%		1.2%		15%	
1120	4.95	62.1	1.653	2.7%	-0.669	-1.1%	-0.120	-0.2%
			±0.075		±0.042		±0.024	
			4.5%		6.2%		20%	

$V_{\parallel} = \vec{V} \cdot \hat{B}$

$V_{\perp 1} = \vec{V} \cdot (\hat{R} \times \hat{B})$ - close to radial

$V_{\perp 2} = \vec{V} \cdot (\hat{B} \times (\hat{R} \times \hat{B})$ - close to azimuthal

$V_{corotation} = 12.551\ |R| \cos$ (Jovigraphic Latitude)

= Difference between corotating and "inertial" frames

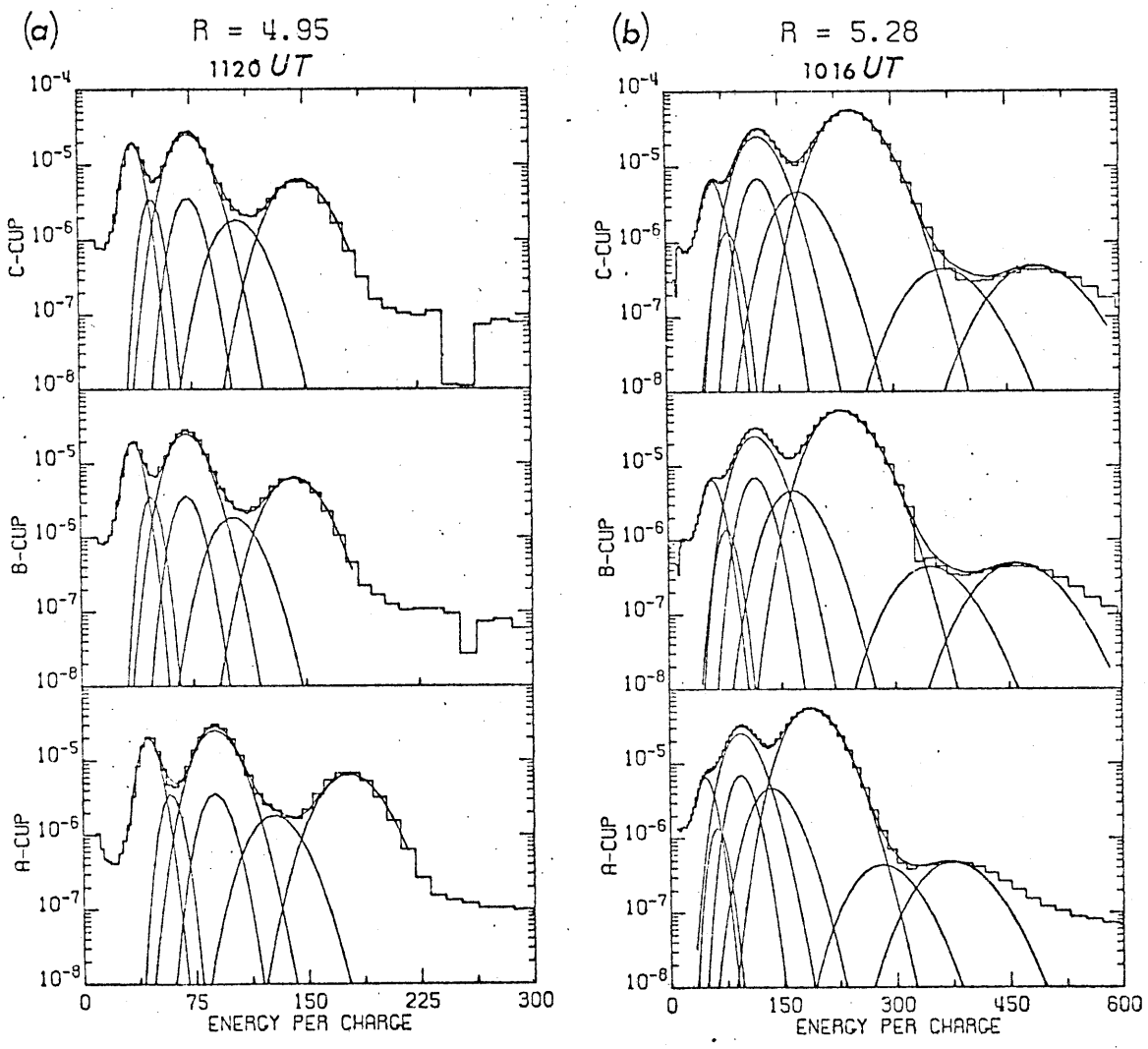

Figure 11. The energy per charge spectra for the A, B and C cups at (a) 1120 UT (4.95 R_J) and (b) 1016 UT (5.28 R_J). The three spectra for each measurement time have been fitted simultaneously to determine the bulk velocity (Table 2), temperature and density (Table 3) of the multi-species plasma.

be associated with any reasonable combination of A/Z^* values if the plasma is taken to be corotating (Sullivan and Bagenal, 1979; McNutt et al., 1979; McNutt et al., 1981). Figure 12 shows the last high resolution spectrum with well resolved peaks which was observed at 11.8 R_J, well before the spacecraft entered the torus. A consistent assignment of A/Z^* ratios of 1, 8, $10^2/3$, 16, 23 and 32 indicates the plasma is moving at about 80% of the corotational speed. Therefore, the assumption of full corotation of the plasma must break down somewhere between 5.4 and ~12 R_J.

Between 5.5 and 9 R_J where the energy per charge spectra of the positive ions are dominated by a single broad peak in F_p, it is not possible to determine independently both composition and bulk speed. In the fits to data taken in this region (cf. Figure 7), the plasma has been assumed to be corotating and the bulk speed was not a parameter of the fit.

(biv) Composition

The determination of ionis composition from the plasma data is a complicated process. The results are summarised at the end of the section. Throughout the inner magnetosphere there is considerable variation in the relative abundances of the different ionic species that comprise the positively charged component of the plasma. The spectra in Figure 8 illustrate the varied nature of the plasma in the inner magnetosphere. For example, in the inner part of the torus a comparison of the spectrum in Figure 13 taken at 4.96 R_J with the spectrum in Figure 6 taken at 5.3 R_J shows the considerable variation in composition in the region. The variability in relative abundance is less evident in the outer torus and further out in the plasma sheet of the middle magnetosphere. In the cold torus the composition is largely determined by the relative heights and positioning

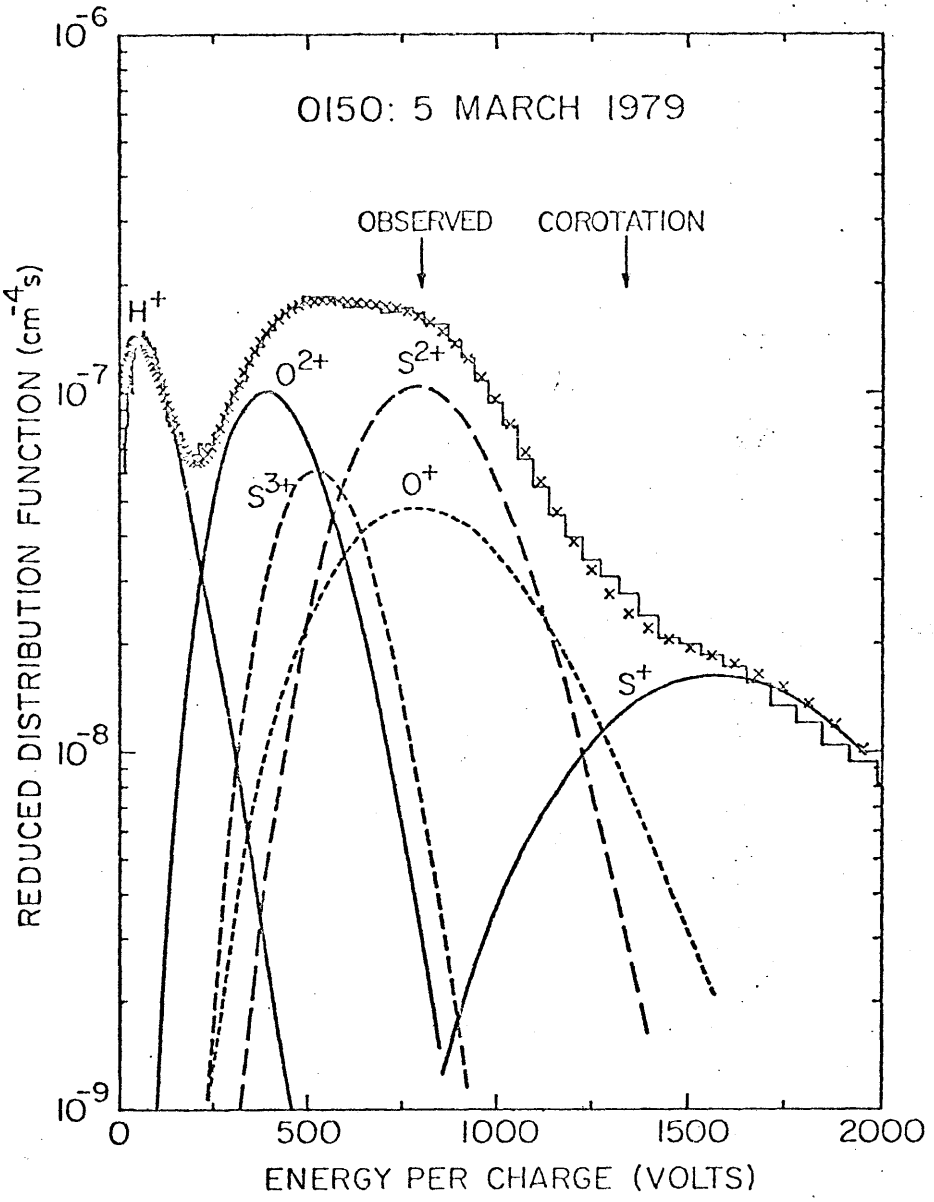

Figure 12. The energy per charge spectrum in the D-cup (side sensor) at 0150 UT, 5 March 1979 (11.6 R_J). The position of the observed spectral peak due to ions with A/Z =16 (shown by the arrows) is at considerably lower energy per charge than that expected for a bulk velocity corresponding to rigid corotation. The data are shown as a histogram and the fit to the current in each measurement channel is shown by x's. The individual Maxwellian distributions of each ion included in the reduced proton distribution function of the fit are shown by the curved lines.

of the well-resolved peaks. In the warm torus where the spectral peaks are unresolved the composition is constrained by i) consistency with composition in other regions, ii) observations of ultraviolet and optical emissions.

The more straightforward situation in the cold torus will be considered first. Table 3 shows the densities of different ionic species at 4.96 and 5.28 R_J from fits to the spectra shown in Figures 6 and 13 respectively. The spectrum at 5.28 R_J was made in the densest part of the cold torus and shows that S^+ is by far the dominant ion. The A/Z^*=16 peak is predominately due to O+ ions rather than S^{2+} and there is some O^{2+} which produces the small emerging peak at the low energy end of the spectrum. There is a distinct peak at A/Z^*=64 corresponding to 14 cm^{-3} of SO_2^+ ions but they comprise less than 1% of the total positive ion number density.

The spectrum made a little later at 1120 and shown in Figure 13 shows that S^+ ions have become less important, O^+ ions are the most abundant at this point and the O^{2+} peak has become quite distinct. As the spacecraft moved in to its closest approach to Jupiter the A/Z^*=8 peak grew until O^{2+} ions had the highest local density while the S^+ peak at A/Z^*=32 subsided until it was little more than a shoulder.

The existence of resolved spectra at radial distances larger than 12 R_J and smaller than 5.3 R_J suggests that the broad spectral feature observed in the warm torus between 5.3 and 12 R_J consists of the sum of peaks corresponding to a similar set of ionic species. If the single peak in the outer torus did in fact correspond to just one corotating ionic species, then it would have an A/Z^* ratio of ~14 and a temperature of ~150 eV. However, the total distribution is poorly represented by a single

Table 3

Cold Torus Composition

TIME	R(R_J)	O^{2+}	S^{3+}	S^{2+}	O^+	Na^+	S^+	SO^+	SO^{2+}	T^+
64 1120	4.95	45 (.7)	5.0 (.5)	11 (5)	220 (10)	20 (2)	82 (1)			0.39 (.006)
64 1016	5.28	24 (1.5)	3.2 (1.2)	37 (8)	370 (20)	82 (6)	1170 (5)	11 (3)	14 (2)	1.09 (.005)

Ion densities are in cm^{-3}.

The numbers in parentheses are standard errors from the least-squares fit to the spectrum.

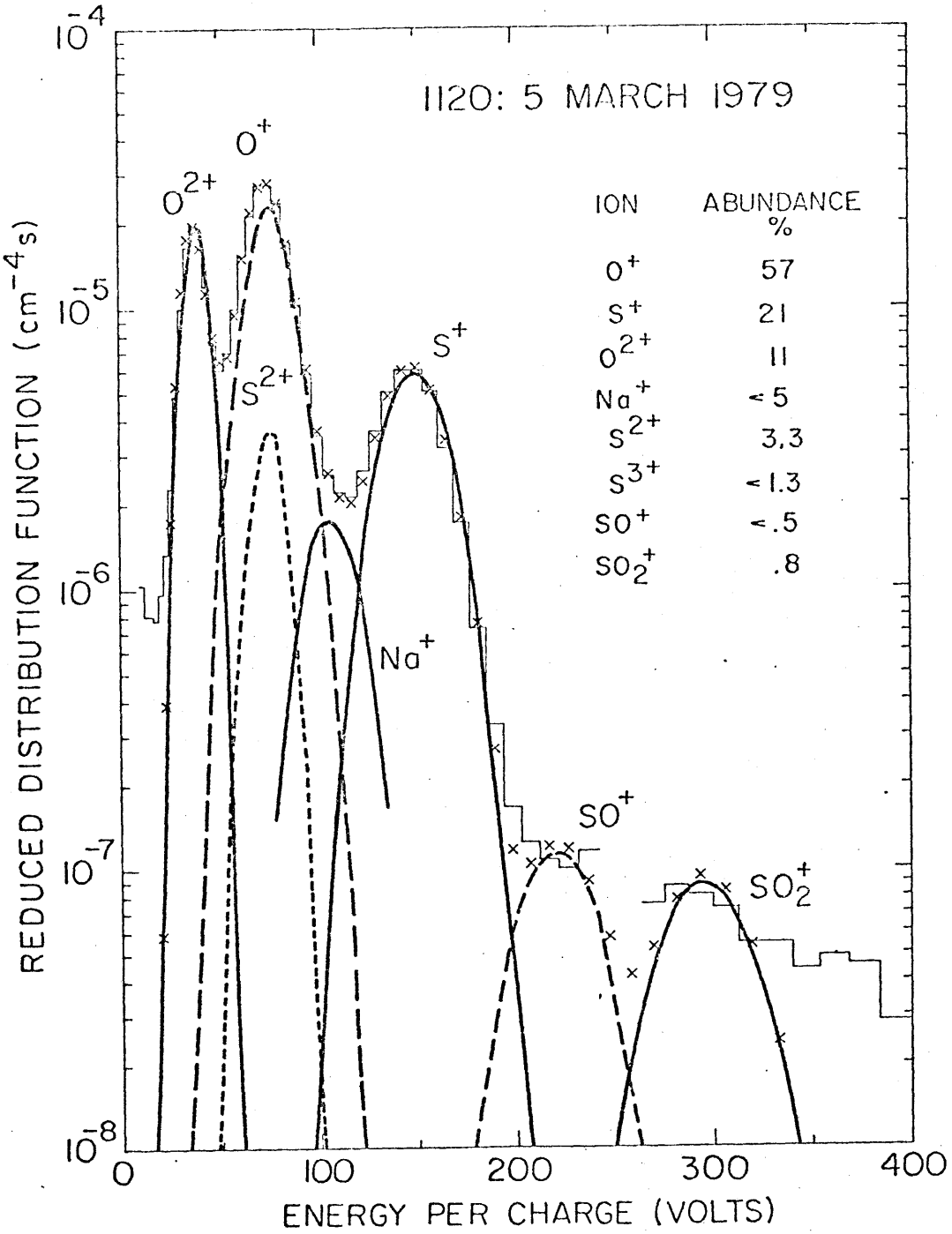

Figure 13. The energy per charge spectrum made in the C-cup at 1120 UT, 5 March 1979 (4.95 R_J). The data are shown as a histogram and the fit to the current in each measurement channel is shown by x's. The individual Maxwellian distributions of each ion that make up the reduced proton distribution function of the fit are shown by the curved lines.

Maxwellian function. Therefore is had been assumed that the spectra in the warm torus consist of a superposition of overlapping Maxwellian peaks corresponding to ions with A/Z^* ratios of 8, $10^2/3$, 16 and 32. This is probably quite a reasonable assumption at the lower end of the spectrum. At higher energies there is evidence (see section 3(d)) of a considerable contribution to the specturm from ions with a non-Maxwellian distribution function. Consequently, the density of ions with higher energies (particularly S^+ ions at $A/Z^* = 32$) are probably overestimated in the present analysis.

Preliminary analyses of the ultraviolet emission spectrum measured by the Voyager UVS experiment suggested that in the warm torus there were few O^+ ions (Broadfoot et al., 1979; Shemansky, 1980). Therefore the ambiguity of the $A/Z^*=16$ peak in the plasma spectra was initially avoided by taking the peak to be entirely due to S^{2+} ions and assuming any contributions due to O^+ ions to be insignificant.

In the early analysis of the ion plasma data the simplest case was considered with the plasma assumed to be fully corotating and the spectrum from only one cup analysed at a time. Figure 7 shows the spectrum at 0859 UT (5.93 R_J) which has been fitted in this way with the added assumption that the ions have either a common (a) temperature, (b) thermal speed. The results of these fits are given in the first two rows of Table 4. With the isothermal model S^{2+} is the most abundant ion though there are also large quantities of S^+ ions. There are few S^{3+} ions and only a moderate amount of O^{2+} ions. The common thermal speed model produces similar results except S^{3+} ions replace any O^{2+} ions so the composition is essentially entirely of sulphur ions. Despite the fact that the fit to the data appears to be pretty good the resolution matrix shows the composition is

Table 4

Composition of Warm Torus

TIME	R (R_J)	$\Phi_{S/C}$ (VOLTS)	THERMAL STATE	O^{2+}	S^{3+}	S^{2+}	O^+	S^+	SO_2^+	$\bar{T}^\dagger$	χ^2
64 0859	5.93	0	§ T	162 (11)	43 (9)	606 (7)		446 (14)	50*	32.7 (.4)	12
			§ W	8.7 (12)	163 (15)	613 (13)		391 (24)	50*	42.1 (.6)	25
		0	T	115 (45)	83 (36)	632 (13)		490 (30)	50*	3.50 (1.2)	96
			W	0 (18)	210 (22)	605 (18)		456 (26)	50*	43 (.8)	98
		-15	T	160 (18)	196 (16)	467 (11)		382 (18)	50*	46.8 (.6)	65
		-15	T	126 (82)	208 (79)	263 (21)	300*	336 (40)		45.9 (2.1)	67
			W	0 (51)	471 (77)	301 (73)		393 (47)	50*	58.2 (2.0)	119
		-30	T	350 (60)	208 (71)	263 (44)		336 (18)	50*	54.0 (2.1)	78
64 0808	6.56	0	T	99 (23)	49 (19)	342 (8.2)		229 (19)	50	46.4 (14)	104
			W	0 (4)	129 (4)	330 (5)		215 (10)	50*	58.0 (6)	100
		-8	T	131 (5)	53 (3)	305 (4)		218 (8)		50.3 (.5)	78
		-15	T	152 (30)	70 (30)	268 (11)		195 (19)	50*	55.1 (1.9)	72
			W	-40 (30)	279 (45)	152 (45)		205 (37)	50*	75.6 (2.6)	119

Numbers in parentheses are standard errors. Ion densities are in cm^{-3}.

†Average temperature. T-Isothermal model. W-Common thermal speed model. *-Fixed density.

§-Fit to data for one sensor only. The remaining fits used the data from all three main sensors.

poorly constrained.

The corotating plasma flowed into the three cups of the main sensor at slightly different angles so that the position of the various spectral peaks differ from cup to cup. Therefore a simultaneous fit has been made to the three spectra assuming corotation, a common temperature or thermal speed and a single set of ion densities in the hope that the additional information will constrain the composition.

The left panels of Figures 14 and 15 show simultaneous fits to the 0859 UT spectra for the two thermal models. The results are tabulated on rows 3 and 4 of Table 4. The fit to the data does not appear as good as for only one cup which suggests that to model the ion distribution function with Maxwellian functions and a simple common thermal state is inaccurate (i.e. the good fit to a single spectrum was misleading). However, a comparison of the results of fitting single versus multiple cups shows that both analyses indicate basically the same composition with some minor changes at lower energies.

An additional concern when considering the composition in the warm torus is the question of spacecraft charging (see Appendix II). When the spacecraft becomes charged it is no longer at the same electrostatic potential as the surrounding plasma so that the channel voltages are correspondingly shifted. In the warm torus a comparison of the electron and positive ion charge densities suggest the spacecraft was at a potential of about -15 volts with respect to the surrounding plasma. The voltage shift due to a spacecraft potential is the same for all sensors so each spectrum appears displaced by a constant amount. The expected positions of spectral peaks for different ions are fixed for each cup but varies between cups according to the angle that the plasma flows into the cup. Therefore

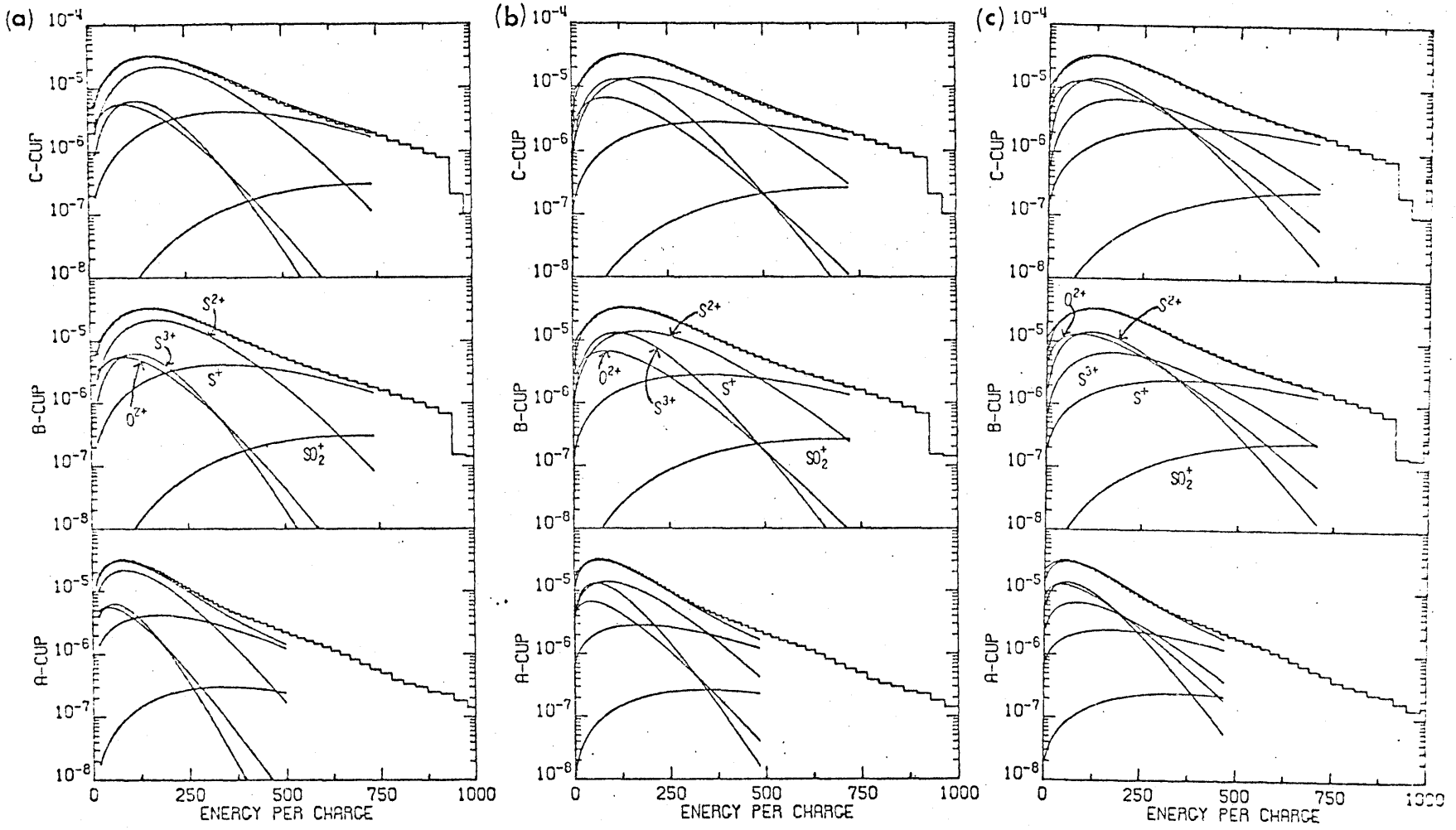

Figure 14 - The energy per charge spectra for the A, B, and C cups at 0859 UT (5.93 R_J) which have been fitted simultaneously when the spacecraft potential has been set at (a) 0 volts, (b) -15 volts and (c) -30 volts. The ions were assumed to be corotating and have the same temperature in all three cases. The density of SO_2^+ ions was set at 50 cm^{-3}.

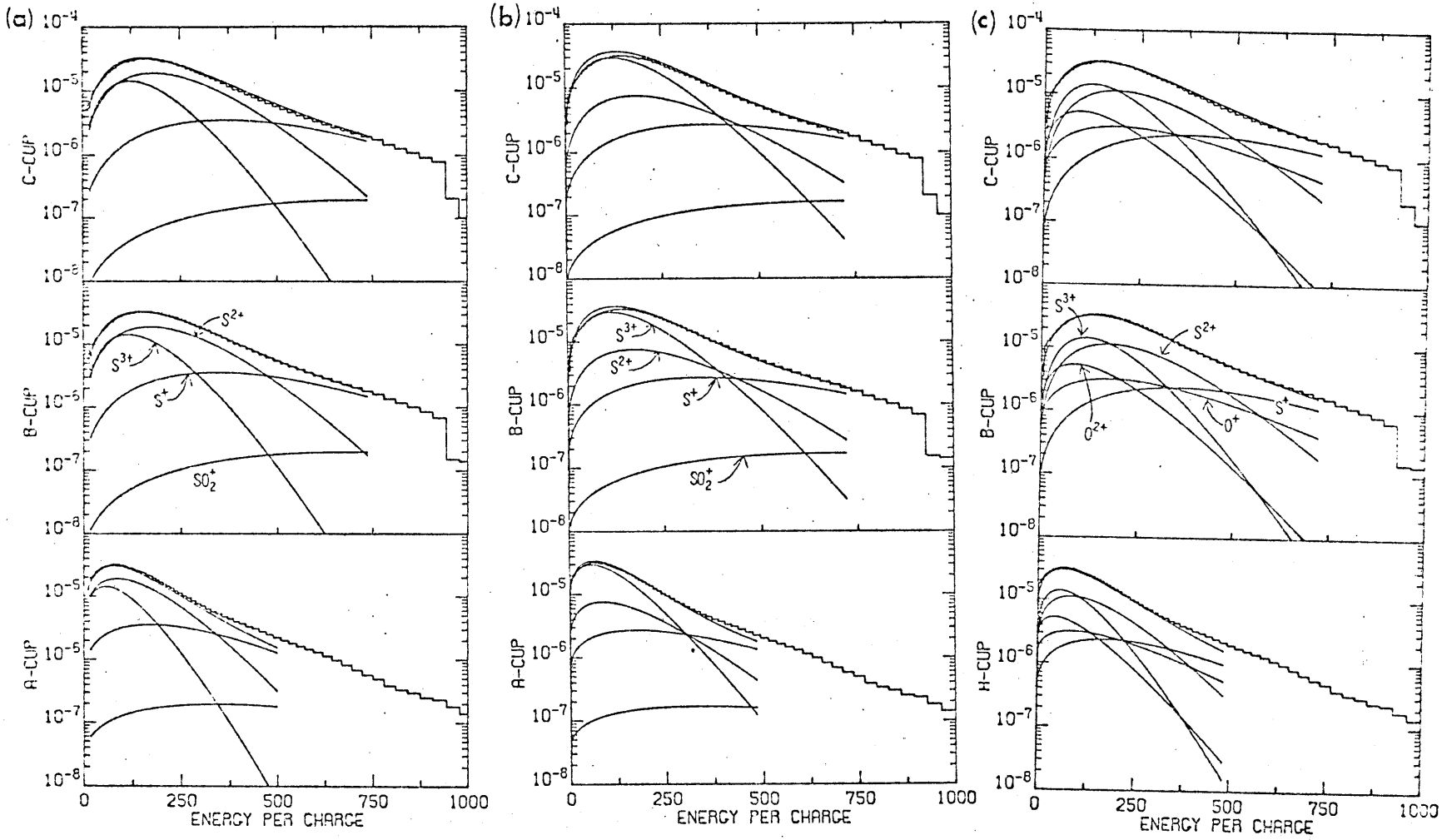

Figure 15. The energy per charge spectra for the A, B and C cups at 0859 UT (5.93 R_J) which have been fitted simultaneously under different assumptions. The assumptions were (a) the ions have a common thermal speed and the spacecraft has a zero potential; (b) the ions have a common thermal speed and the spacecraft has a potential of -15 volts; (c) the ions have a common temperature, the spacecraft potential is set at -15 volts and the density of O^+ ions is set at 300 cm^{-3}. The plasma assumed to be corotating in all three cases.

comparing the goodness of fit when the spacecraft potential is set at different values should give some indication of both the spacecraft charge and the plasma composition.

Figure 14 shows fits to the data under isothermal conditions when the spacecraft is assigned a potential of (a) 0 volts (b) -15 volts and (c) -30 volts. The resulting fit parameters are given in Table 4. The effect of shifting the spectrum to lower energies due to the increasingly negative potential is to increase the amount of ions with low values of A/Z^* and decrease the amount of ions with higher A/Z^*. Thus O^{2+} becomes the dominant ion at -30 volts. The best fit is obtained at -15 volts and fits at -10 and -20 volts support this estimate of the spacecraft potential for 0859 UT. The fits made under the assumption that the ions have a common thermal speed (Fig. 15(a) and (b)) do not improve when the spacecraft is given a negative potential. If O^{2+} ions are included in the fit their density is driven to negative values. The remaining ions are then just the first three ionisation states of sulphur. With larger negative spacecraft potentials S^{3+} becomes the dominant ion.

An analysis of the ultraviolet spectrum, recently published by Brown et al. (1981), suggests that there may well be a considerable density of O^+ ions in the warm torus, contrary to the earlier conclusions of Broadfoot et al. (1979) and Shemansky (1980). The justification for these disparate conclusions is discussed in Chapter 4. In view of these results, the third panel in Figure 15 shows an isothermal fit to the 0859 UT spectrum where the density of O^+ ions was fixed at a value of 300 cm^{-3} and the spacecraft charge was set at a value of -15 volts. The fit to the data is as good as in Figure 14 (b) where the $A/Z^* = 16$ peak was assumed to be all S^{2+}. The effect of including O^+ ions is mainly to reduce the density of S^{2+} and, to

a lesser extent, S^+ and O^{2+} ions.

At the bottom of Table 4 are the results of fitting spectra made at 0801 UT at 6.56 R_J. This was the furthest distance at which the flow angle into all three main sensor cups was less than 60° so all three spectra can be fitted simultaneously. At this distance the total density is less than at 5.93 R_J but the composition appears to be very similar. Again the fit improves if the spacecraft is given a negative potential though, because of the lower density of the plasma the potential is probably less than 15 volts in magnitude.

The discussion above has been confined to the ionic species that dominate the plasma in number density. There is also evidence for various minor species. Sometimes there is a resolved spectral peak such as the proton peak in Figure 11; the SO_2^+ peak in Figure 6; or the Na^+ peak in Figure 12. At other times, the minor species may produce a shoulder on the edge of a spectral peak (for example SO_2^+). In addition, upper limits can be put on the densities of ions which come between two resolved spectral peaks as illustrated for Na^+ and SO^+ in Figure 6. When fitting a gap in a spectrum between two peaks, the minor ionic species is chosen for its plausibility. An upper limit for the density of a different ionic species with a similar A/Z^* ratio could be determined in a similar way.

In the middle magnetosphere protons comprise up to ~30% of the number density, their importance increasing with distance away from the plasma sheet (McNutt et al., 1981). In the inner magnetosphere the kinetic energy of protons is generally insufficient to produce measurable fluxes above the energy per charge threshold of the plasma instrument. However, there are a few spectra before closest approach (where the cold plasma flows directly into one of the cups) with a feature below the well-resolved $A/Z^* = 8$

spectral peak which might be the tail of a distribution function in the lowest channels. If this feature corresponds to either H^+ or He^{2+} ions with the same temperature as the heavy ions then a fit to the data gives density estimates of ~16 or 1.8 cm^{-3} respectively. This is about 3% or 0.4% of the total ion number density. These values should be regarded with caution because the density is estimated from the tail of the distribution since the data does not include the peak.

There is often a well-defined spectral peak corresponding to $A/Z^*=64$ (Figure 6) which is probably SO_2^+ (or maybe S_2^+ which has the same A/Z^* ratio). Fitting the $A/Z^* = 64$ peak at 5.3 R_J produces a density of ~13 cm^{-3} which is <1% of the ion population. When the plasma becomes too hot for separate spectral peaks, then the density of SO_2^+ ions has been arbitrarily set at a value of 50 cm^{-3} (about 4% of the total ion density) because it is not possible to separate the contribution of SO_2^+ ions from the other factors contributing to the high energy region of the spectra. Filling the gap between the S^+ and SO_2^+ peaks in the 1016 UT spectrum (Figure 6) produces an upper limit of 8 cm^{-3} (~0.5% of the ions) for SO^+.

Finally, it should be noted that the upper limits on the densities of minor species discussed above are speculative and some of these spectral features could well be due to alternative minor ionic species to those suggested or due to non-Maxwellian components in the distribution of the major ions.

Table 5 gives a summary of the composition of the positive part of the plasma found in the cooler regions of Jupiter's magnetoshere, i.e., the Io torus and the middle magnetosphere plasma sheet. Typical plasma parameters are given for the cold torus (5.3 R_J), the warm torus (5.9 and 6.6 R_J) and five of many places in the middle magnetospere plasma sheet where well-

Table 5 - Summary of Posivite Ion Parameters in the Torus and Plasma Sheet Regions of Jupiter's Magnetosphere

	TIME (UT)	R (R_J)	$\phi_{s/c}$ (VOLTS)	THERMAL MODEL	O^{2+}	S^{3+}	S^{2+}	O^+	Na^+	S^+	H^+	V/V_c	$\bar{T}$ (eV)
					(Density, cm^{-3})								
COLD	64 1016	5.3		T	24	3	37	370	82	1170		0.999	1.1
WARM	64 0859	5.9	-15	T	160	200	470			380		1*	47
			-15	T	130	210	260	300*		340		1*	46
PLASMA SHEET	64 0150	12		T	1.5	0.6	2.2	(2.9)†		1.4	2.2	0.77	23
	63 2323	13		W	.81	.87	2.5	(4.9)†	.52	.61	.18	0.78	21-28
	63 1551	20		W	.09	.11	.35	(.70)†	.11	.06	.18	0.76	16-22
	63 0609	27		W	.07	.05	.18	(.36)†	.03	.04		0.48	6-9
	62 1035	41		W	.04	.04	.13	(.26)†	.03			0.43	16-25

†The A/Z* peak at 16 is normally taken to be S^{2+} outside the cold torus. The values for the density of O+ given here are from assuming the A/Z* is in fact all due to O+.

*Fixed parameter in fit procedure

T = Common temperature for all ions

W = Common thermal speed for all ions

$\bar{T}$ = Average temperature. A range of values are given for the common thermal speed model according to the A/Z* = 16 peak being either all S^{2+} of all O^+.

resolved spectral peaks allow a determination of composition. From the warm torus outwards the composition remains fairly constant with the dominant ions being some combination of O^+ and S^{2+} at $A/Z^* = 16$. Next come O^{2+}, S^{3+} and S^+ with roughly the same degree of importance though the relative abundance of S^{3+} and O^{2+} varies with assumptions about the thermal state of the plasma.

In the cold inner torus the composition is significantly different. When the composition is averaged over the inner region the ions are largely of lower ionisation states. The dominant ion is S^+ accompanied by O^+ ions while there are few ions of higher ionisation states (S^{2+}, S^{3+}, O^{2+}).

c) Spatial distribution of plasma

A two-dimensional model of the torus can be constructed from the in situ density measurements made along the spacecraft trajectory by assuming the distribution of plasma along the magnetic field lines. Warwick et al. (1979) took the electron densities determined from radio data (PRA experiment) obtained on both inbound and outbound legs of the trajectory and drew contours of constant density in a meridional plane by assuming the torus to be symmetric both azimuthally and about the magnetic equator. In a preliminary analysis of the plasma data (Bagenal et al., 1980) the ion temperature determinations from inbound measurements were inserted into a simple expression for an exponential scale height distribution so the in situ ion density measurements could be extrapolated along dipolar magnetic field lines. Azimuthal symmetry was again used with mirror symmetry about the centrifugal equator to construct meridional contour maps of ion and electron densities. In the more detailed analysis presented here (and in Bagenal and Sullivan, 1981) the azimuthal symmetry assumption has been

PAGES (S) MISSING FROM ORIGINAL

69

section of the torus. The surface includes the inbound spacecraft trajectory and the dipole magnetic field line associated with the location of the spacecraft at the time of each measurement. This surface is very similar to a meridional plane. It is a little distorted because the dipole tilt varied with the time (and radial distance) of the measurements. The resulting contour map of total charge density on this surface is shown in Figure 16 as a plot of density as a function of radial distance from the center of Jupiter and distance from the centrifugal symmetry surface (centrifugal equator). The apparent asymmetry about the centrifugal equator occurs because the angle between the magnetic and centrifugal equators varied along the spacecraft trajectory. While both the inbound and outbound trajectories of the spacecraft are shown, the map is based solely on data obtained on the inbound pass. Data from the outbound pass is discussed in the last section of this chapter.

(ci) Torus Structure

Outside the torus (>7.5 R_J) the plasma had a fairly uniform low density of ~100 cm^{-3}. As Voyager 1 moved radially inwards, the density rapidly increased as the spacecraft entered the torus (at ~7.5 R_J) from below the centrifugal equator. After crossing the equator at ~7.1 R_J, the spacecraft remained less than 0.15 R_J above it and traversed the core of the warm torus, passing over the small region of the maximum torus density (~3000 cm^{-3}) at 5.8 R_J which corresponds to the sharp spike (2) in the *in situ* density profile (Figure 9). The plasma in the outer part of the torus was warmer and hence spread away from the equatorial maximum with an effective exponential scale height of ~1 R_J. Inside the sharp temperature drop at 5.7 R_J the plasma was cold and hence closely confined to the

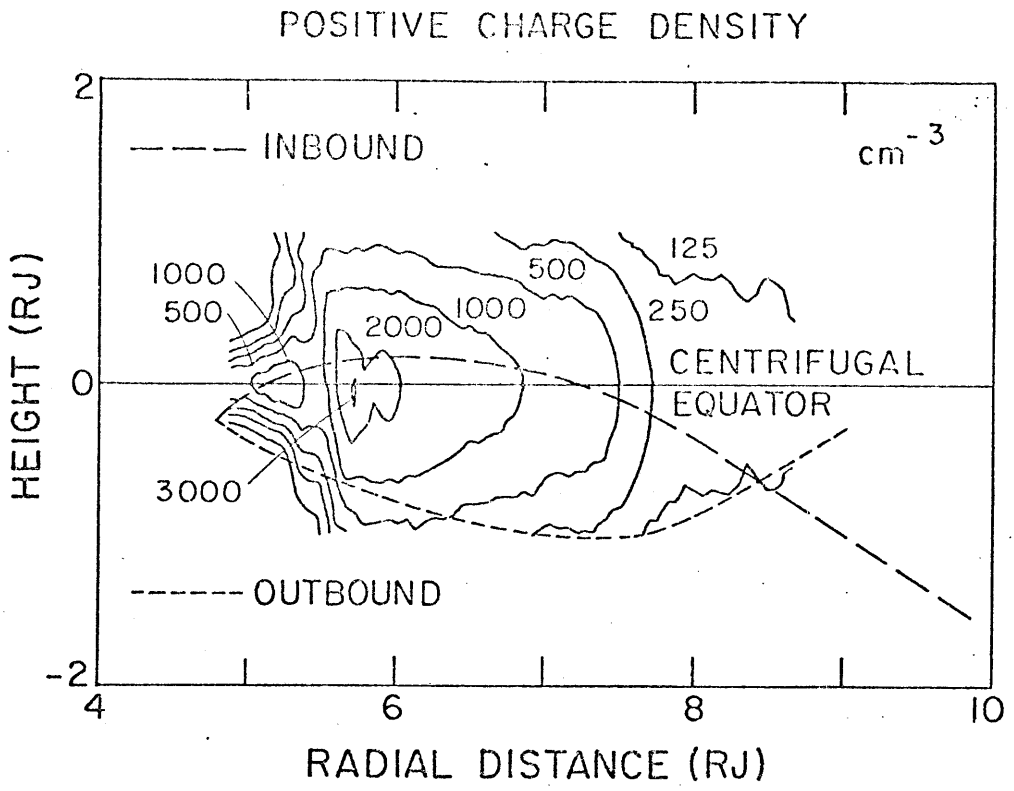

Figure 16. Contour map of positive charge density as a function of radial distance from the center of Jupiter and height from the centrifugal equator. The map has been constructed from plasma measurements made along the inbound spacecraft trajectory (---) by using a theoretical expression for the distribution of plasma along dipolar field lines (Appendix III). The contours are in units of cm^{-3}.

centrifugal equator with an effective scale height of <0.2 R_J. The centrifugal equator was crossed again in the locality of the local density maximum in the inner torus at ~5.3 R_J (3).

The *in situ* charge density (Figure 9) dropped rapidly as the spacecraft moved inside the density maximum at 5.3 R_J. However, as illustrated in Figure 16, this sharp density drop is largely due to the spacecraft's increasing southerly latitudes. Because of the small effective scale height in the cold torus the spacecraft did not have to go far from the centrifugal equator to see a large change in density. The decrease in measured density was not totally a latitude effect as the equatorial density drops markedly inside 5.3 R_J. Figure 17 shows a comparison of the radial profile of charge density along the centrifugal equator (from Figure 16) with the charge density measured at the location of the spacecraft on its trajectory.

The two-part nature of the plasma torus is apparent in Figure 16 and in the radial profiles of charge density and ion temperature (Figure 10). Between the two parts of the torus, the spacecraft passed through a transition region where there was a sharp temperature gradient of $\sim 7 \times 10^5$ K R_J^{-1}. The transition region around 5.5 R_J is one of the three regions where whistler mode plasma waves were observed by the Voyager 1 Plasma Wave Science (PWS) experiment (Gurnett *et al.* 1979). The other two regions were at ~6 R_J on both inbound and outbound legs of the trajectory. The measured frequency dispersion of the whistlers is largely determined by the density of electrons in the plasma through which these waves have propagated. Gurnett *et al.* (1981) conclude that the dispersion of these whistlers suggests there are considerably more electrons between the point of measurement and the source of the whistlers in the ionosphere of Jupiter

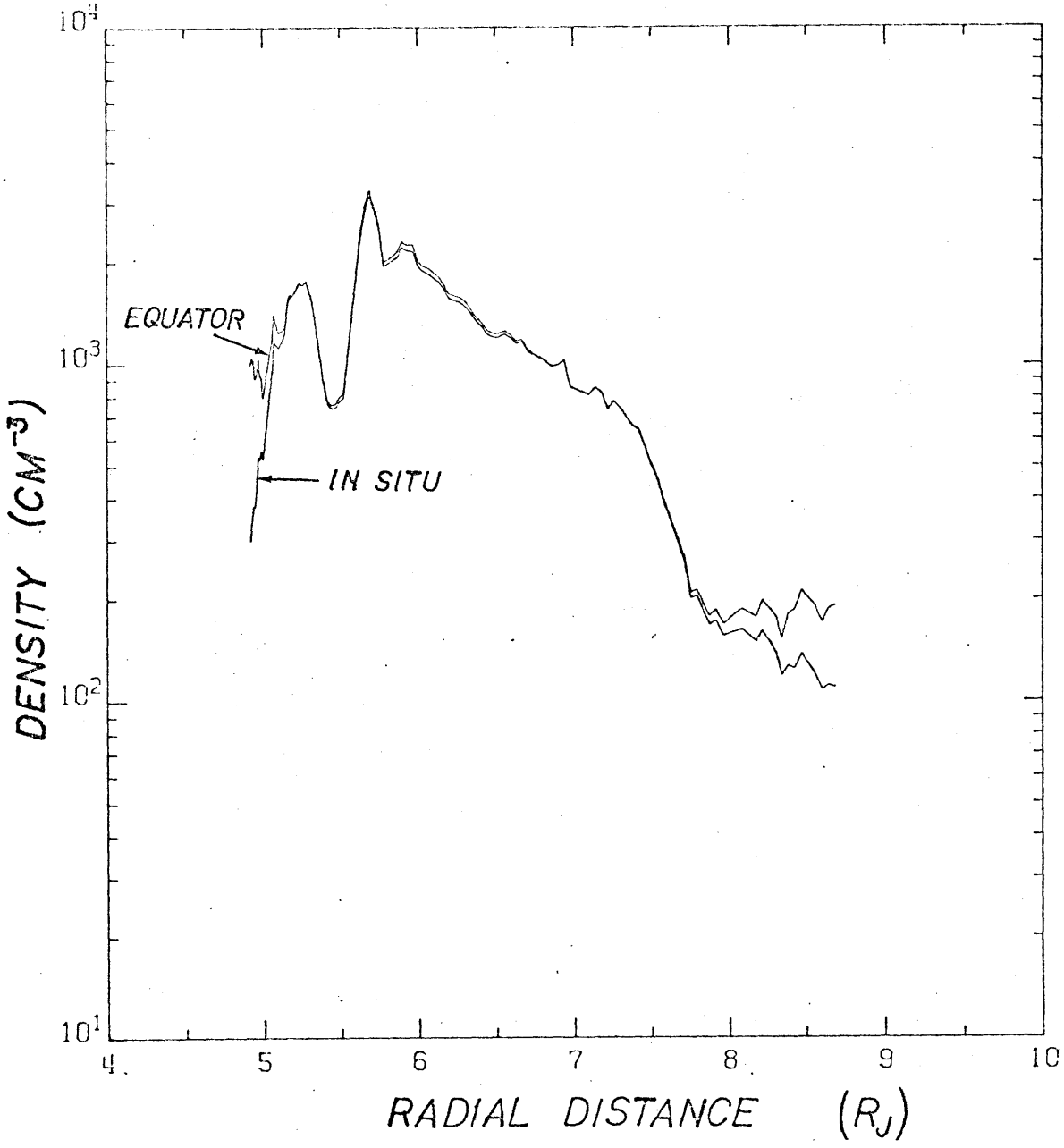

Figure 17. Radial profile of charge density. The in situ plasma measurements (illustrated by the lower curve) have been extrapolated using the theoretical expressions in Appendix III for the distribution of plasma along a magnetic field line to determine the total positive charge density at the centrifugal equator (the upper curve).

than are accounted for by the model of the torus discussed above. If there are additional electrons, they could be associated with light ions such as protons which would not be as closely confined to the centrifugal equator as the heavy ions. These light ions would have larger effective scale heights so that they would form a small proportion of the plasma near the equator (where the measured total positive charge density is very close to the electron density) but could dominate the ion composition closer to the planet. Determining the density of ions outside the torus region should give an estimate of the importance of the ionosphere of Jupiter as a source of plasma for the magnetosphere.

Although the plasma detector was less favorably oriented on the outbound traversal of the torus, considerable fluxes were measured. The individual spectra will be discussed in the last section of this chapter, but generally speaking the global structure on the outbound pass was found to be very similar to that observed inbound. Lower densities were measured during the outbound passage due to the greater distance of the spacecraft from the centrifugal equator. This effect is especially noticeable in the inner torus where the effective scale height is small.

The magnitude and location of the three local density maxima and the location of the transition region and the outer boundary are tabulated in Table 6. The local density maxima on the outbound trajectory have been found from the PRA and plasma profiles. Although the radial distances of the first and second maxima vary by 0.2 R_J between the inbound and outbound passes, the L-shells of the maxima nearly coincide when the offset of the magnetic dipole from the center of Jupiter is taken into account. If the offset of the field were neglected, then the electron densities determined by Birmingham et al. (1981) would be larger than the values along the

Table 6 - Regions of the Torus

		Time (UT)	LT	R (R_J)	λ III (°)	L-Shell centered	L-Shell offset	Ne (cm^{-3})	Experiment+	
Outer Boundary	Inbound	0630	1500	7.7	128	7.7	7.6			
	Outbound	~1700	2400	7.2	15	7.5	7.5			
Peak 1	Inbound	0902	1445	5.90	197	5.94	5.87	2160 2170	PLS PRA	
	Outbound	1445	2245	5.70	317	5.79	5.89	*1500± 50 1650	PLS PRA	
Peak 2	Inbound	0924	1600	5.69	206	5.72	5.66	3130 3500	PLS PRA	WARM
	Outbound	1420	2200	5.49	307	5.55	5.64	*1600± 50 1950	PLS PRA	
Transition Region	Inbound	0945	1630	5.5	215	5.5	5.5			
	Outbound	1400	2210	5.3	300	5.4	5.5			
Peak 3	Inbound	1016	1730	5.27	225	5.27	5.28	1740 1750	PLS PRA	COLD

*Predicted by model of torus from measurements on the inbound leg of the trajectory.
+ PLS - Voyager 1 Plasma Science Experiment.
PRA - Voyager 1 Planetary Radio Science Experiment.

outbound trajectory shown in Figure 16 by about a factor of 2 at ~6 R_J and to a lesser extent further out. The effect of including the dipole offset is to change the apparent outbound trajectory shown in Figure 16 with the result that the electron densities (Table 2) predicted from the inbound plasma data are in good agreement with those determined by Birmingham et al. (1981).

(cii) Variations in Composition with Latitude

Figure 18 shows two-dimensional density plots for three individual ionic species, S^+, S^{2+} and O^{2+} which have been constructed in the same manner as Figure 16. The in situ ion densities, which have been extrapolated along corresponding field lines to make this figure, were derived from fits to the data assuming the plasma was corotating and isothermal. The spacecraft potential was taken to be zero which means that in the warm torus the densities of O^{2+} and S^{3+} ions have been underestimated while the densities of S^+ and S^{2+} have been overestimated. The contour map for S^{3+} ions is very similar to the S^{2+} map shown here in that there are insignificant densities of S^{3+} ions in the inner torus. The contour map for O^+ is similar to that of S^+ in shape but with lower densities.

Figure 18(c) illustrates how at 5.3 R_J the minor quantity of doubly ionized oxygen present has been drawn away from the equator by the field-aligned polarization electric field that has been set up by the predominant heavy sulphur ions which are held close to the equator by centrifugal forces. The electrons are too light to be affected much by centrifugal forces so they are only constrained by electrostatic interaction with the ions. Lighter ions of higher charge state are more easily pulled off the

centrifugal equator by the electrons so their density distribution along the field lines has a larger effective scale height (the O^+ torus is thicker than that of S^+). In the more extreme case shown in Figure 18c, sufficient O^{2+} ions have been drawn along the field lines to form double maxima in their density distribution approximately 0.2 R_J away from the centrifugal equator.

The predominance of heavy ions with lower ionization state near the centrifugal equator means that the composition measured there is not typical of the whole of the torus. At greater distances from the centrifugal equator, the average ion mass number decreases and if multiply-charged ions are present the average charge state increases with distance from the equator. Thus away from the equator oxygen ions become more abundant than sulphur ions and at high latitudes protons must become the dominant ionic species as they have very large scale heights due to their low mass relative to sulphur and oxygen.

d) Non-Maxwellian spectral features

In the three-dimensional plot of the spectra from the inbound pass (Figure 8) there are a few spectral features which are of minor importance with respect to the gross properties of the plasma but may indicate some interesting phenomena. For example, the currents measured by the detectors reached the saturation level for one spectrum in two (B and C) cups of the main sensor at 0937 UT and increased by and order of magnitude in the two cups that pointed further away from the coratating flow. This single saturated spectrum shows up as a spike at 300 volts in Figure 8 (the saturated channels are not plotted). Comparison with spectra before and after 0937 UT suggests that this anomalous spectrum was due to a variation

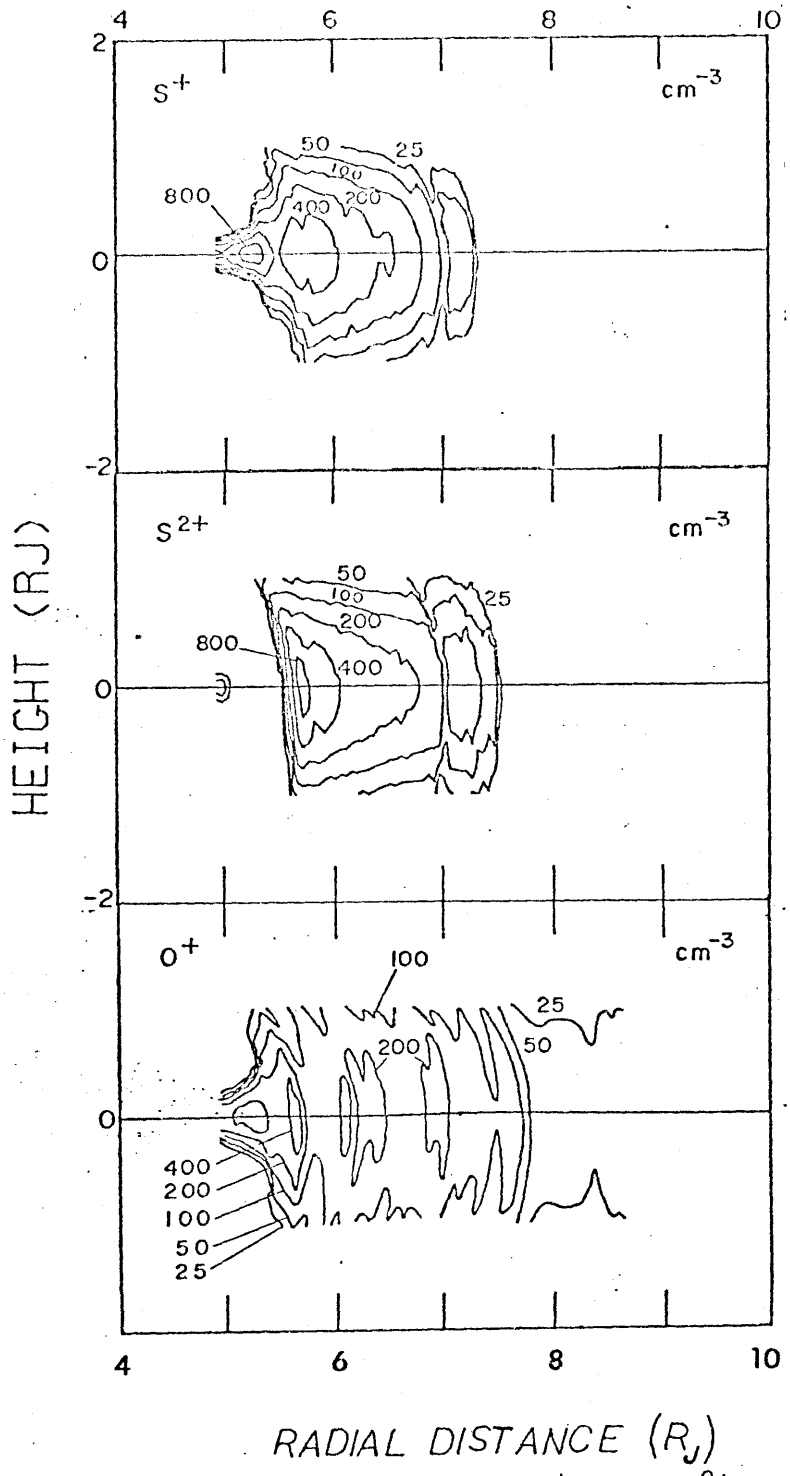

Figure 18. Contour maps of the density of (a) S^+ ; (b) S^{2+} and (c) O^{2+} ions as a function of radial distance from the center of Jupiter and height from the centrifugal equator. The maps have been constructed from plasma measurements made along the inbound spacecraft trajectory using theoretical expressions for the distribution of plasma along dipolar magnetic field lines (Appendix III). The contours are in units of cm^{-3}.

surrounding plasma, each grid spaced duration converts to a spatial scale of ~2000 km. There is no special significance in the location of the spacecraft which was at 5.6 R_J, well inside the orbit of Io at this time. There my be some clues in the electron plasma measurements and the energetic particle data for this period, but as yet the cause of this anamolous spectrum remains a puzzle.

Another interesting spectral feature is the significant particle flux that was detected throughout the inner magnetosphere at energies well above the energy of the bulk of the plasma. For example, Figure 19 shows two spectra made at 0931 UT and 1000 UT. Before 0936 UT every spectrum for all three main sensors shows large fluxes at energies of a few keV, well above the energy of corotating thermal population (a few 100 eV). Although the high energy fluxes are about three orders of magnitude less than the flux of thermal plasma, they are well above the instrument noise level (dashed lines in Figure 19a) and represent a significant non-Maxwellian tail to the distribution function. High energy tails to the distribution function are observed throughout the Jovian magnetosphere but despite considerable theoretical interest in the phenomenon the origin of these energetic particles is not understood. They could be torus particles which have been accelerated to higher energies, or particles from other regions, such as the ionosphere or outer magnetosphere, that have diffused into the torus region.

Perhaps a more puzzling question is posed by the fact that suddenly at 0936 UT the high energy tail cuts off at ~1500 eV. From 0936 UT onwards the fluxes at energies above ~1500 eV fall below the instrument threshold

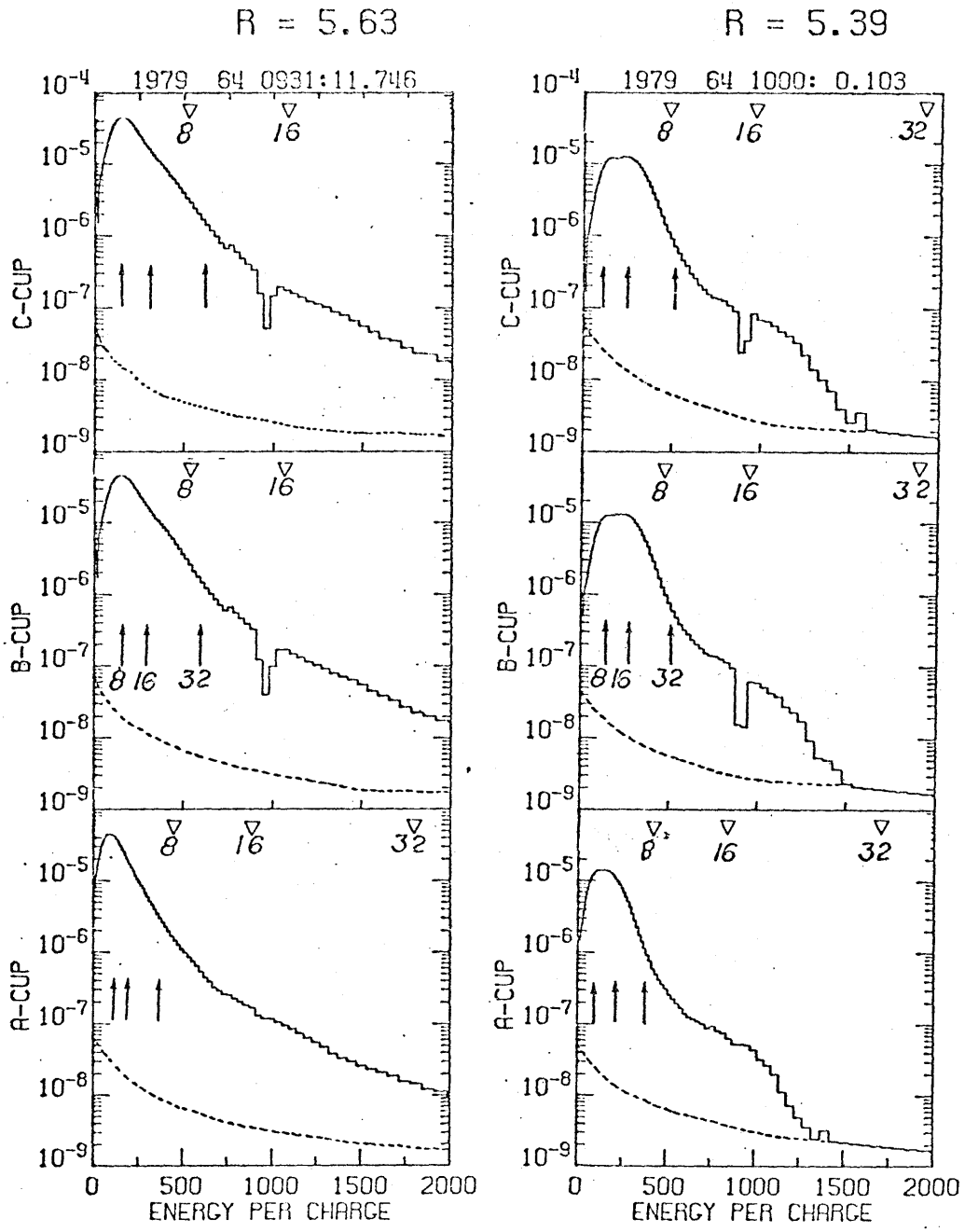

Figure 19. The energy per charge spectra of the A-, B- and C-cups made at (a) 0931 UT (5.63 R_J) and (b) 1000 UT (5.39 R_J). The arrows mark the locations of spectral peaks corresponding to corotating ions with various A/Z values. The triangles mark the pick-up energies for the different ions. The dashed curve shows the instrument noise level. The notches near the center of the spectra are caused by interference from another experiment on the spacecraft.

(Figure 19b). In addition, the properties of the bulk of the plasma are also changing quite rapidly around this time. The density decreases and the plasma becomes cooler. Therefore it is not clear whether the particles with energies greater than~ 1500 eV suddenly disappear after 0936 UT or whether the non-thermal particle populations observed before and after 0936 UT have completely different origins. Another factor that may or may not be purely coincidental is that the saturated spectrum came immediately after the transition in spectral shape at higher energies.

The position of the high energy cut off in the spectra inside 5.6 R_J is not quite the same for all three main sensors. The arrows at the top of each panel show the energy per charge of ions with A/Z^*=8, 16, and 32 at the local pick up energy, the energy at which the tin-can distribution function of newly ionised material would have a sharp cutoff (see Figure 2). The observed cutoffs are less sharp than those expected for a purely tin-can distribution and fall about midway between the expected pick up energies of ions with A/Z^*=16 and 32 (Figure 19b). It is tempting to suggest that the observed cutoff in the spectrum is due to a combination of tin-can distributions of newly ionised S^{2+} (or O^+) and S^+ ions but the evidence is not compelling. There remains no explanation of why there is a sudden change in the spectrum at 5.6 R_J (well inside the orbit of Io) or why, outside 5.6 R_J, the spectrum extends quite smoothly to energies of over 6 keV.

e) Data from the outbound pass

Figure 20 shows a 3-dimensional plot similar to Figure 8 for the outbound passage through the plasma torus. As the spacecraft swung round the planet the plasma flowed into the sensors at increasingly oblique

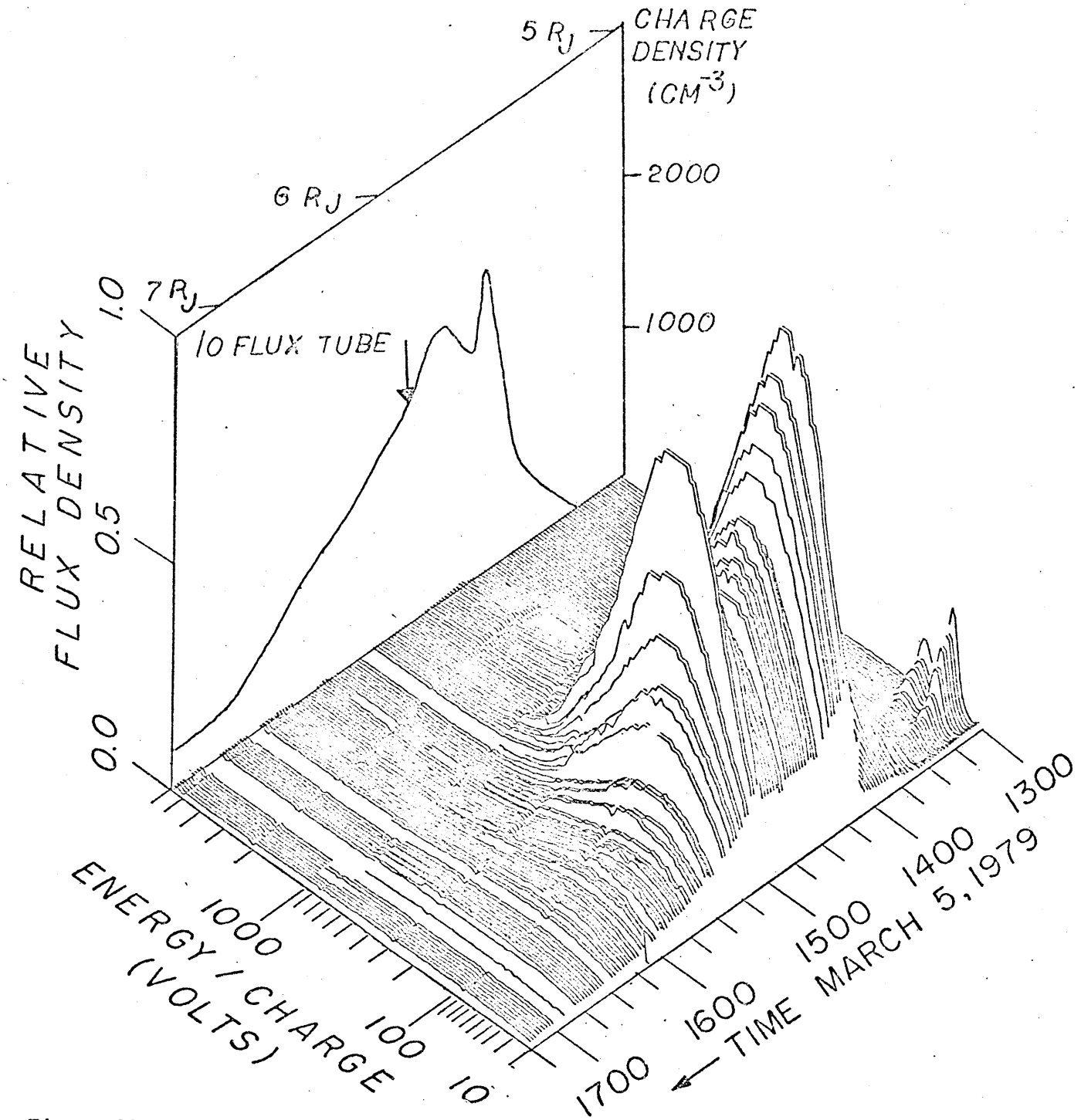

Figure 20. A three-dimensional plot of reduced proton distribution function against energy per charge for spectral measurements made in the A-cup of the main sensor between 1300 UT (~5R_J) and 1715 UT (~7.4 R_J) on 5 March 1979. The back panel shows the electron density measured by the PRA experiment (Birmingham et al., 1981) as a function of time.

angles. This means that much lower fluxes were measured on the outbound passage and that the analysis of these spectra is less straightforward because the response of the instrument to these fluxes is more complex. However, some of the spectral features of the inbound passage can be recognised in Figure 20. There were a few well-resolved peaks in the cold inner region but these soon disappeared as the spacecraft moved to larger southern latitudes. As observed during the inbound leg, the fluxes sharply increased at ~5.3 R_J (1400 UT outbound), briefly reaching maximum values at 1420 UT before decreasing rapidly due to the decreasing response of the plasma sensor. The back panel of Figure 20 shows the electron density profile from PRA measurements which has a spike at 1420 UT. This spike is similar to the density maximum (2) on the inbound pass. Similarly there was a broad density maximum (1) a little further out corresponding to first inbound maximum. The large fluxes measured for just a few spectra around 1500 UT are due to the plasma flow being perturbed by Io which was reported by Belcher et al. (1981) and will be discussed later.

Chapter 4

Comparison of direct plasma measurements with plasma characteristics determined from indirect measurements.

The bulk properties of the plasma in the Io torus can be inferred from both the direct plasma measurements and various types of radio, optical and ultraviolet emissions that the plasma radiates. The indirect measurements can be compared with the direct plasma measurements presented above.

(a) Radio Emissions

Plasma properties can be inferred either from the characteristic frequencies of radiation emitted by the local plasma or from the attenuation of electromagnetic waves through the plasma. Throughout the outer and middle Jovian magnetosphere the local electron density was determined by the Plasma Wave Science (PWS) experiment on the Voyager spacecraft from the low frequency cutoff of the continuum radiation which was assumed to occur at the local plasma frequency f_p (Scarf et al., 1979). In the dense plasma of the Io torus f_p moves up into the higher frequency range of the Voyager Planetary Radio Astronomy (PRA) experiment. Inside ~10 R_J Jupiter's magnetic field is strong enough that the electron gyro frequency (f_0) also enters the PRA range. In the Io plasma torus the PRA experiment observed a series of emissions which have been identified as locally generated electrostatic waves. These appear to be closely related to waves observed in the Earth's magnetosphere (Warwick et al., 1979; Birmingham et al., 1981). They are termed

"gyro-harmonic" emissions because they are narrow banded and occur between harmonics of the local gyrofrequency. Strong emission also occured at the local upper hybrid resonance frequency (f_{uhr}). The variation of f_{uhr} and the gyro harmonics as the spacecraft moved through the torus indicates variations in the local electron density. Figure 9 shows how the resulting profile of local electron density published by the PRA experimentors (Birmingham et al., 1981) is in excellent agreement with the positive charge density determined from plasma measurements on the inbound leg of the trajectory. The PRA outbound profile of electron density shows a similar structure to the inbound profile but with lower densities because the spacecraft was further away from the center of the torus. When the geometry of an offset dipole magnetic field is used the L-shells of the main features of the inbound and outbound features coincide as shown in Table 5. The outbound densities also roughly match those expected from the two-dimensional model constructed from the inbound plasma data shown in Figure 16.

Finally, the shape of the plasma torus has been studied from the propagation of the radio signal that was transmitted from the spacecraft through the torus by the Voyager Radio Science experiment (Levy et al., 1981). The phase shift experienced by the coherent radio waves passing through the torus is directly proportional to the line integral of electron density along the ray path and proportional to the wavelength. Therefor measurement of the differential phase shift between the two telemetry signals (at 13 and 3.6 cm wavelengths) determine the changes in the column density of electrons between the spacecraft and the Deep Space Network receivers on Earth. The measured variation in integrated electron density due to changes in the spacecraft's location were

compared by Levy et al., (1981) with column densities predicted by various models of the plasma torus from other experiments (Warwick et al., 1979; Birmingham et al., 1981; and an early model of the torus density determined from plasma data and published by Bagenal et al., 1980). There is a reasonable agreement between the measured and predicted column densities (which would probably be improved by using the more recent plasma model shown in Figure 16) but there are fairly large uncertainties in the Radio Science measurements because of uncertainties in the column density of the Earth's ionosphere that has to be subtracted from the total line integral to obtain the contribution due to the torus plasma.

(b) Ground-based photometric observations

The Io torus was first discovered when Kupo et al. (1976) detected emission at a pair of spectral lines (λ = 6731 Å and 6716 Å) at the red end of the spectrum. These lines correspond to first two excited levels of S^+ ions and are "forbidden" because the ions can only be excited by electron collisions. The radiative relaxation times for these excited states are τ_{6731} = 10 minutes and τ_{6716} = 33 minutes. Just less than 2eV is released from each transition. In the limit of low electron density the intensity of the two lines will have a fixed ratio of $J_{6716}/J_{6731} \sim 1.5$. However in the limit of high electron density, de-excitation by collision (without radiation) becomes more important so that the line with the shorter relaxation time becomes stronger and $J_{6716}/J_{6731} \sim 0.4$. Conveniently, the torus plasma density is in the middle of the range where the line intensity ratio is a sensitive indicator of local electron density. The application of these techniques which are traditionally applied to emisssion from remote nebulae was first carried out by Brown

(1976) who deduced $N_e = 3200^{+3100}_{-1600}$ cm^{-3} and $T_e = 2^{+6.5}_{-1.5}$ eV from the line ratio observed by Kupo et al. (1976).

The third and fourth excitation levels of S^+ produce a pair of forbidden lines in the blue region of the spectrum at (λ = 4069 Å and 4076 Å) which have been observed by Morgan and Pilcher (1981). These emission lines correspond to energies just over 3 eV and have much shorter life times, 3 and 8 seconds respectively.

Because of the much shorter life times, the intensity ratio J(4069A)/J(4076A) is much less sensitive to the density of electrons unless the density is much larger than that observed in the Io torus. However, in the low density limit, the intensity ration of either blue line to either red line is sensitive primarily to the average energy of the electrons and hence may be used to estimate electron temperature.

These two pairs of spectral lines have been studied at a variety of observatories (Brown, 1978; Trafton, 1980; Trauger et al., 1980; Morgan and Pilcher, 1981; Oliverson et al., 1980). The electron density estimates vary from 1000 to 4000 cm^{-3} with large intensity variations occuring on time scales of a few hours upwards. Such densities are a little larger than the in situ plasma measurements as illustrated in Figure 17, which shows the equatorial positive charge density had values of ~800 to ~3000 cm^{-3} in the torus during the Voyager 1 encounter. Various estimates of the electron temperature from the S^+ emission generally agree with Brown's value of ~2 eV (Trauger et al., 1980; Trafton, 1980) though larger values are indicated at larger radial distances (Pilcher, 1980). These results suggest most of the S^+ emission comes from a region inside the steep drop in ion temperature at ~5.7 R_J which separates the inner cold torus from the outer warm torus (Figure

10). It is generally agreed that the emission is consistent with a torus of S^+ ions near the orbit of Io tilted away from the rotation equator towards the magnetic equator, though the spatial resolution is too poor to distinguish the $\lesssim 3°$ difference between the centrifigual and magnetic equators. There have been some claims that the emission intensity systematically varies with magnetic longitude (Trafton, 1980; Pilcher and Morgan, 1980; Trauger et al., 1980) but the evidence is not strong.

Four weeks after the Voyager 1 encounter Pilcher (1980) obtained images of the S^+ emission near Io. Figure 21 shows a map of the emitting region with contours corresponding to values of equal intensity. The observed intensities are integrals of emission along a line of sight through the torus. Therefore, for comparison, a map of column density has been constructed from the two-dimensional density distribution shown in Figure 16 and using the geometry of an azimuthally symmetric torus. Of course the probability of emission must also be folded into the calculations before the two measurements can be compared directly, but Figure 21 shows how the general structure appears to be the same. Integrating along a line through a torus moves the maxima radially inward so the maxima of equatorial column density are at ~5.5 R_J and ~5 R_J (while the local density peaks at ~6 and 5.5 R_J). These maxima of column density are also the regions of peak emission intensity. In the warm torus the column density of S^+ ions shown here has probably been overestimated because in this case no account has been taken of the non-Maxwellian components to the spectrum and no effects of spacecraft charging have been included. Therefore the large column densitites outside 6 R_J do not imply a real disagreement with the ground-based observations.

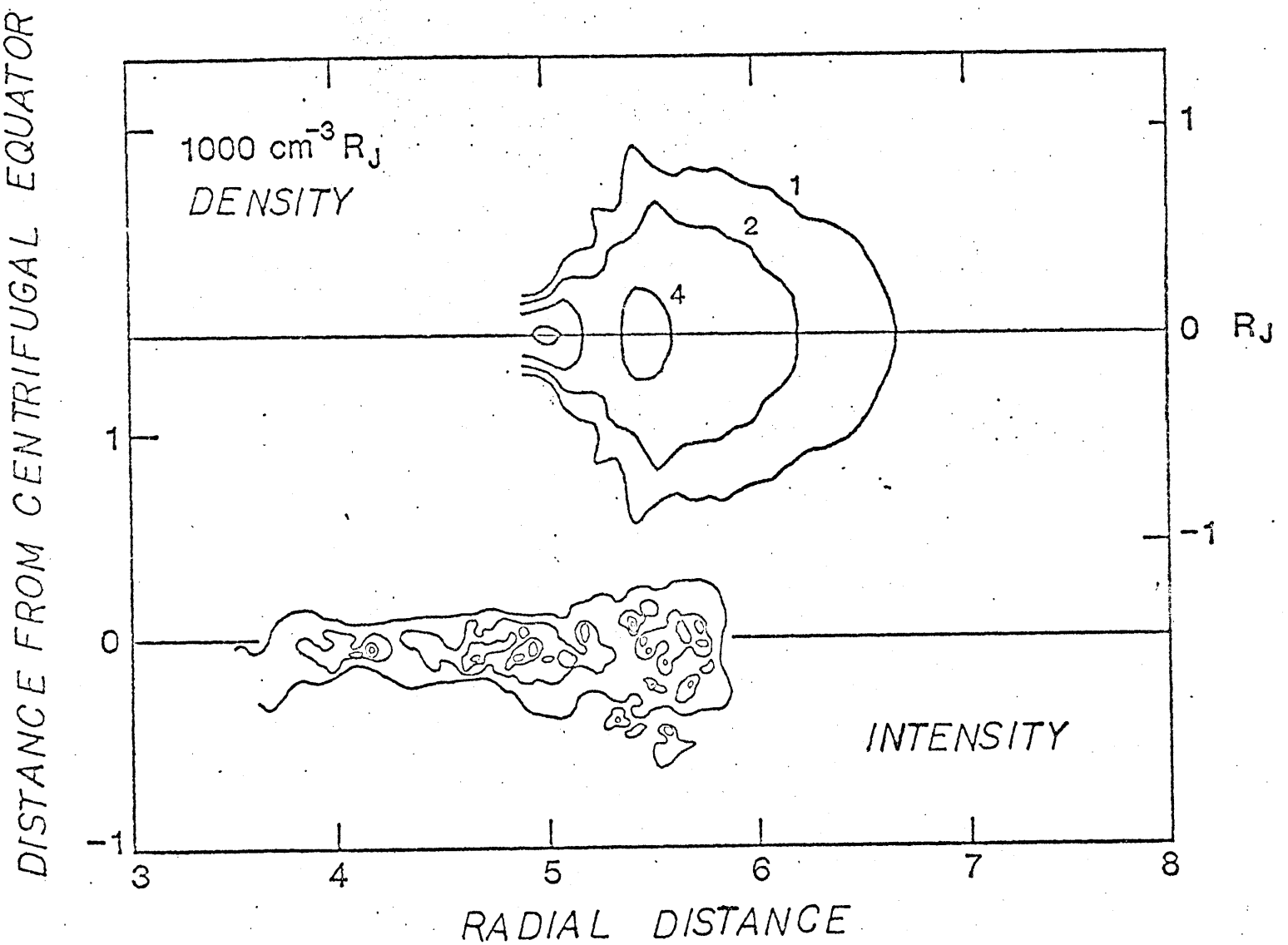

Figure 21. Comparison of the observed S^+ emission at λ = 6731 Å (Pilcher, 1980) with column density of S^+ ions calculated from the in situ plasma measurements.

Imaging techniques have been improving rapidly over the past year or so and some preliminary pictures taken by Oliverson et al. (1980) suggest that long term monitoring of the Io torus with good spatial and temporal resolution can soon be carried out relatively easily from the ground.

In addition to the emission lines of S^+ several forbidden lines of other ions have also been observed from the ground. These include the first two "forbidden" lines of O^+ near ultraviolet wavelength of 3726 and 3729 Å which have been observed by Pilcher and Morgan (1979). Morgan and Pilcher (1981) note that more recent observations indicate that the O^+ torus is thicker than the S^+ torus which is conistent with the O^+ ions having a larger effective scale height due to their lower mass (see Appendix III). Emissions from S^{2+} ions have been observed at various wavelengths: 9532 Å in the infrared (Trauger et al., 1979; Oliversen et al., 1980); a red line at 6321 Å (Brown, 1980) and at a near ultraviolet line 3722 Å (Morgan and Pilcher, 1981). The temperature of the ions that have been deduced from the S^{2+} emissions vary from 26 eV (Trauger et al., 1979) to as much as ~80 eV (Brown 1980). These higher temperatures are consistent with most of the emission coming from outside Io's orbit in the warm torus. The in situ plasma observations suggest the S^{2+} ions have a temperature of ~30-60 eV and are confined to the warm torus.

Finally, two ground based optical observations have been made recently which bear directly on the nature of the source mechanisms for the torus ions. Firstly Brown (1980) reported the detection of emission from neutral oxygen atoms in the vicinity of Io's orbit. The observations suggest a tenuous cloud of ~30 atoms cm^{-3} in the warm torus and an electron temperature of ~4-5 eV. The intensity of emission implies a source rate of $\sim 10^{28}$ oxygen atoms s^{-1}. Secondly, Brown and Ip

(1981) looked at the S^+ emission from a region outside Io's orbit and found that when the two red S^+ lines are superposed the width of the main spectral peak corresponds to a thermal doppler spread for ions at a temperature of ~18 eV while there is an underlying broad peak, presumably due to S^+ ions at much higher energies. The temperature of 18 eV is compatable with ion temperatures measured by the plasma instrument at ~6 R_J. The S^+ ions at higher energies that are observed by Brown and Ip may be responsible for the high energy tail in the energy per charge spectra obtained by the plasma instrument in this region. Brown and Ip (1981) fitted the broad underlying peak with a Maxwellian function for ions with a temperature of 540 eV which is the corotational energy of S^+ ions at 6 R_J and correspondingly the gyro-energy of freshly ionised ions. They found that the wings of the spectral feature could be fitted with the hot (540 eV) component containing up to one third of the total S^+ density. These two recent observations support the idea that ions are produced from a diffuse source (i.e. a neutral cloud) rather than in a very localized region near Io, and that the new ions pick up large gyro energies which have to be partly dissipated as radiation to produce the observed low plasma temperatures.

(c) Ultraviolet observations from Voyager and IUE spacecraft

The Earth's atmosphere absorbs most of the ultraviolet light at wavelengths less than ~3000 Å so it is necessary to mount a spectrometer on a spacecraft to measure extraterrestial emission at shorter wavelengths. The Voyager Ultraviolet Spectrometer (UVS) experiment spanned a wavelength range of 500 to 1700 Å with a resolution of ~30 Å (Broadfoot et al., 1979). The Earth-orbiting International Ultraviolet

Explorer (IUE) carries a spectrometer spanning 1175 to 1950 Å wavelengths with a resolution of ~11 Å (Moos and Clarke, 1981). The UVS spectrometer loses sensitivity at the longer wavelengths so that in fact there is little overlap between the two experiments. The wavelengths between 500 and 1950 Å correspond to electron transitions in the energy range ~6 to ~25 eV and therefore the instrument is very appropriate for detecting emission lines associated with the excitation of the first few allowed levels of sulphur and oxygen ions. There are a total of 21 allowed transitions for the five ionization states, S^+, S^{2+}, S^{3+}, O^+, and O^{2+} ions in this energy range. Only four of these lines are in the IUE range.

The 6 to 25 eV energy range also includes the thermal energy of the cold component of the electron population in the warm part of the Io torus. Scudder et al., (1981) report electron temperatures of 5 to 26 eV for the cold compoment of the plasma measured at 5.5 - 8.9 R_J by the Voyager plasma experiment. Correspondingly the ultraviolet emission appears to come from a toroidal region of internal radius ~1 R_J centered just outside the orbit of Io (Broadfoot et al., 1979).

To deduce the properties of the emitting plasma from the intensity of the emission lines it is not only necessary to know all the appropriate rate coefficients for the atomic transitions but also to consider the time scales of the emission processes compared with the characteristic lifetime of the ions in the torus. The allowed excited states of oxygen and sulphur ions are very short-lived with characteristic lifetimes against radiative de-excitation on the order of nanoseconds (Shemansky and Smith, 1981). Each of the ionization states of sulphur and oxygen may be assumed therefore to be in radiative

equilibrium. However the timescale for ionization equilibrium between the different ionization states is months which is probably longer than the timescales for diffusion in the torus (10-100 days). This means that the relative abundances of the different ionization states (such as $n(S^+)$; $n(S^{2+})$; $n(S^{3+})$) will not necessarily be as predicted by ionization equilibrium.

A sample spectrum from the Voyager UVS experiment is shown in Figure 22. Full descriptions of the UVS spectra are given by Broadfoot et al. (1979) and Sandel et al. (1979). There are two main spectral features (at ~685 Å and 833 Å) and several smaller peaks at higher wavelengths. The lack of resolution causes considerable difficulty in interpreting the spectrum because for each peak there are several possible emission lines. For example, the 685 Å feature coincides with three overlapping S^{2+} multiplet transition lines with a contribution from an O^{2+} line. It is flanked by multiplets of S^{2+} and S^{3+}. The 833 Å feature spans nearly-coincident multiplets of O^+ and O^{2+} which makes it hard to determine the contribution of the two ionization states of oxygen. At longer wavelengths there are multiplets of S^{2+}, S^{3+} and S^+. When analyzing this spectrum it was first assumed that the plasma was in collisional ionization equilibrium (Broodfoot et al., 1979; Shemansky 1979). The resulting ionic composition is given in Table 7. To increase the abundance of ions at higher ionization states that were not originally accounted for under ionization equilibrium, Strobel and Davis (1980) included a fraction of hot (~100 eV) electrons. Alternatively, Shemansky and Smith (1981) did not assume ionization equilibrium but took the 833 Å feature to be largely due to O^{2+} emission (Table 7).

Of the four emission lines in the IUE wavelength range there are two

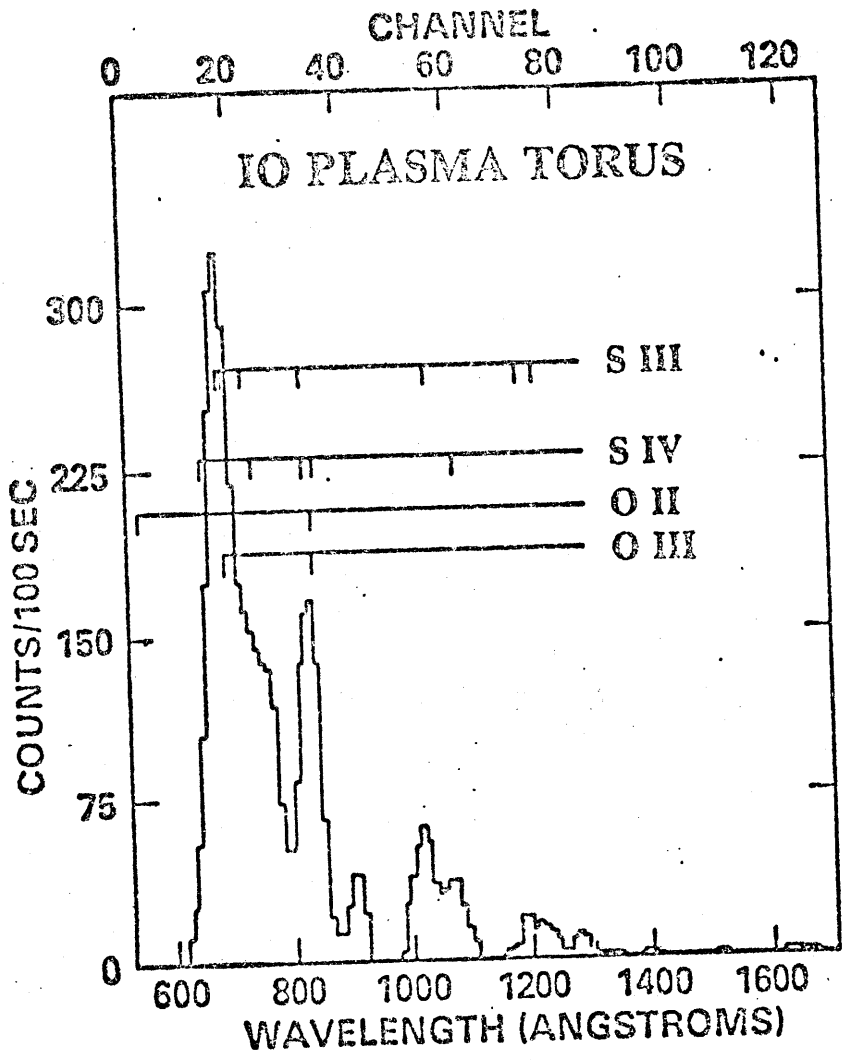

Figure 22. The ultraviolet emission spectrum measure by the Voyager Ultraviolet Spectrometer when the spacecraft was ~70 R_J from Jupiter (from Pilcher and Strobel, 1981). Multiplets of identified species are indicated.

Table 7

Warm Torus Composition Determined By Different Experiments

		O^{2+}	S^{3+}	S^{2+}	O^{+}	S^{+}	Comments
Voyager Plasma Experiment	$\phi S/C$ = 0 volts	115 (45)	83 (36)	632 (13)		490 (30)	Simultaneous fit to three main sensor spectra at 0859 UT (5.93 R_J), under assumptions of 1.) corotation and 2.) common temperature for all ionic species
	$\phi S/C$ = -15 volts	160 (18)	196 (16)	467 (11)		382 (18)	
	$\phi S/C$ = -30 volts	350 (60)	208 (71)	263 (44)		336 (18)	
	$\phi S/C$ = -15 volts	126 (82)	208 (79)	373 (21)	300 (fixed)	318 (40)	
UVS	Shemansky (1980)	190 → 740	80	95	<46	25	Analysis of Voyager Ultraviolet Science spectrometer measurement at 67 R_J from Jupiter when aperture slit centered at the brightest part of the torus (~5.9 R_J)
	Strobel and Davis (1980)	110 (60)	160 (30)	500 (100)	300 $^{+200}_{-80}$	<300	
	Shemansky and Smith (1981)	336 (60)	216 (50)	160 (30)	49 (20)	44 (22)	
	Brown, Pilcher and Strobel (1981)	110			300		Combines both UVS and IUE observations
IUE	Moos and Clarke (1981)	110		160 → 320		140	International Ultraviolet Explorer spectral measurement from Earth orbit

strong lines of S^+ and S^{3+} as well as weak emission lines of O^{2+} and S^{3+}. Because of the better resolution of the IUE spectrometer and also because of the long exposure times which could be used for IUE, it is possible to put good upper limits on these weak emissions (See Table 7) as well as for lines of many other ionic species (Moos and Clarke, 1981).

Rather than assume the 833 A feature was largely due to O^{2+}, Brown et al. (1981) compared the two sets of observations to see if it is possible to pin down the relative densities of the two oxygen ions. They calculated the expected ratios of emission intensity for two different lines of each ion for five electron temperatures between 3 and 9 eV. (The ratios were J(539 A)/J(834 A) for O^+ and J(1664A)/J(835A) for O^{2+}). Upper limits on the intensity of emission from the 539A line (from the UVS experiment) and the 1664 line (from IUE) were then used to put upper limits on the emission of each of the 834 Å and 835 Å lines as a function of electron temperature. The total emission in the 833 A feature was then used to constrain the electron temperature to ~6 eV and the densities of O^+ and O^{2+} at ~300 and ~110 cm^{-3} respectively. Similar comparisons led Brown et al. (1981) to conclude that the large intensities measured by IUE at the S^+ 1256A line are incompatable with the UVS observations unless the S^+ emission actually comes from a colder region than the warm torus, closer to the cold region inside Io's orbit. This could quite possibly be so considering the size of the aperture and pointing accuracies of the IUE experiment.

Included in Table 7 are the fits to the plasma spectrum at 0859 UT (5.93 R_J). When comparing the in situ measurements with the remote observations it is important to realize that the densitites have been derived from emission intensities assuming a homogeneous torus 2 R_J thick

while the plasma measurements were made near the equator. As a result the measured plasma values should be on the order of ~20% higher than those deduced from remote observations. However the UVS experimenters assumed a uniform total charge density of ~2000 cm^{-3} which is probably on the order of ~20% larger than suggested by the plasma data (as shown in Figure 16) for a 2 R_J thick torus. Therefore given the uncertainties in each set of measurements, the densities can be directly compared.

The plasma data in the warm torus were originally analysed under the assumption that the A/Z = 16 peak was due to S^{2+} rather than O^+ ions under the misunderstanding that O^+ emission lines were absent in the UVS spectra (Broadfoot et al., 1979). The result was that even with a large spacecraft charge the plasma fits suggested much more S^{2+} and less O^{2+} than the early fits to the UVS data. When the plasma data are fitted with a constant O^+ density of 300 cm^{-3} and a spacecraft charge of -15 volts the resulting composition is quite compatable with the UVS fits of Strobel and Davis (1980) and the estimates of Brown et al. (1981). The only inconsistency occurs with the S^+ density. However the S^+ density has probably been overestimated in the warm torus (perhaps by as much as an order of magnitude) in the analysis of the plasma measurements because the high energy end of the spectrum near A/Z*=32 contains contributions from freshly ionized matter with a non-Maxwellian (maybe "tin-can") distribution. There are probably also effects due to the presence of heavier ions (SO^+, SO_2^+, etc.) as well as the response of the instrument at higher energies, which have not been fully included as yet.

In summary, the in situ plasma measurements and the remote ultraviolet observations of the warm region of the torus are found to be quite compatible though there remain considerable uncertainties in each

of the measurements due to the poor resolution of both instruments and many assumptions that consequently must be made in the analysis of both data sets.

Chapter 5

The role of Io in the Jovian magnetosphere

The Voyager 1 plasma instrument made the first direct measurements of the plasma in the inner magnetosphere. Many theories of the magnetospheric processes were developed befor Voyager 1 reached Jupiter and the theorists have since been enthusiastic in using the data to test and expand these theories. For example composition and rate of renewal of the torus plasma are needed to constrain the mechanisms for removing material from Io. Similarly, it is necessary to know the spatial distribution of plasma around Io in order to model the interaction of the satellite with the magnetospheric plasma. This chapter discusses some of the theories that have been proposed and how the Voyager plasma data presented above can be used by various investigators to study the role of Io in the inner magnetosphere.

(a) Plasma source

The detection of an SO_2 atmosphere by Pearl et al. (1979) and SO_2 frost on the surface of Io (Fanale et al., 1979; Smythe et al., 1979) make SO_2 an obvious source material for the plasma torus. The characteristics of the dissociation and ionisation processes for SO_2 are not well known. However, Shemansky (1980) and Kumar (1980) suggest they probably involve O_2 and SO molecules and their ions, especially on the nightside of Io where O_2 may dominate the atmosphere (Kumar and Hunten, 1980). The existance of intermediate dissociation products as well as the fact that oxygen is less readily ionized than sulphur may explain why more sulphur was observed in the torus than expected from the full

dissociation and ionisation of SO_2.

It has been noted by Cheng (1980) and Brown et al. (1981) that charge exchange reactions should be included when considering the relative abundances of sulphur and oxygen in the torus. If a charge exchange reaction occurs between a corotating ion and a slowly orbitting neutral atom, the ion becomes a fast neutral atom retaining its original corotational speed which is far greater than necessary to escape the Jupiter system. The originally slow neutral atom is accelerated on ionisation up to corotation and picks up a gyro-speed of roughly the local corotational value (see Chapter 1(d)). The total number of ions remains constant in charge exchange processes but the new ion picks up a larger gyro-energy than the old ion and the neutral atom is lost from the system. Brown et al. (1981) calculated that for typical ion energies and a neutral atom density of 100 cm^{-3}, the reaction times for neutral sulphur atoms exchanging charge with S^+ or O^+ ions are 55 and 71 hours respectively. Being smaller, oxygen atoms are less likely to undergo a charge exchange reaction. This means that oxygen ions are preferentially lost from the system (as fast as neutrals).

On the other hand, there is probably a significant amount of elemental suphur on the surface of Io (Masursky et al., 1979). There must be some mechanism such as sputtering for removing from Io material which is not a major constituent of the atmosphere because neutral sodium has been observed in the vicinity of Io for many years and sodium ions have been detected in the magnetosphere (Krimigis et al., 1979; Vogt et al., 1979; Sullivan and Bagenal 1979). Therefore, additional sulphur may be supplied to the torus by a similar process.

The rate at which plasma is injected into the torus has been

estimated by various means to be on the order of 1 tonne per second (specifically, $\sim 6 \times 10^{29}$ atomic mass units per second or $\sim 2 \times 10^{28}$ sulphur ions per second). Hill (1979) predicted that injecting plasma into the magnetosphere will cause the plasma to lag behind strict corotation because of the finite conductivity of the Jovian ionosphere. He then used the observed deviation in plasma flow from corotation (McNutt et al., 1979) to obtain a mass-loading rate (Hill, 1980). Richardson et al. (1979) found the source rate that would produce the observed radial distribution of plasma (discusssed in section (b), below) under time-dependent radial diffusion. Another way of estimating the source rate is to balance the power dissipated in the torus ($1\text{-}3 \times 10^{13}$ watts in the aurora and 6×10^{11} watts as ultraviolet emission from the torus, according to Broadfoot et al., 1981) with the maximum energy that would be available from the cyclotron motion of freshly ionised material (Dessler, 1980; Eviatar and Siscoe, 1980).

Although the source rate is generally agreed to be within an order of magnitude of 1 tonne per second, there is controversy remaining over where the material is actually ionised. There are two main possibilities: the plasma comes from the ionisation of (i) a diffuse cloud of neutral gases which is spread over a large portion of Io's orbit; (ii) the atmosphere of Io during the complex interaction of magnetospheric plasma and the satellite. The "diffuse" source mechanism (which produces "hot" ions) requires a small source rate (i.e. lower limit of the estimate) and longer average residence time for particles in the torus (i.e. 50 - 100 days) while the "local" source mechanism (which produces "cool" ions) requires a large source rate (i.e. upper limit of estimate) and short residence time ($\sim$10 days).

The evidence in favour of a diffuse source is:

(i) Brown (1980) has reported the observation of a spectral line of neutral oxygen atoms in the vicinity of Io.

(ii) Longer residence times would provide greater opportunity for the ions to be ionised to the higher ionisation states that are observed (though would not imply ionisation equilibrium).

(iii) There may be evidence that a fraction of the S^+ ion population has energy well above the average thermal energy from (a) the high energy tail of the energy per charge spectra and (b) the underlying broad peak in the S^+ emission spectrum, reported by Brown and Ip (1981).

The problems with the diffuse source are:

(i) The source rate would be a little too small to explain the observed deviations from corotation in the middle magnetosphere.

(ii) How can the energy be transferred from the energetic new ions to the electrons (and hence into radiation) when coulomb colisions are very infrequent and inefficient?

The argument in favour of a local source is that the mechanism produces ions of about the observed thermal energies.

The problems with the local source are:

(i) The mechanism requires an intense localised source which would produce an enhancement of ultraviolet emission in the vicinity of Io far larger than the upper limits imposed by the Voyager Ultraviolet Spectrometer measurements (Broadfoot et al., 1979).

(ii) As each new ion starts out with less energy per ion, there may not be enough energy available to fuel the total observed ultraviolet emission.

(iii) How do the ions become ionised to higher ionisation states in the

shorter residence time?

There is no doubt that both ionisation processes must be taking place, but is not clear which is of over-riding importance.

Finally, the ionosphere of Jupiter and, probably to a lesser extent, the solar wind must also contribute plasma to the magnetosphere. Protons are observed in the middle magnetosphere and they may well dominate the plasma composition away from the equatorial regions to which the heavier ions from Io are strongly confined. (McNutt et al.,1981)

(b) Diffusion of plasma in the inner magnetosphere

The ions produced at Io are found dispersed throughout the inner magnetosphere. The spread of ions in the azimuthal direction is a result of corotation enforced on ions coming from a non-corotating source. The spread in latitude is controlled by the field-aligned component of the centrifugal force.

Dispersion of plasma away from L-shells of the source region requires cross-L diffusion. The time scale for diffusion is much longer than the time scales for dispersion in azimuth (i.e., the rotation period) or latitude (i.e., the 'bounce' period). Therefore it is generally assumed that there is axial symmetry and that diffusion in only one dimension need be considered (Fälthammer, 1966). For dipole geometry the equation for the conservation of ions is then

$$\frac{\partial N}{\partial t} = \frac{\partial}{\partial L}\left(\frac{D_{LL}}{L^2}\left(\frac{\partial}{\partial L}\left(NL^2\right)\right)\right) + S - R \qquad (5.1)$$

where N is the total number of particles in a magnetic L-shell per unit L; D_{LL} is the diffusion coefficient; S and R are the appropriate source and loss terms. The main loss mechanism is recombination but the time scales for recombination are large even in the densest part of the torus so R may be neglected. The source is fairly well confined to the L-shells near Io's orbit but probably varies with time. The diffusion coefficient D_{LL} depends on the actual diffusion mechanism and probably varies with L.

The quantity NL^2 has been calculated at M.I.T. from plasma data obtained during the inbound pass of Voyager 1 using the relation derived by Siscoe (1977).

$$NL^2 = \sum_i 2\pi R_J^2 L^3 H_i n_{oi} \qquad (5.2)$$

under the assumption that the ions are distributed along a field line exponentially with a scale height H and an equatorial density n_o (see Appendix III). This rather crude approximation is probably sufficient at present and considerably simplifies the calculations. The resulting radial profile of NL^2 is shown in Figure 23. Siscoe and co-workers at UCLA have fitted this profile with several different diffusion models to determine the ion source strength S and the nature of diffusion in the inner magnetosphere at the time of the Voyager encounter. (Richardson et al., 1980; Richardson and Siscoe, 1981; Siscoe and Summers, 1981).

The radial profile of equatorial charge density in Figure 17 shows

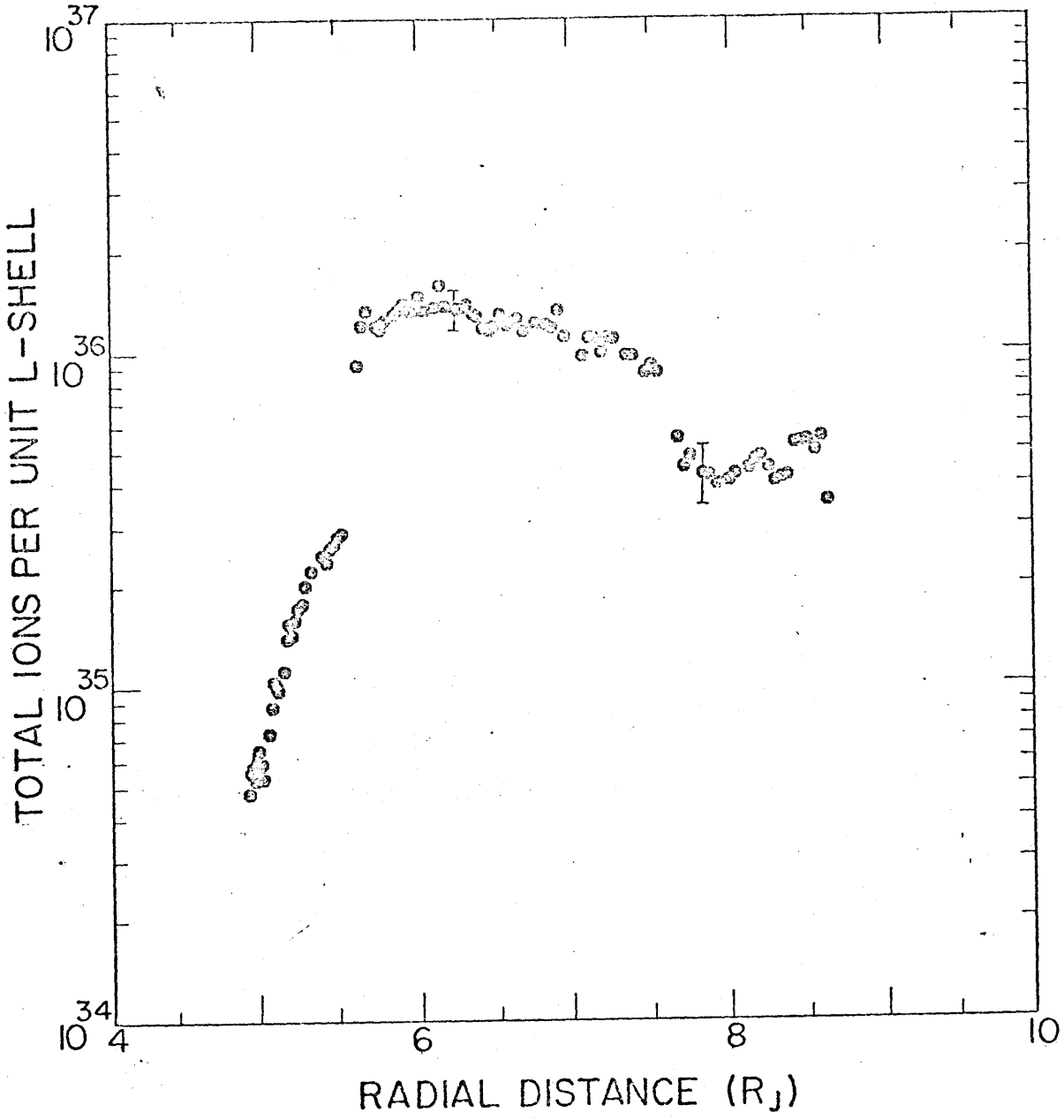

Figure 23. Radial profile of the total number of ions per unit L-shell constructed from in situ plasma measurements, assuming a dipole magnetic field and a simple exponential scale height distribution for the ions along the field lines. The uncertainties due to thermal-model dependences are shown by the vertical bars.

two maxima, one at ~5.3 R_J and another near the orbit of Io at 5.9 R_J. However the single maximum in the NL^2 profile implies a single source region near Io. This confirms that the local charge density maximum at 5.3 R_J results from the confinement of the cold plasma to the equatorial plane rather than from the presence of an additional source of plasma.

Differences in steepness of slope in the NL^2 profile suggest that different diffusion mechanisms (with corresponding charges in D_{LL}) are operating in different regions. Inside ~6 R_J the gradient is much steeper than outside so that D_{LL} must be correspondingly smaller for inward diffusion.

The mechanism for cross-L diffusion in the inner magnetospheres of both Earth and Jupiter has traditionally been thought of in terms of the interchange of adjacent flux tubes as a result of fluctuations in the magnetospheric circulation. At the Earth the source of these fluctuations is thought to be atmospheric turbulence which perturbs the atmosphere/ionosphere coupling. This has the result of making stochastic changes in the third adiabatic invarient of azimuthally drifting particles and consequently radial diffusion of their guiding centers. In the case of atmospherically driven flux tube interchange the diffusion coefficient has the form

$$D_{LL} = k\, L^m \tag{5.3}$$

where k is a constant and $m \leq 3$. From the Pioneer measurements of the radial distribution of energetic particles outside L ~ 6 in the Jovian inner magnetosphere Goertz and Thompson (1979) estimated k to be $2 \times 10^{9\pm1}$ and m = 2.5%s~ However the diffusion coefficient for energetic particles may not be applicable to low energy plasma.

Richardson et al. (1980) fitted the NL^2 profile near Io using a diffusion coefficient of the form $D_{LL} = k\ L^3$ and found that

$$\frac{k(out)}{k(in)} \sim 50 \qquad (5.4)$$

The fit is shown in Figure 24. Richardson et al. (1980) included time dependence in the fit procedure using a step function for the time dependence of the source. Inserting values of $2x10^{9\pm1}$ for $k_{in} = 2x10^{9\pm1}$ the source was turned on between 1 and 100 days before Voyager reached Jupiter.

However the sharp change in D_{LL} at the L-shells of the source raises doubts about the diffusion being driven by a remote process such as turbulence in the atmosphere of Jupiter and instead implies a local driving mechanism. With the strong centrifugal force due to Jupiter's rapid rotation any outward motion of plasma releases potential energy. This means that when the flux tube content decreases with distance potential energy is released in interchange of two adjacent flux tubes. However if the gradient of flux tube content is positive energy is required to interchange flux tubes. Siscoe and Summers (1981) have developed a theory of centrifugally driven flux tube interchange diffusion where the diffusion coefficient becomes

$$D_{LL} = -k\ L^{4+p} \frac{d(NL^2)}{dL} \qquad (5.5)$$

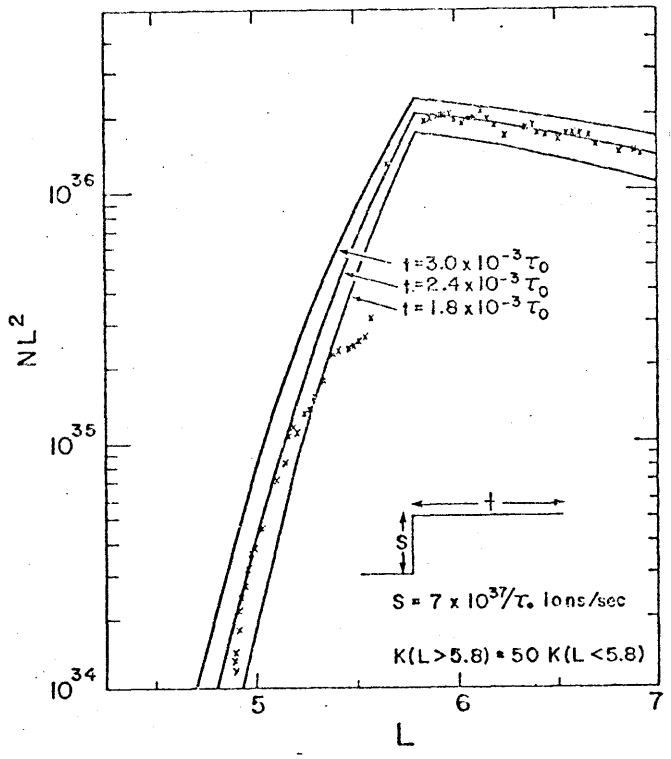

Figure 24.

Fit to radial profile of NL^2 by Richardson et al. (1979). Three solutions of the time-dependent diffusion equation are shown. The middle solution gave the best fit of all parameter combinations tried.

Richardson and Siscoe (1981) fitted an extended NL^2 profile with both linear (eqn 5.3) and non-linear (eqn 5.5) diffusion models and found fairly similar solutions as shown in Figure 25. The fit parameters were found to be insensitive to boundary conditions at the near and distant magnetosphere but some form of time-dependence was suggested in either case.

Although the fits shown in Figure 25 are quite reasonable given the uncertainty in the determination of NL^2, there appears to be a step in the profile between ~7 and 8 R_J. As this region is outside the source and the gradient of NL^2 is still negative, centrifugally driven diffusion would imply a continuous value for D_{LL}. The feature is not close to any satellites which might produce or remove plasma so there must be another factor which decreases the diffusion coeficient. It has been pointed out by Siscoe et al. (1981) that this region of inhibited radial diffusion coincides with the outer boundary of the torus as well as the inner edge of the Jovian ring current. The ring current at Jupiter, as at Earth, is a population of energetic particles that has diffused inwards from the outer magnetosphere. Their number density is low compared with that of the low energy plasma but they contribute the major part of the total energy density in the region of the ring current . As the volume of magnetic flux tubes decreases, the local density of energetic particles generally increases as they diffuse inwards. These energetic particles are removed by being swept up by satellites or scattered in pitch-angle so that they precipitate into the ionosphere of Jupiter.

The Voyager Low Energy Charged Particle experiment observed a rapid

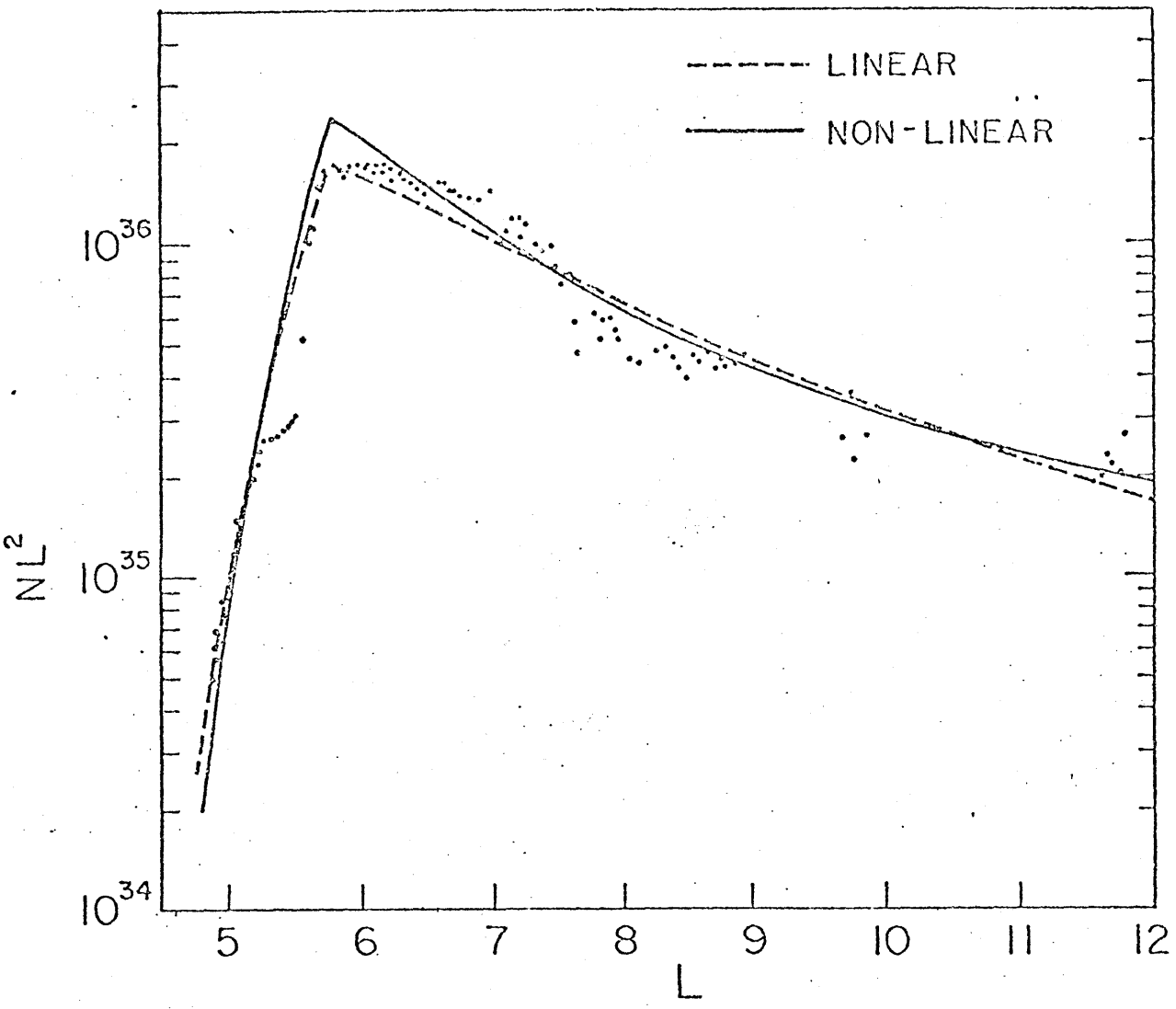

Figure 25.

Fit to the radial profile of NL^2 by Richardson and Siscoe (1981) using both linear and non-linear, time-dependent diffusion equations.

drop in the fluxes of 0.5 to 1.05 MeV particles inside 7 R_J on the inbound leg (Krimigis et al., 1979). Conversely, on the outbound leg the fluxes increased by the same two orders of magnitude between 7 and 8 R_J. There are no nearby satellites to sweep up the particles which implies they must be scattered into the ionosphere. In fact the L-shells near L=7 map onto the latitudes on Jupiter where considerable auroral activity has been observed by the Voyager Ultraviolet Spectrometer (Broadfoot et al., 1979). Thus the inwardly diffusing energetic particles appear to be scattered by the dense low energy plasma that they encounter at the outer edge of the torus, so that their pitch-angles are increased and the particles precipitate into the upper atmosphere where they trigger the aurora. Near the outer boundary of the torus the PWS experiment observed considerable low-frequency emission (Scarf et al., 1979). Several types of emission have been identified as similar to electrostatic plasma waves observed in the auroral regions of the Earth's magnetosphere. They are generally associated with precipitation of non-thermal (energetic) electrons and ions into the ionosphere (Scarf et al., 1981).

To consider what happens to the low energy plasma at the outer edge of the torus it is necessary to include the effects of the energetic particle population on flux tube interchange motion. Siscoe et al. (1981) calculated the gain in internal energy of the low energy plasma when a flux tube is interchanged and compared it with the energy required to compress the ring current particles from the outer flux tube into the inner flux tube of smaller volume. The calculations showed that the compression of the ring particles requires more energy than is available from the low energy plasma so that flux tube interchange is inhibited. This means that the plasma is confined at the outer boudary of the torus

by the ring current. The "weight" of the whole torus under centrifugal "pseudo-gravity" is $W = \int_{5.9}^{7.0} \rho R_J \Omega^2 L \, dL \cong 4.8 \times 10^{-8} \, N m^{-2}$ while the termal pressure of just the 0.5 MeV particles measured by Krimigis et al. (1979) is $P \cong 2/3 \, n E$ at least 2 x 10^{-8} N m^{-2} (Siscoe et al., 1981). The probable existence of a considerable population with energies between the 6 keV threshold of the plasma experiment and 0.5 MeV would easily increase this estimate of the confining pressure sufficiently to withstand the "weight" of the torus.

Figure 26 shows the inner magnetosphere can be divided into four regions according to the four different diffusion regimes that are summarized in Table 8. Over 90% of the plasma produced near Io's orbit rapidly diffuses outwards because of the instability of flux tube interchange under a strong centrifugal force. Outward diffusion is inhibited between ~7 - 8 R_J where the inwardly diffusing energetic ring particle population meets the outwardly diffusing torus plasma so that the diffusion coefficient in the interaction region decreases by a factor of ~6. Because of the sharp radial gradient in energetic particle density the confining pressure of the ring current decreases outside ~8 R_J, the radial diffusion coefficient in the middle magnetosphere reverts to a value similar to that in the warm torus. Diffusion inward of the source proceeds very slowly because of the difficulty in pushing the heavy ions up the steep gradient of the centrifugal potential. Therefore the plasma in the inner region of the torus is cold because it has had plenty of time to emit radiation and cool.

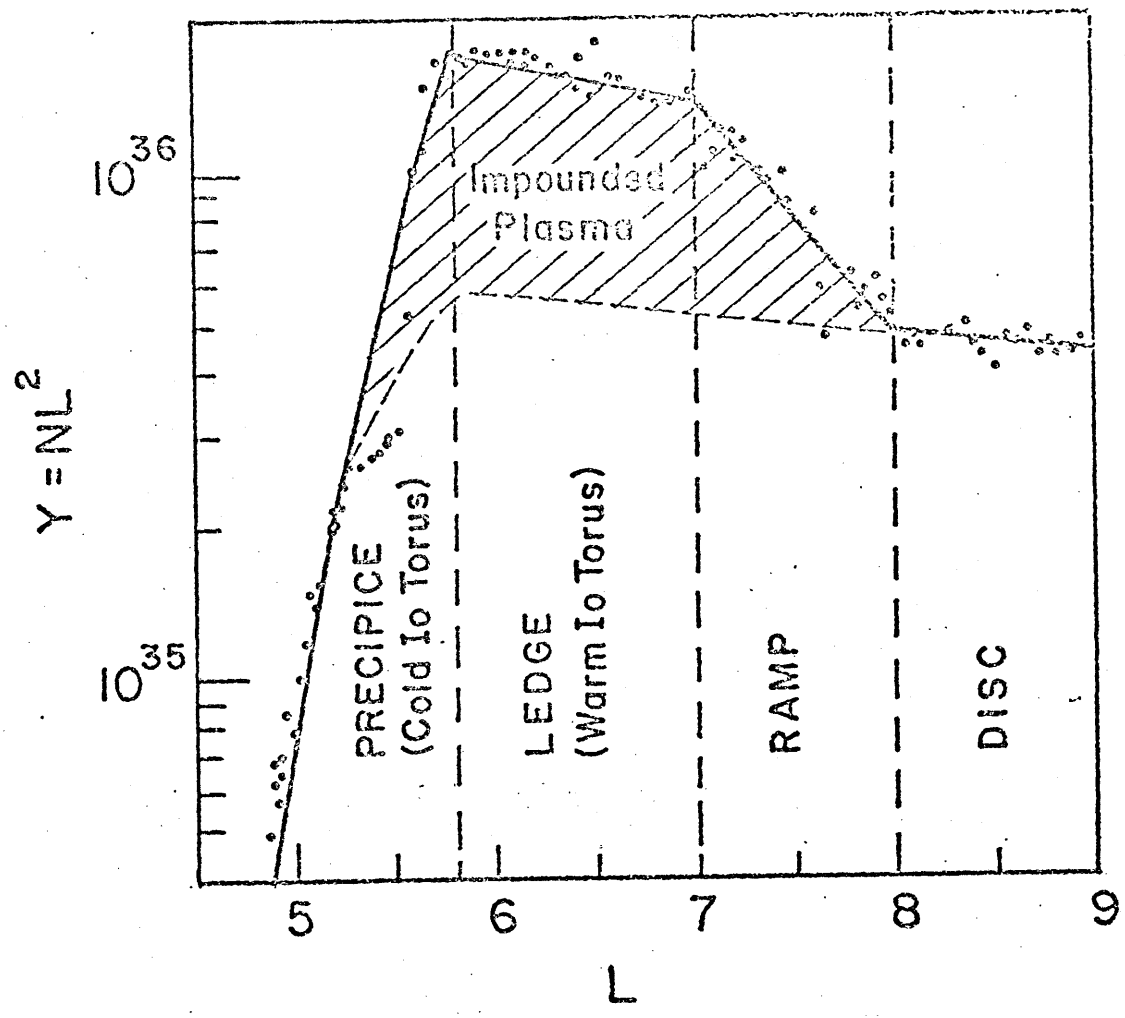

Figure 26. Fit to the rdial profile of NL^2 by Siscoe et al. (1981). The region has been divided into four diffusion regimes where the diffusion coefficient has different L-dependence. The resulting parameters are given in Table 8.

Table 8 - Diffusion Parameters

	Inner Torus	Warm Torus	Outer Boundary	Plasma Disk
Radial Range (R_J)	5.8	5.8-7.1	7.1-8.0	8.0
D_{LL}	kL^3	$kL^{4.5}$	kL^{12}	kL^4

(From Siscoe et al., 1981)

$\frac{D_{LL}(out)}{D_{LL}(in)}$	~16 - 20 at Io
Source	$S \sim 5 \times 10^{28 \pm 1}$ ions S^{-1}
Timescale	τ ~18 x $10^{\pm 1}$ days
$\frac{\text{Inward Flux}}{\text{Total Flux}}$	~0.08 - 0.12

(From Richardson and Siscoe, 1981)

(c) Interaction of Io with the Jovian Magnetosphere

(i) Theoretical background

Bigg's observation in 1964 that Io modulates the intensity of radio waves emitted from the vicinity of Jupiter provoked many early models of the satellite's interaction with the magnetosphere. (Piddington and Drake, 1968; Goldreich and Lynden-Bell, 1969; Gurnett, 1972; Goertz and Deift, 1973). These theoretical studies were carried out before any spacecraft had made direct measurements of the magnetic field or plasma in Jupiter's magnetosphere. They examined how Io's motion in the planetary magnetic field caused the satellite to act as a unipolar generator and investigated the possibility that large field-aligned electric currents connect the satellite to the planet. Goertz and Deift (1973) proposed that Alfvén (transverse) mode M.H.D. waves would be generated by Io and propagate along the field, carrying the field-aligned currents towards Jupiter. The description of a large conducting body generating Alfvén waves as it moved through a planetary magnetic field was first put forward by Drell et al. who was considering the affects of large artificial Earth-orbiting satellites moving in the Earth's magnetic field. Goertz and Deift (1973) applied the theory to Io but were hampered by the fact that very little was known about the conductivity of Io and the properties of the surrounding plasma. Since Voyager 1's passage through the inner magnetosphere, both Neubauer (1980) and Goertz (1980) have extended the theory and inserted the observed plasma properties.

The emerging picture of Io's interaction with the magnetospheric plasma is illustrated in Figure 27. The currents flowing in the vicinity

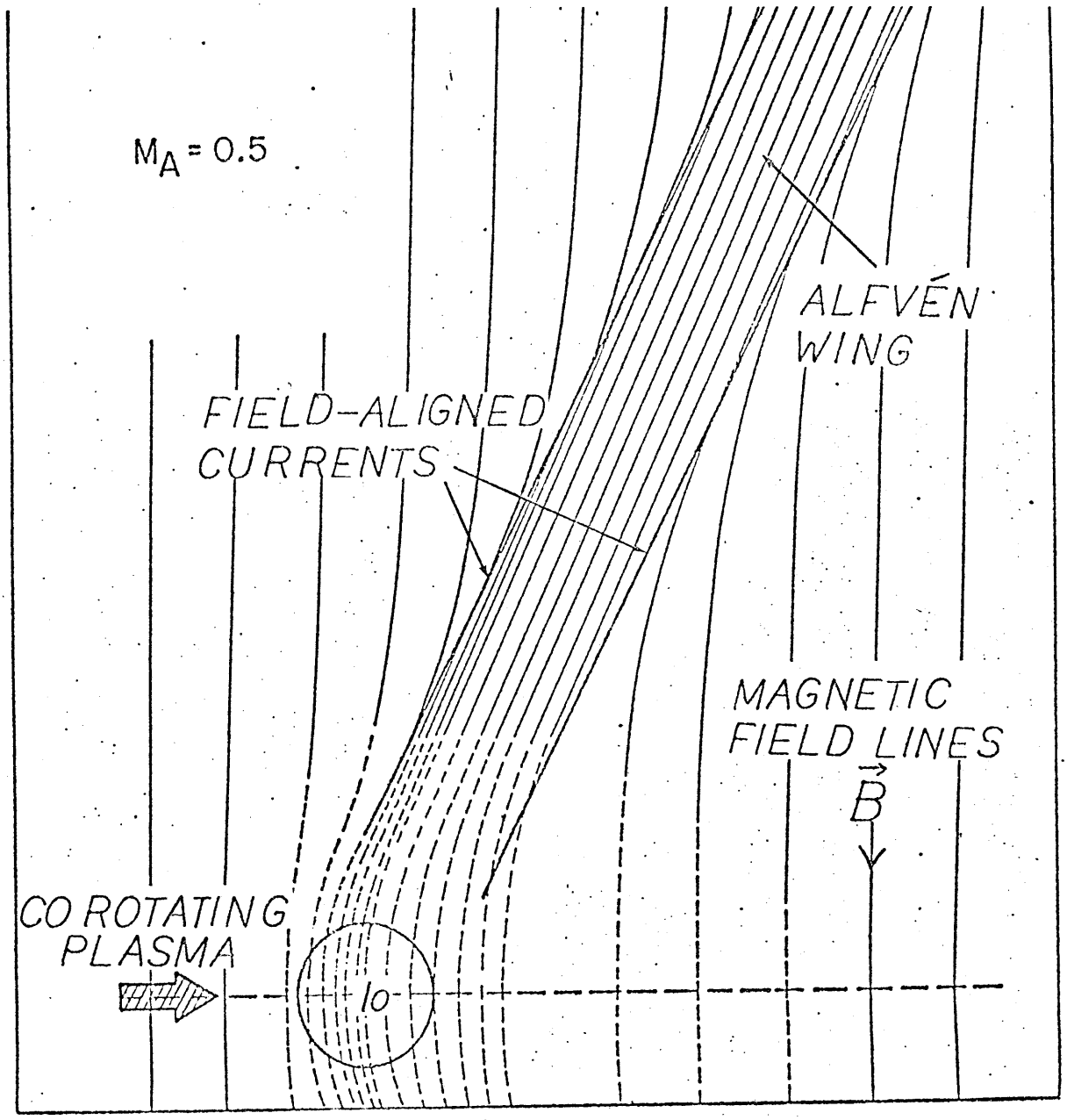

Figure 27. Perturbations of the magnetic field by Io (After Naubauer, 1980). The sketch is in a plane parallel to the magnetic dipole axis, looking towards Jupiter (the radial direction is out of the plane).

of Io are probably quite complex because not only is the conductivity of the satellite's interior proabably non-uniform but there are many other complicating factors involved with the interaction of the magnetospheric plasma with Io's atmospher and ionosphere (Cloutier et al., 1978; Neubauer, 1980; Goertz, 1980). Complications due to the possibility that Io might have an intrinsic magnetic field and its own magnetosphere have also been considered (Kivelson et al., 1980; Southwood et al., 1981). The ambient electric field in Io's rest frame is due to its motion with respect to the planetary magnetic field and is about $0.1 Vm^{-1}$ in roughly the radial direction. Therefore whatever the internal current configuration may be the voltage drop across the satellite is transmitted along the magnetic field by field-aligned currents emanating from Io's inner and outer faces.

In the rest frame of the ambient plasma (the corotating frame) the field-aligned currents are carried by Alfvén waves along the magnetic field. In Io's rest frame, the currents are carried downstream by the corotating plasma in addition to moving along the field. The result is a pair of standing convected Alfvén waves, which were described by Drell et al. (1965) as Alfvén wings, dragged back from Io at the Alfvénic Mach angle θ_A where

$$\tan \theta_A = M_A$$

M_A is the Alfvénic Mach number. i.e., the ratio of the plasma flow speed V to the Alfvén wave speed V_A.

The local Alfvén speed V_A is given by $V_A = \frac{B}{\sqrt{\mu_0 \rho}}$

where B is the local magnetic field strength and ρ the mass density of the plasma. It was originally thought that the magnetospheric plasma was sufficiently tenuous that an Alfvén wave could travel to Jupiter, be reflected by the conductive ionosphere and return to Io before the 66 seconds Io takes to move the distance of its diameter along its orbit in the corotating frame. If that were so then the current circuit would be closed in Jupiter's ionosphere. However, with the discovery of the plasma torus the local Alfvén speed is found to be 250 km s^{-1} so that the wave has barely traveled 0.25 R_J in 66 secs. This means the Alfvén wings emanating from Io may be regarded as open circuit transmission lines (Drell et al., 1965; Neubauer, 1980) where the characteristic impedance is $\mu_o V_A$. In a fully non-linear analytical study of the standing Alfvén wave system at Io, Neubauer (1980) has derived a more accurate expression for the Alfvén conductance (inverse impedance), the following approximation is good to 10% unless $M_A \geq 0.4$.

$$\Sigma_A = \frac{1}{\mu_o V_A} = \frac{1}{B\sqrt{\mu_o}}$$

The conductance of an Alfvén wave relates the local electric field to the currents carried along the magnetic field. In the transmission line analogy

$$I_A = \Sigma_A \Delta\mathcal{E}$$

where I_A is the field-aligned current and $\Delta\mathcal{E}$ the potential drop across the wings. Unless Io becomes charged up the currents carried away from Io in the wings must match the currents induced in (or near) the satellite

$$I_{I_o} = 2\,\Sigma_A \Delta\mathcal{E}$$
$$= \Sigma_{I_o}(\mathcal{E}_{co} - \Delta\mathcal{E})$$

where Σ_{IO} is the effective conductance of Io and the voltage drop across the satellite has been reduced from the corotational value, ϵ_{co} by the Alfvén wave. The nature of Io's interaction with the magnetospheric plasma is best characterized by the ratio

$$\frac{\Delta\mathcal{E}}{\mathcal{E}_{co}} = \frac{\Sigma_{Io}}{\Sigma_{Io} + 2\Sigma_A}$$

In the extreme case that Io is a very good conductor and the plasma tenuous, then $\Sigma_{IO} >> \Sigma_A$ and this ratio approaches unity. If $\Delta\epsilon \sim \epsilon_{co}$, then the corotational electric field is almost screened out by the Alfvén wave so the plasma flow comes to a halt in the wings, making the flux tubes appear "frozen" to Io. In the opposite extreme, where Io is a poor conductor and the plasma is dense ($\Sigma_A >> \Sigma_A$) then $\Delta\epsilon < \epsilon_{co}$ and the plasma flow is only slightly perturbed. The magnetic field easily diffuses through the satellite which then just acts as an obstacle in the magnetospheric flow and sweeps up the corotating particles. Of course, the realistic situation lies somewhere between these two extremes so that the corotational electric field is reduced because of the ohmic currents in (or near) Io which dissipate some of the plasma's kinetic energy as Joule heating. On approaching Io, some of the corotating plasma is absorbed by the satellite while the rest is directed around the sides to be accelerated downstream of Io back to corotation by the magnetic field.

(ii) Voyager observations of the interaction

Although there is no way of directly measuring the conductance of Io, the Voyager plasma and magnetic field measurements have provided considerable evidence of Io's interaction with the magnetosphere. When the Voyager 1 spacecraft passed directly beneath Io the magnetometer measured a magnetic field perturbation which strongly suggests field-aligned currents were flowing from Io (Ness et al., 1979; Acuña et

al., 1981). Figure 28 shows the geometry of the currents that would produce magnetic perturbations consistent with the data. The Alfvénic Mach angle subtended by the Alfvén wings with respect to the background field suggests a Mach number of $0.1 < M_A < 0.25$ depending on the shape and size of the currents used in the model (Acuña et al., 1981; Southwood et al., 1980).

Figure 20 shows shows some of the positive ion spectra obtained by the plasma experiment on the Voyager 1 outbound leg. The high fluxes measured at ~1510 UT correspond to the passage of the spacecraft beneath Io. Unfortunately, the plasma detectors were not pointed in directions favourable for measuring the corotating flow at this time. The plasma flowed obliquely into all sensors which means the detector response function cannot easily be approximated in the analysis of the positive ion data. However, for a plasma of given composition, temperature and bulk speed, the expected fluxes in the different sensors can be calculated using a lengthy computer simulation of the detector response (developed by V. M. Vasyliunas, J. W. Belcher and J. D. Sullivan). The composition and temperature of the plasma observed near Io's orbit on the inbound passage were used by Belcher et al. (1981) to simulate the fluxes into the sensors assuming that the plasma flow was perturbed from corotation by the Alfvén wings emanating from Io. The flow perturbation due to an Alfvén wave is directly related to the magnetic field perturbation $\Delta\vec{B}$ by

$$\frac{\Delta\vec{V}}{V_A} = -\frac{\Delta\vec{B}}{B}$$

where B is the background magnetic field. Therefore, the observed magnetic field perturbations could be used to predict the flow

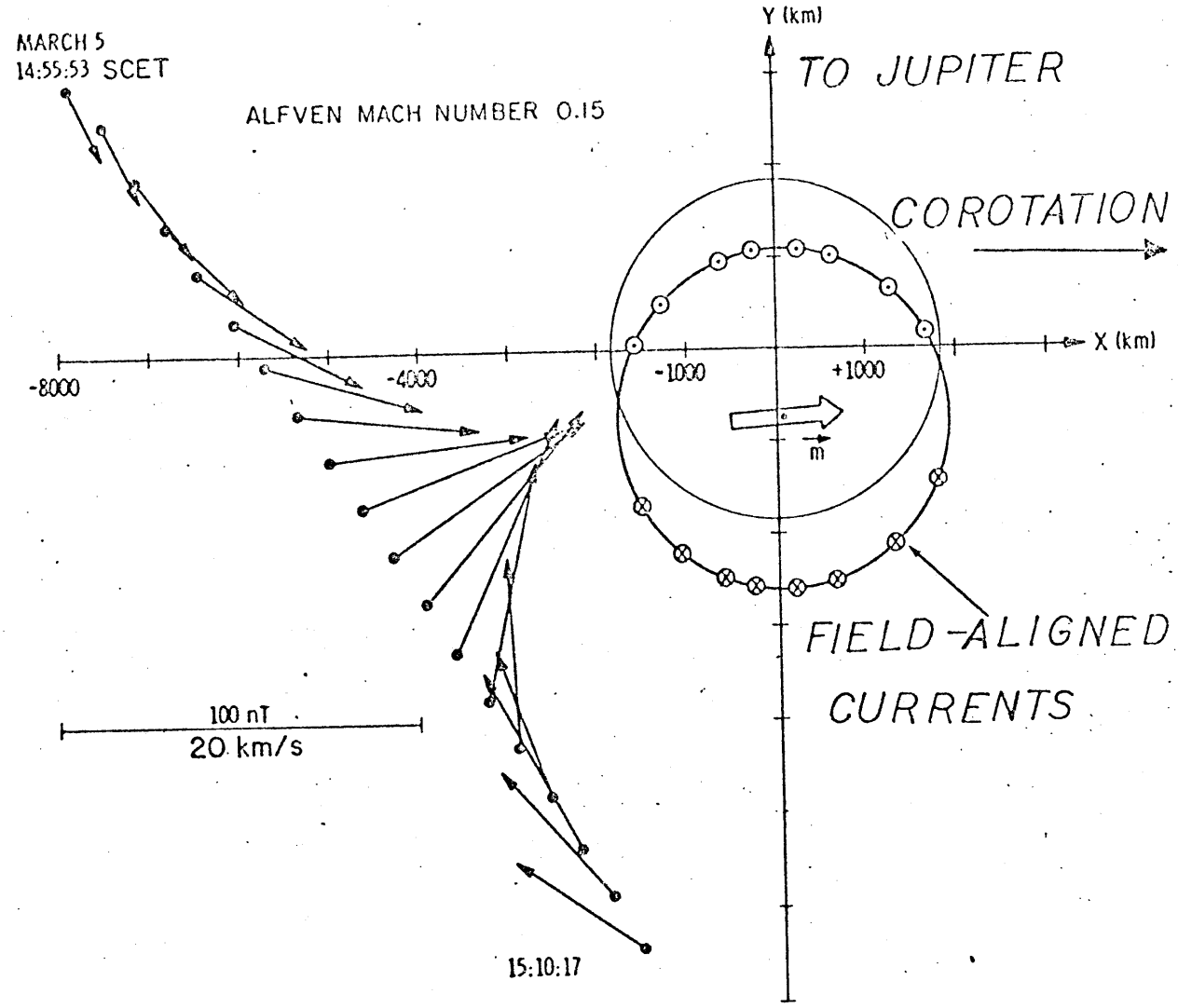

Figure 28. Perturbation magnetic field due to the Io current system as observed by Voyager 1 along its trajectory. Also shown are the position of the equivalent dipole moment of the current system and the current density along a circle of Io's radius (For an Alfvén Mach number of 0.15). The figure is in a plane roughly parallel to Jupiter's rotational equator, ~20,500 km beneath Io. (From Acuña et al., 1981)

perturbations.

The result of this procedure is shown in Figure 29. The predicted fluxes show at least a qualitative agreement with the data. In particular, the fact that the fluxes increase (rather than decrease) is consistent with an Alfvén wave propagating south. A southward propagating wave is to be expected if the wave emanated from Io, 20500 km above the spacecraft. The fit to the plasma data will probably be improved considerably when the spectral analysis techniques have been extended to incorporate a more accurate detector response function. It may then be possible to show whether the observed changes are due solely to Alfvénic perturbations in the plasma velocity and require no changes in ambient densities or temperatures.

Since these measurements confirm then an Alfvén wave triggered by Io, the torus model obtained above from the plasma measurements made during the inbound passage can be used to calculate the propagation of Alfvén waves through the torus from Io to the ionosphere of Jupiter. The total mass density of the plasma in the warm torus can be determined from the energy per charge spectra with few assumptions about composition (see Appendix 1). Therefore the variation in Alfvén speed due to uncertainties in composition (~12%) is less than the effects of the local magnetic field changing in magnitude along the orbit of Io (~20%). The results of fitting the spectrum made at 0859 UT (L=5.93) are tabulated in Table 4 and give a range of values for the local Alfvén speed of $209 < V_A < 295$. The difference between Io's orbital speed and corotation is 57 km s^{-1} so that the Alfvénic Mach number near Io is $0.19 < M_A < 0.2$. Although this range conflicts with the estimate of 0.15 ± 0.01 for M_A from Acuña et al. (1981), Southwood et al. (1981) point out that the

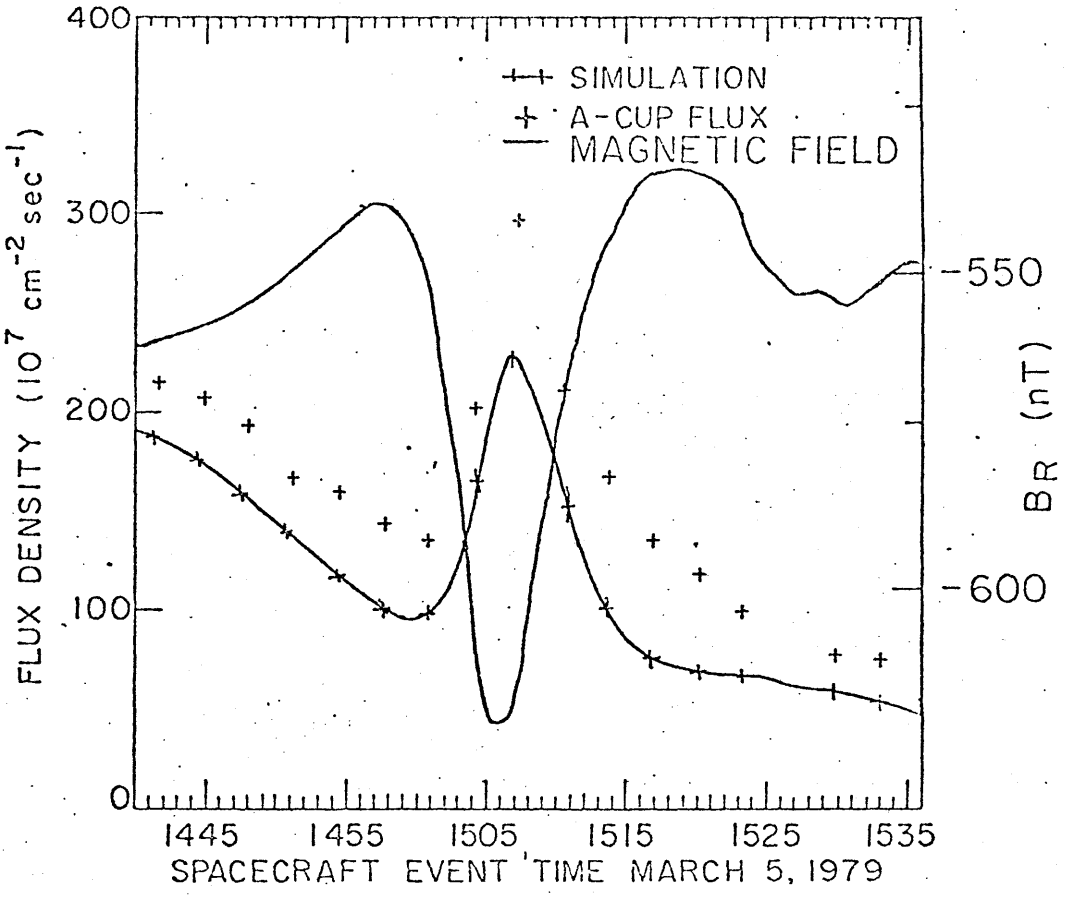

Figure 29. Flux density in the A-cup when Voyager 1 passed close to Io. The theoretical simulation of the flux densities were calculated using the plasma parameters measured during the inbound passage of the Io L-shell and the observed magnetic field perturbation. (From Belcher et al., 1981)

magnetic field measurements are compatable with $0.1 < M_A < 0.25$ when a range of current distributions are allowed.

The propagation characteristics of an Alfvén wave generated at Io have been calculated using the composition and temperature estimates from the spectrum at 0859 UT (5.93 R_J) which are presented in Chapter 3. The local plasma density has been calculated along the field line using the theory described in Appendix III. The local magnetic field strength has been calculated using the O_4 model of Acuña and Ness (1976). The local Alfvén speed, Mach number and Mach angle have then been calculated and plotted in Figure 30 as a function of latitude along the L-shell assuming Io to be in the center of the torus (System III longitude λ = 112° or 292°. Because the density scale height ~1 R_J the Alfvén speed increases by a factor of 10 in 20° from Io's orbital plane (which is essentially equal to Jupiter's rotational equator). At higher latitudes, the assumptions made to calculate the distribution of plasma along the field line are no longer valid. However the asymptotic values of Mach angle θ_A and the total travel time are probably quite realistic because very large proton densities would be required to significantly affect the Alfvén speed.

As the Alfvén wave leaves the equator, the Mach angle drops sharply from a maximum value of ~17° to less than 1° by a latitude of 20°. As the Alfvén wave moves along the field line towards Jupiter the system III longitude of Io increases according to the difference between Jupiter's rotation rate and Io's orbital motion. This angular separation of the longitude of Io and the wave front approaches an asymptotic value of ~3°. This means that if the wave is reflected at the ionosphere of Jupiter, by the time it returns to the orbit of Io the satellite will be

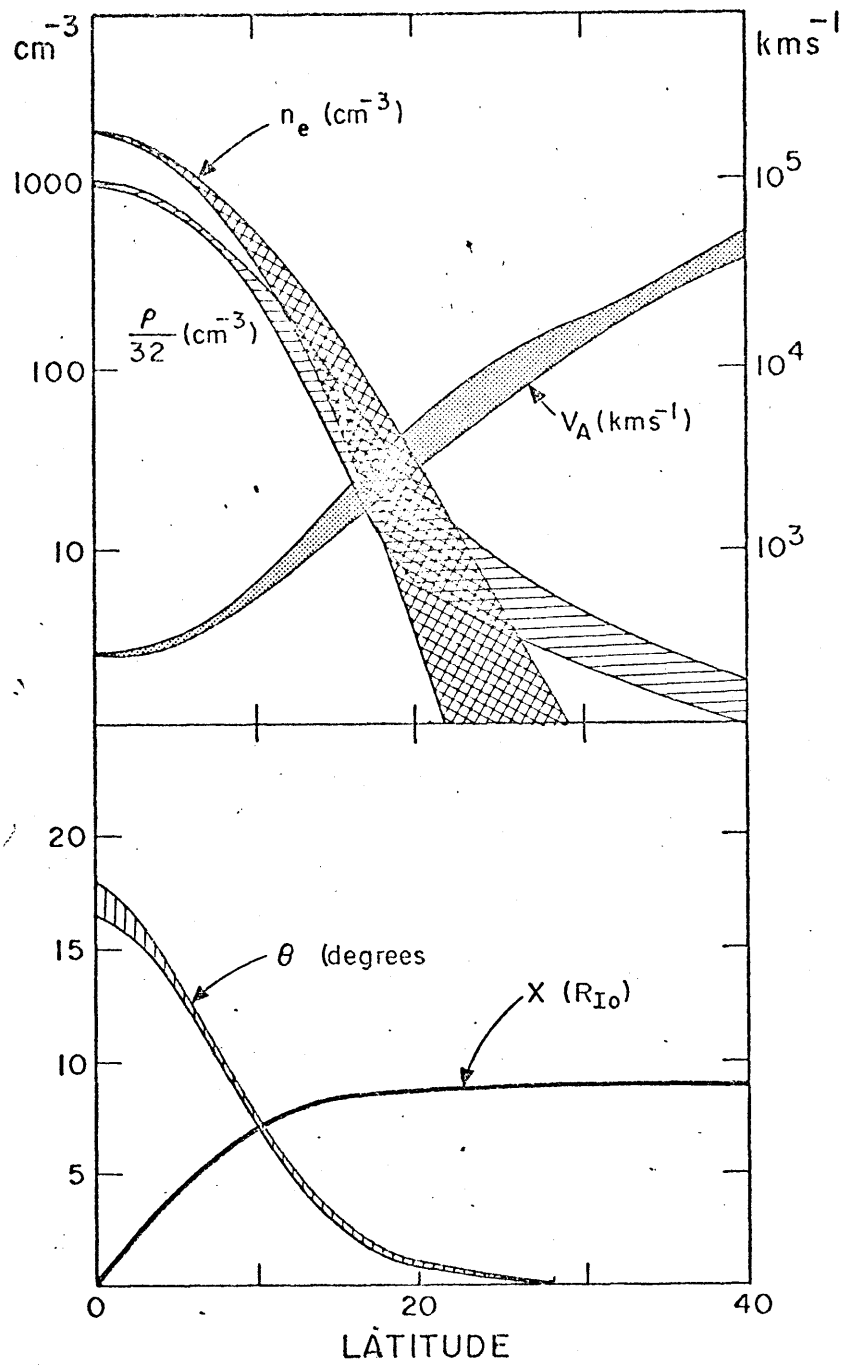

Figure 30. (a) Variation in electron (n_e) and mass (ρ) densities as well as Alfvén speed as a function of latitude for the Io L-shell when Io is at System III longitude of 112°. (b) Variation in Alfvén Mach angle (θ) and the distance moved by Io (in System III) with the latitude of an Alfvén wave front. The width of the curves corresponds to the range in the parameters due to uncertainties in the plasma composition.

6° or 16 Io radii away.

The torus is aligned with the centrifugal equator which is tilted ~7° to Io's orbital plane. This means Io's position varies by ±1 R_J from the center of the torus with System III longitude. At λ_{III} = 22° (202°) Io is below (above) the torus. Figure 31 shows how the various propagation characteristics vary with the System III longitude of Io at the time the Alfvén wave is launched. When Io is south of the torus at λ_{III} ~22° the northwardly propagating wave takes up to ~600 seconds to reach the ionosphere because it has to travel right through the torus while the south bound wave passes through the tenuous plasma below the torus to the ionosphere in as little as 75 seconds. The north/south asymmetry is reversed at λ_{III} ~202°. The azimuthal distance moved by Io in these times correspondingly varies from 3 to 17 Io radii with System III longitude.

The non-dipole components to the magnetic field produce a small difference between the north and south bound legs. The magnetic field is stronger in the north so that the northbound wave takes ~7% longer to reach the ionosphere. In addition, the longitudinal asymmetry of the ionosphere may considerably enhance the asymmetry in the propagation characteristics.

(d) Io - Modulation of Decametric Radio Bursts

Over ~25 years of observing the decametric radio emissions from Jupiter a wealth of information has been gathered about the characteristics of the phenomena; see for example, the review by Carr and Desch (1976). Considerable effort has been made to interpret these and provide models of the source mechanism; see the review by Smith (1976).

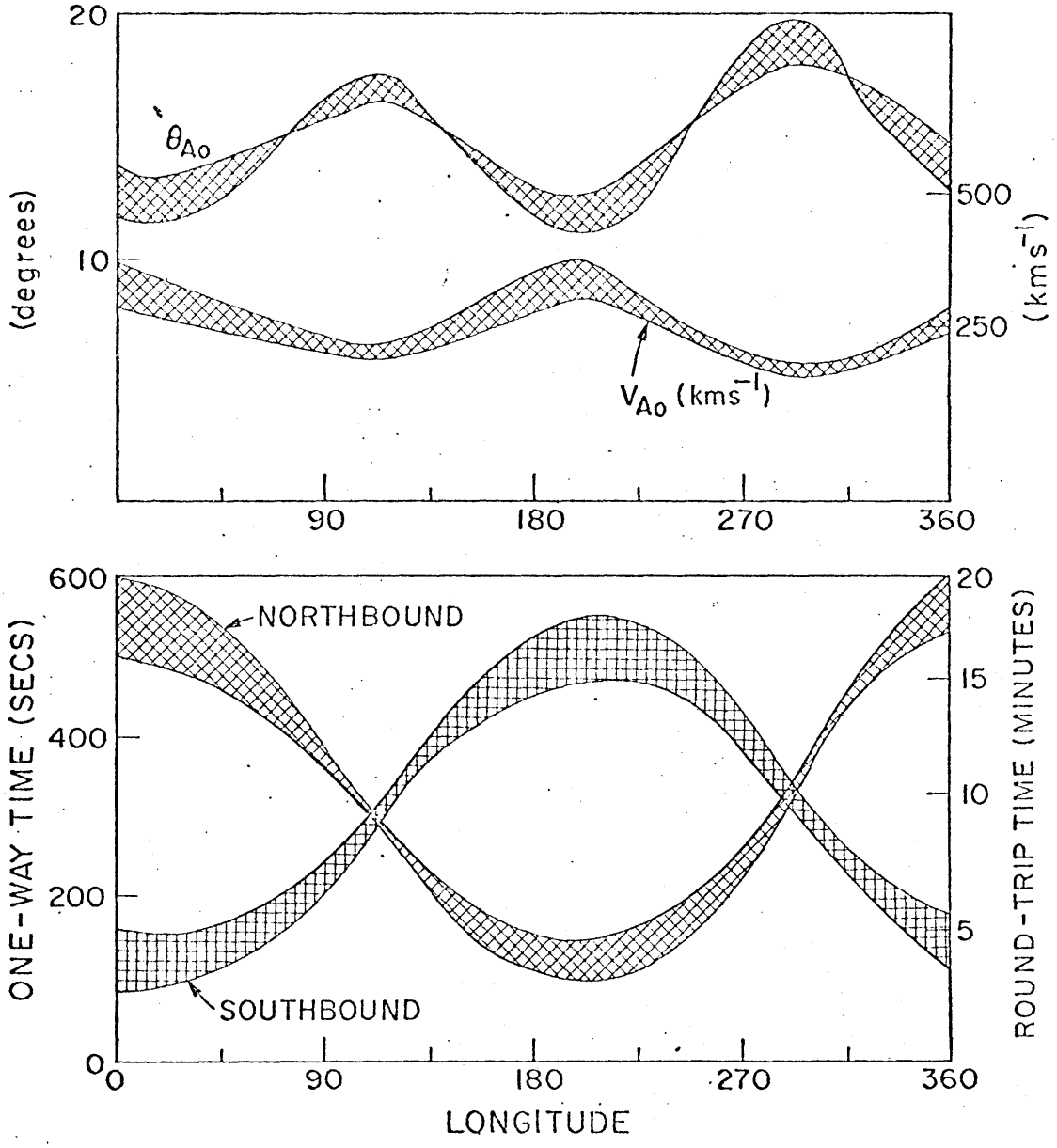

Figure 31. (a) Variation in the local Alfvén speed and Alfvén Mach angle near Io as a fuction of longitude. (b) Variation in the travel time between Io and the ionosphere of Jupiter. The width of the curves corresponds to the range in the parameters due to uncertainties in the plasma composition.

A particularly puzzling problem was to explain why the probability of an emission is very greatly enhanced at the System III longitudes of λ_{III} = 140 and 280 and especially when the phase of Io in its orbit is $\gamma_I \simeq$ ~90° or ~240° from superior conjunction.

The Planetary Radio Astornomy (PRA) experiment on the Voyager spacecraft has contributed some vital clues because not only did the instrument have much better sensitivity and frequency coverage than is possible from Earth, but also the spacecraft's trajectories allowed a large range of viewing geometries that are not possible from Earth. Figure 32a shows some PRA data that was presented by Warwick et al. (1979) to illustrate how the emissions from discrete arcs on frequency-time spectrograms. At high frequencies the emissions occur preferentially near System III longitudes of ~140° and 240° but at lower frequencies the emissions occur at all longitudes. The structures are very similar from rotation to rotation, independent of emission strength, which suggests their shape is due to the geometry of the magnetic field and plasma distribution rather than the source mechanism. The convex ("vertex-early") arcs are associated with the source at λ_{III} ~140° while the λ_{III} ~240 source produces concave ("vertex late") arcs. Warwick et al. (1979) proposed that the arc structure is consistent with a conical emission pattern where the cone angle varies with frequency. The decametric radiation is thought to be emitted just above the local electron gyrofrequency by fluxes of kilovolt electrons precipitating into the ionosphere (Smith, 1976). Therefore the frequency of emission will decrease with decreasing magnetic field strength at source locations farther away from Jupiter along a field line. Goldstein and Theiman (1981) have reproduced most of the arc structure by assuming that the

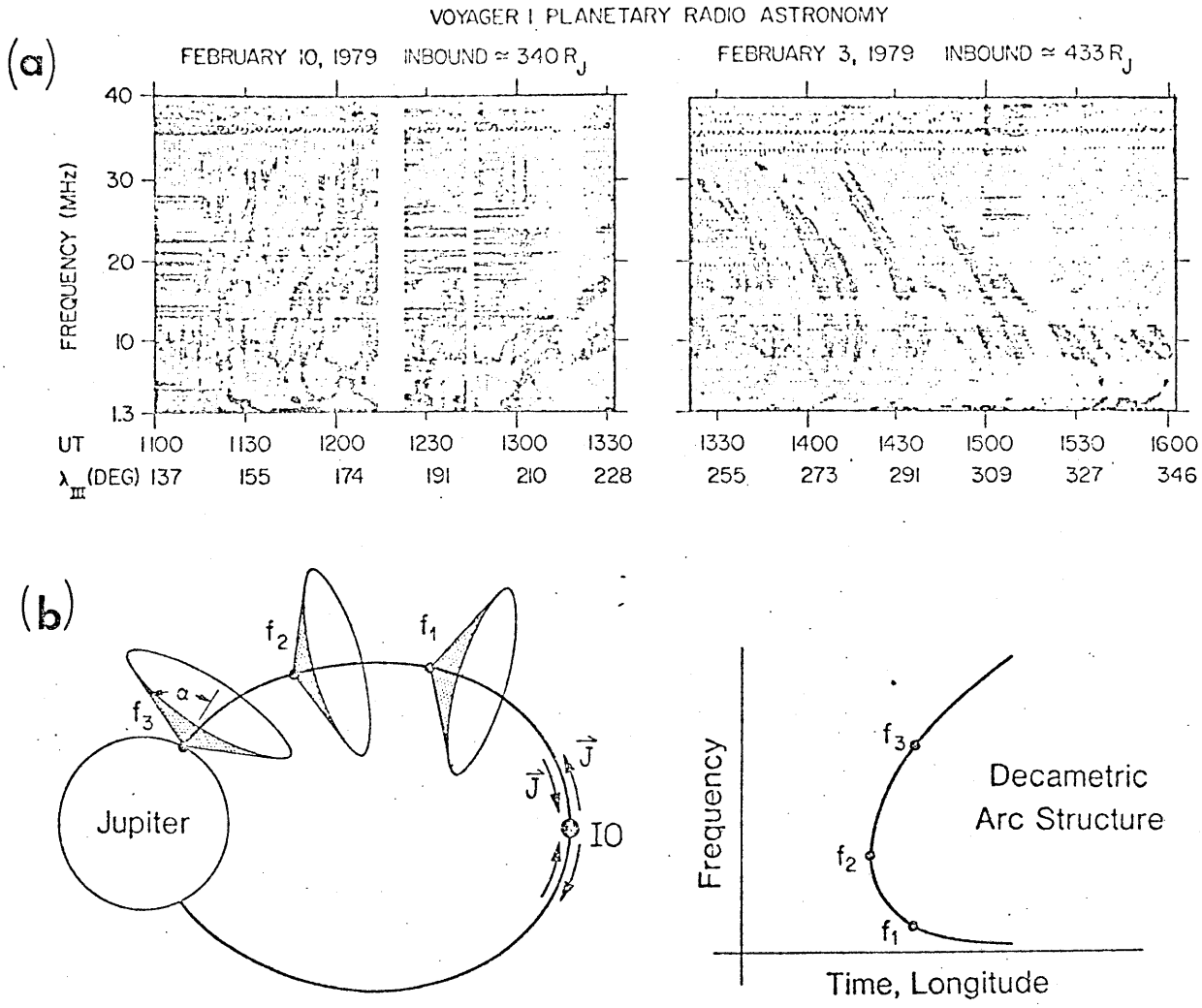

Figure 32. (a) Representative frequency-time spectrographs of decametric arcs observed by Voyager 1 during the approach to Jupiter by the Planetary Radio Astronomy experiment (Warwick et al., 1979).
(b) The arc structure observed above may be explained by the decametric radiation being emitted in cones with half-angle a , which varies with frequency. (From Gurnett and Goertz, 1980)

emission cones are generally wider at higher frequencies but that refraction due to the higher plasma densities nearer the ionosphere causes the emission cones to become narrow again at even higher frequencies. This means the cone angle is ~45° to 65° at high and low frequencies and larger (~80°) in-between. Figure 32b shows how a continuous distribution of sources along a field line that rotates with Jupiter will produce first an vertex-early arc then a vertex-late arc as the emission cones are swept past the observer.

Gurnett and Goertz (1980) have proposed that the occurance of descrete multiple arcs is due to a series of separate standing Alfven waves. The arcs are very narrow, about 3 minutes wide, roughly independant of frequency and spaced by intervals varying from a few to ~30 minutes. Gurnett and Goertz (1980) point out that 3 minutes corresponds to

(3 minutes)/(Io's rotation in System III) x 360° = 0.42°

of System III longitude while Io's diameter subtends

$$\frac{2\ R_{Io}\ (=1820 km)}{2\pi\ a_{Io}\ (=5.9\ R_J)} \times 360° = 0.45°$$

Thus the arc width is in very good agreement with the longitudinal scale size of the Io flux tube. If an Alfvén wave generated near Io just travelled to Jupiter's ionosphere and triggered radio emission there, then there would only be two arcs per rotation, one either side of Io's system III longitude, instead of the 100 or so arcs that are observed. However, the multiple arcs are readily explained if the Alfvén waves are

reflected by Jupiter's ionosphere and bounce between the north and south hemispheres. In Io's reference frame the corotating wave system is swept away producing a three-dimensional standing pattern as illustrated in Figure 33.

Assuming a uniform torus with an Alfvén Mach number of $M_A = 0.15$ Gurnett and Goertz (1980) estimate that if the repeated arcs correspond to multiple reflections of the Alfvén waves at Jupiter's ionosphere then angular separation of successive reflections should be

$$\Delta\phi = 360° \times 2\ell M_A / (2\pi a_{Io})$$
$$\cong 5.8°$$

(Where ℓ is the height of the torus, ~2 R_J; and a_{IO} is the orbital radius, ~6 R_J) This corresponds to a round trip travel time for the Alfvén wave of ~40 minutes which they say will be modulated by Io's position in the torus to produce an average period of ~20 minutes (1200 seconds). Figure 31 shows that models of the torus from the plasma data put the round trip time at 2.5 to 20 minutes (150 to 1200 seconds). However if there is a significant quantity of protons at high latitudes that have come from the ionosphere (as suggested by the dispersion of whistlers in the torus) the round trip time could be larger.

The next question to consider is how many times can the wave be reflected in Jupiter's ionosphere before being completely damped? The power in the current system is $\sim 10^{12}$ watts (Acuña et al., 1981) while the total power emitted as decametric radiation is estimated at 10^8 W (Warwick, 1967) so that if the triggering mechanism had perfect efficiency there would be enough power available for $\sim 10^4$ reflections. On the other hand Gurnett and Goertz (1980) extended the transmission line analogy to estimate the reflection coeficient for the Alfvén wave

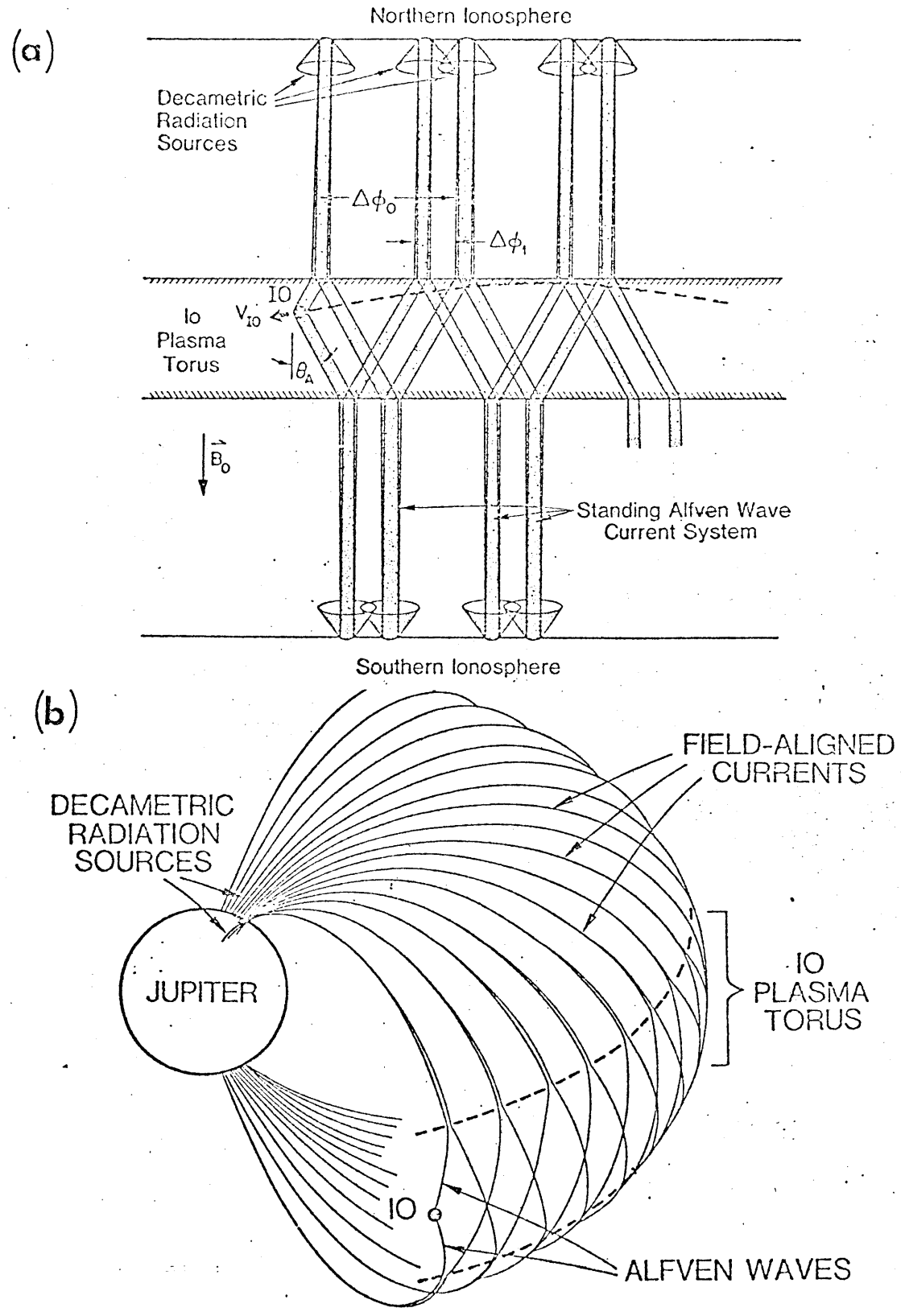

Figure 33. The standing wave pattern formed by Alfvén; waves excited by motion of Io through the plasma torus. (a) Projection on the Io L-shell. (b) Three-dimensional representation.

energy at the ionosphere boundary

$$R = \frac{\Sigma_J - \Sigma_A}{\Sigma_J + \Sigma_A}$$

where Σ_J is the integrated Pederson conductivity of the Jovian ionosphere and Σ_A is the Alfvén wave conductance at the ionosphere. The number of relfections suffered by the wave before its energy is reduced e-fold is then $N \sim \Sigma_J/2\Sigma_A$. Unfortunately the ionosphere conductivity is poorly determined. Estimates range from 0.1 mho (Dessler and Hill 1979) to 2-20 mho (Brice and Ioannidis, 1970). With $\Sigma_A \sim 5.7 \times 10^{-3}$ mho from an ionospheric density of 5×10^4 cm^{-3} and magnetic field strength of 14 G the number of reflections varies from 9 to over 1700. The fact that arcs are observed all the way round Jupiter suggests there must be on the order of 100 reflections. Thus the shape, width and spacing of the arcs seem to be consistent with the decametric emission being controlled by the Alfvén wave current system emanating from Io.

Chapter 6

Conclusions

(a) Summary of results

When Voyager 1 traversed the inner magnetosphere of Jupiter on March 5, 1979, the plasma detector on the spacecraft measured the characteristics of the low energy plasma which forms a dense torus of plasma near the orbit of Io. Energy per charge spectra for positive ions in the range of 10 eV to 6 keV have been analysed for the three main plasma sensors to determine the flow velocity, density and temperature of the plasma. The measurements of the characteristics of the plasma along the spacecraft trajectory have been combined with the assumption of azimuthal symmetry and theoretical expressions for the distribution of plasma along a magnetic field line to construct a two-dimensional map of plasma density.

The main features of the inner magentosphere that have been determined from the Voyager plasma measurements are:

A) There are two distinct regions of plasma torus. In the inner part ($< 5.5\ R_J$) the cold (< 1 eV) plasma is closely confined to the centrifugal equator (density scale height of $\sim 0.2\ R_J$). Between 5.5 and 7.5 R_J the plasma is warm (~ 50 eV) and forms a thick torus near the centrifugal equator (density scale height $\sim 1\ R_J$).

B) The ions in the inner cold region corotate with Jupiter; are of low ionisation state (predominately S^+ with some O^+); and appear to have the same temperature. The low temperature (< 1 eV) and high densities ($\sim 10^3\ cm^{-3}$) imply the ions probably are in thermodynamic equilibrium with

electrons, though no measurements of the electron temperature could be made in this region. The in situ measurements of S^+ ions are consistant with the ground-based observations of emission at optical wavelengths corresponding to forbidden transitions of the S^+ ion.

C) When the ions in the warm torus are assumed to be corotating and have the same temperature, the spectral measurements suggest the ions are of higher ionisation states (S^{2+} and S^{3+} with probably little S^+; O^{2+} as well as O^+) which is consistant with the observations of ultraviolet emission from this region. The ionic composition derived from plasma measurements in the warm torus can be matched with the composition determined by Voyager Ultraviolet Spectrometer investigators, but there are large uncertainties in the results of both experiments. Most of the electrons are a factor of 3 to 5 colder than the ions in this outer region.

D) The transition region between the two parts of the torus is very narrow (0.1 RJ at 5.5 R_J). In this region the plasma temperature has a very steep gradient of $-7 \times 10^5 K\ R_J^{-1}$. Although the radial profile of local plasma density has a local minimum at 5.5 R_J, the total number of ions in a flux tube does not. The flux tube content decreases either side of the single source region near Io's orbit ($\sim$6 R_J) with a much steeper gradient inward than away from Jupiter. The different gradients either side of the source suggests that plasma diffused outward much more rapidly than inward due to the de-stabilising effect of the strong centrifugal force in the outward direction.

E) The outer boundary of the torus is around 7.5 R_J where the plasma density sharply drops and the gradient in the radial profile of flux tube content steepens. The change in gradient may be due to the

outward radial diffusion of plasma being inhibited by energetic ring current particles which diffuse inward until they reach the torus where they are scattering into the auroral region of Jupiter's ionosphere.

F) The sulphur and oxygen ions found in the torus are consistant with the dissociation and ionisation of about 1 tonne per second of SO_2 (from the volcanoes on Io) if oxygen atoms are preferentially lost (for example, by charge exchange processes) or sulphur atoms are preferentially ionised (possibly due to their lower ionisation energy) to leave roughly equal quantities of sulphur and oxygen ions.

G) The kinetic temperature of the bulk of the plasma throughout the torus is well below that expected if the ions were picked up by the magnetic field and had retained gyro-speeds equal to the speed of corotation. However, there may be evidence from high energy tails in the energy per charge spectra that a small fraction of the ions do have gyro-speeds of roughly the corotational value. The presence of these "hot" ions suggests new plasma has recently been ionised in a region where the magnetic field is relatively unperturbed (If ionisation took place in the close vicinity of Io where electric currents strongly perturb the magnetic field then the new ions would be much cooler).

H) The perturbations of the magnetic field and plasma flow that were observed when Voyager 1 passed beneath Io are consistant with an Alfvénic disturbance travelling along the magnetic field away from the satellite. It has been proposed that decametric radio bursts are emitted in conical beams when the Alfvén waves reach the ionosphere of Jupiter. The arc-like structure observed in the frequency-time spectrograms at decametric wavelengths can then be explained by a variation in cone angle with frequency while the width and spacing of the arcs roughly correspond

to the diameter of Io and the time the Alfvén wave takes to reach the ionosphere respectively. Multiple reflections of the Alfvén wave in the ionosphere at the northern and southern ends of the magnetic field line would produce repeated arcs similar to those observed. The emission is modulated by the magnetic longitude of Io because the characteristics of the Alfvén waves vary as the satellite moves between the center and edge of the torus (due to the 7° tilt of the cnetirfugal equator from the orbit of Io).

(b) Important remaining questions

There are many detailed observations that have not yet been explained. However before the details are understood there are three basic questions to be answered:

(i) Where is the plasma initially produced? Is there a large neutral cloud that is ionised or is there considerable ionisation in the vicinity of Io due to magnetospheric particles bombarding the satellite's atmosphere? How much of the magnetospheric plasma comes from Jupiter's ionosphere or the solar wind?

(ii) What is the thermal state of the plasma in the warm torus? Is there equipartition of energy between a) the different ionic species b) the electrons and ions, despite the fact that the residence time is short and collisions are infrequent?

(iii) What is the nature of the interaction between Io and the magnetospheric plasma? Is Io's ionosphere produced by the magnetospheric plasma ionising Io's atmosphere? To what extent are the plasma flow and magnetic field perturbed near Io?

(c) Further studies

(i) Further analysis of the Voyager plasma data

When the full response of the sensors can be included ion the spectral analysis the data obtained on the outbound traversal of the inner magnetosphere can then be analysed. Because the spacecraft was at different magnetic longitudes and latitudes during the two traversals it will be possible to test the assumption of asimuthal symmetry and see if the plasma is distributed along magnetic field lines according to theory. Of particular interest on the outbound passage are the data obtained when the spacecraft passed close beneath Io. It will be interesting to see if there is a perturbation in density as well as flow direction near the satellite.

(ii) Photometry

The best prospect for learning more about the inner magnetosphere is probably in ground-based observations of emission from ions in the torus at the various forbidden spectral lines. Recent advances in observational techniques make it relatively easy to obtain high resolution images of the emission regions. With these it will be possible to moniter the spatial and temporal variability of the plasma in the torus which may be the key to answering the three questions above.

(iii) Finally, there is always hope of future missions to Jupiter, preferably with orbiting spacecraft and a full complement of magnetospheric experiments.

Appendix I

Analysis of Multi-Peaked Spectra

a) The Measurements

The Faraday cup is an electrostatic device which measures ion charge flux as a function of energy per charge. For positive ions with a distribution in velocity space described by the function $f(\vec{v})$ the currents measured by a Faraday cup are related to $f(\vec{v})$ in the following way (see Vasyliunas, 1971, and Belcher et al., 1980). If $\hat{n}$ is the unit normal to a given cup aperture, a positively charged particle will reach the collector plate if V_n, its component of velocity parallel to $\hat{n}$, satisfies

$$\frac{1}{2} A m_p V_n^2 > e Z^* \phi \qquad (1)$$

where e and m_p are the charge and mass of a proton; Z^* and A are the charge and mass numbers of the ion and ϕ is the retarding potential between the modulator grid and the spacecraft (see Figure 34). Suppose $\{\phi_j\}$ represents the set of contiguous voltages of the K energy channels (j = 1 to K+1), with ϕ_j the lower voltage of the j-th channel. Let $\{v_j\}$ represent the corresponding set of velocities where

$$v_j = \left(\frac{2 e Z^* \phi_j}{A m_p} \right)^{1/2} \qquad (2)$$

The average and incremental velocities for the j-th channel are defined by

$$\bar{v}_j = \left(\frac{v_j + v_{j+1}}{2} \right)$$

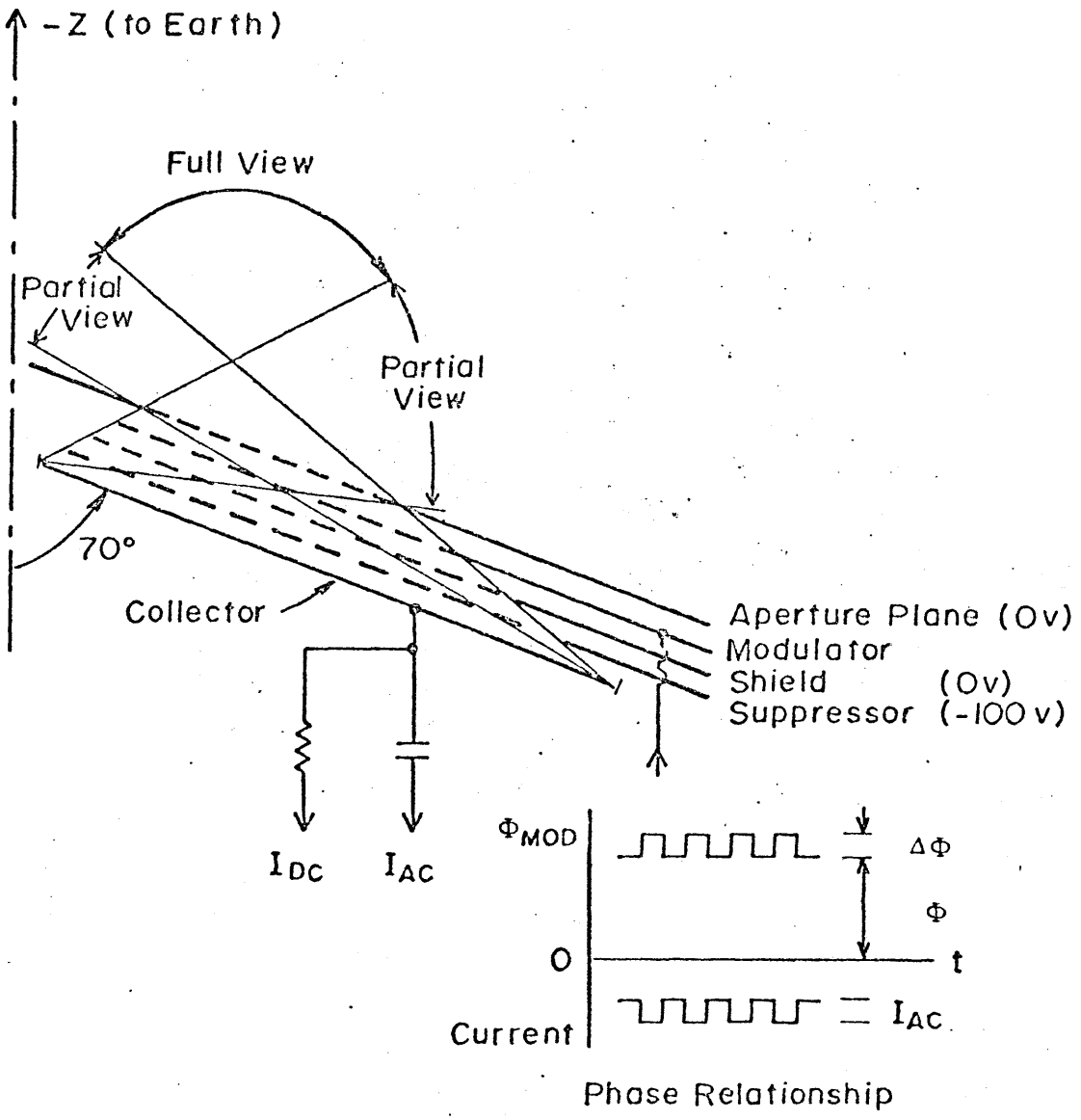

Figure 34. A cross-sectional view of the grid structure (schematic) for one of the three main sensors of the plasma detector. (From Bridge et al., 1977). For clarity only a single shield grid and a single modulator grid are shown. In the actual sensor six shield grids are used to obtain sufficient electrical isolation between the modulator and collector, and three grids are used for the modulator so that the retarding potential is defined to 0.5%.

and

$$\Delta V_j = V_{j+1} - V_j$$

Then the modulated AC current (I_{AC} in Figure 4) in the j-th energy channel corresponding to a modulator voltage varying between ϕ_J and ϕ_{j+1} is

$$I_j = Z^* e A_{eff} \int_{V_j}^{V_{j+1}} V_n \, dV_n \int_{-\infty}^{\infty} dV_{t1} \int_{-\infty}^{\infty} dV_{t2} f(\vec{V}) \, G(V_n, \hat{n}) \tag{4}$$

where A_{eff} is the effective area of the aperture; $\hat{t}_1$ and $\hat{t}_2$ are mutually perpendicular unit vectors which are orthogonal to $\hat{n}$ and $G(\vec{v},\hat{n})$ is the response function of the sensor. In this preliminary analysis the response function has been taken as unity so that

$$I_j = Z^* e A_{eff} \int_{V_j}^{V_{j+1}} V_n \, F(V_n) \, dV_n \tag{5}$$

where $F(v_n)$ is the "reduced" one-dimensional distribution function

$$F(V_n) = \int_{-\infty}^{\infty} dV_{t1} \int_{-\infty}^{\infty} dV_{t2} \, f(V_n, V_{t1}, V_{t2}) \tag{6}$$

This means that each detector samples the full distribution function in a

manner which is differential for the velocity component parallel to the detector normal and integral for the velocity components perpendicular to the detector normal. Figure 35 is a schematic illustration of this concept for a model proton distribution function with a pronounced heat flux.

In our present analysis the distribution functions of the positive ions are assumed to be characterized by a convected, isotropic Maxwellian function. Therefore, the "reduced" one-dimensional distribution function of each ionic species of density n_i, thermal speed w_i and bulk velocity $\vec{V}_i$ is

$$F_i(v_n) = \frac{n_i}{\omega_i \sqrt{\pi}} \exp\left[- \frac{(v_n - V_{in})^2}{\omega_i^2} \right] \tag{7}$$

where V_{in} is the component of the bulk flow along the cup normal $\hat{n}$. Thus for a multi-species plasma the current in the j-th energy channel becomes

$$I_j = e A_{eff} \sum_i \int_{v_j}^{v_{j+1}} v_n Z_i^* F_i(v_n) \, dv_n \tag{8}$$

Substituting $F_i(V_n)$ from above, this expresion can be integrated to give

$$I_j = \frac{e A_{eff}}{2\sqrt{\pi}} \sum_i Z_i n_i \left[\omega_i \left\{ e^{-u_j^2} - e^{-u_{j+1}^2} \right\} + \sqrt{\pi} V_{ni} \left\{ \mathrm{erf}(u_{j+1}) - \mathrm{erf}(u_j) \right\} \right]$$

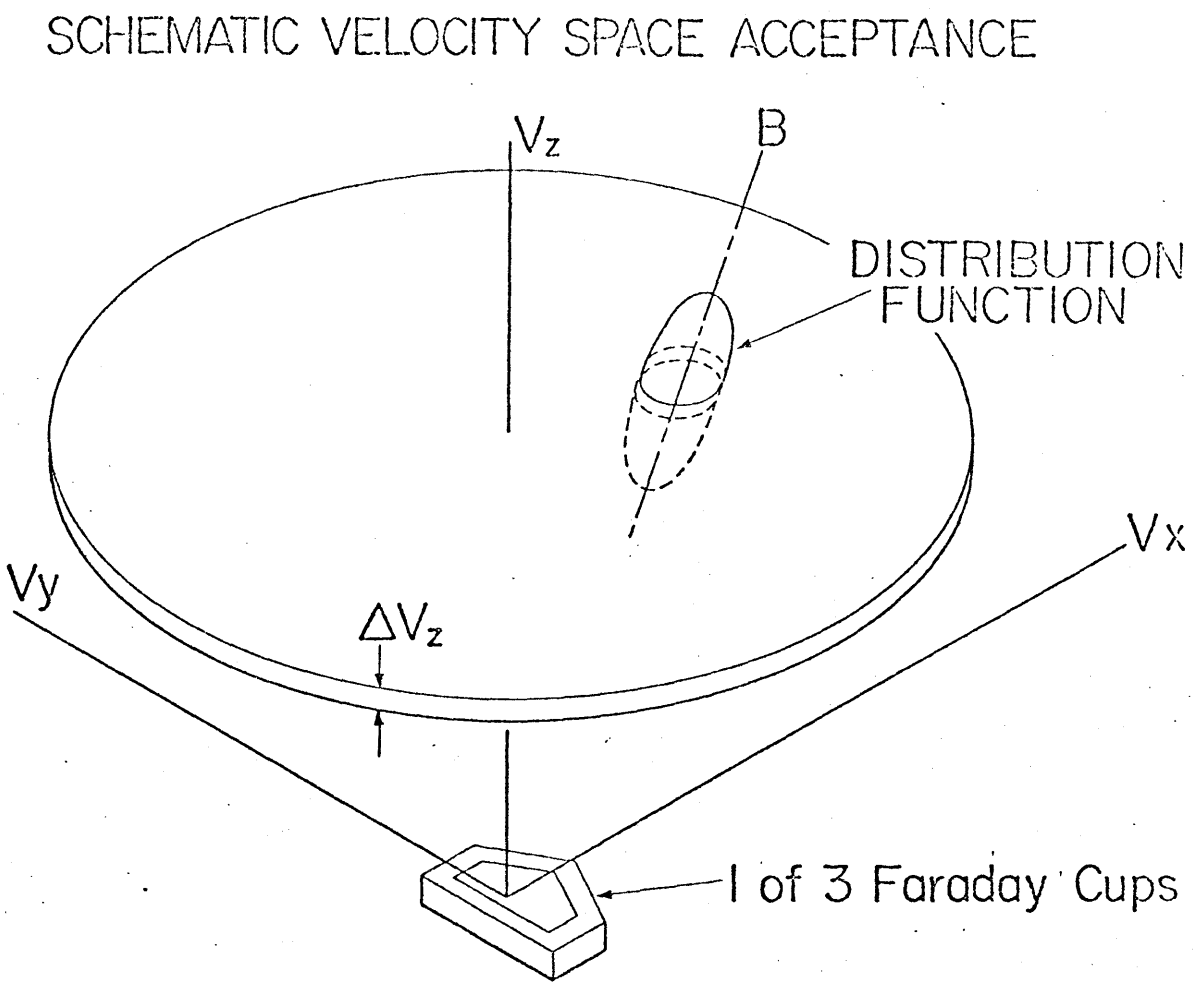

Figure 35. Schematic velocity space acceptance of the main sensors of the Voyager plasma instrument. Only particles within a narrow range of V_z (component of velocity normal to the cup aperture) are accepted into the sensor. The x and y components of velocity of the accepted particles can be within a wide range. This means the three-dimensional distribution of ions in velocity space is sliced differentially in the direction normal to the cup aperture and integrated in the x and y directions.

where

$$u_j = \left(\frac{v_j - V_{in}}{\omega_i}\right) \quad \text{and} \quad u_{j+1} = \left(\frac{v_{j+1} - V_{in}}{\omega_i}\right) \tag{9}$$

The above function is used to fit the measured currents (in a least squares sense) and hence find the plasma parameters n_i, w_i, V_{in} for each species.

Before the details of the full fitting procedure is described it should be realized that there are quantities that can be estimated independent of assumptions about composition. Because the velocity interval ΔV_j is much less than the average channel velocity v_j equation can be approximated by

$$I_j \cong e A_{eff} \sum_i Z_i^* v_j \Delta v_j F(v_j) \tag{10}$$

Summing over all the channels gives

$$\sum_j I_j \cong e A_{eff} \sum_i Z_i^* \left[\sum v_j \Delta v_j F(v_j)\right] \tag{11}$$

Using the fact that $\Delta v_j \ll v_j$ again means

$$\sum_j I_j \cong e A_{eff} \sum_i Z_i^* \left(\int_{-\infty}^{\infty} v_n F_i(v_n) d v_n\right)$$

$$= e A_{eff} \sum_i Z_i^* V_{in} n_i \tag{12}$$

so that if V_{in} is known (e.g., taken to be the value corresponding to rigid corotation) then the total positive charge density n_+ is given by

$$n_+ = \sum_i Z_i^* n_i = \frac{\sum_j I_j}{e A_{eff} V_n} \tag{13}$$

which is completely independent of any assumptions of composition. In addition, if there are well-resolved peaks in the spectrum at velocities $V_i=(A/Z^*)_i V$ then the mass density $n_m = \sum_i n_i A_i$ as well as the charge density n_+ can be determined given the ratio $(A/Z^*)_i$ without knowing the independent values of A_i or Z_i^*. Since

$$\sum_i n_i A_i = \sum_i n_i Z_i^* \left(\frac{A}{Z}\right)_i \tag{14}$$

The quantity that has been plotted as "reduced distribution function" in the figures showing spectra has been determined as follows. Equation (10) relates the current in the jth channel to the one-dimensional distribution function $F(v_j)$. The voltage width of each channel is given by

$$\Delta\phi_j = \frac{m_p}{e}\left(\frac{A}{Z^*}\right)_i V_j \Delta V_j \tag{15}$$

This is combined with equation (10) to give a "reduced distribution function"

$$f_j = \frac{Z^{*2}}{A} F(v_j) = \frac{I_j}{\Delta \phi_j} \left(\frac{m_p}{A_{eff}\, e^2} \right) \qquad (16)$$

which has units of m^{-4} s.

b) Parametric least squares fitting procedure

When the multiple peaks in a spectrum are well-separated then it is possible to fit each peak separately and determine independent values of V_{in}, n_i and w_i for each ionic species. However for peaks that are less well-resolved it is necessary to constrain the fitting function by reducing the number of free parameters. Otherwise the parameters are found to be interdependent and the solution non-unique. The number of variable parameters can be reduced either by constraining the bulk velocity of the ions or by making some assumption about the thermal state of the plasma. A summary of the different conditions that have been used to fit spectral peaks according to the degree of resolution is given in Table 9.

When the plasma flow direction was close to the symmetry axis of the main sensor good spectral measurements were made in all three cups (A, B and C). When the three spectra contain well-resolved peaks it was possible to compare separate determinations of n_i and w_i for each species as well as combine the three components of bulk velocity along the three cup normals to construct the complete bulk velocity vector $\vec{V}$. Alternatively the 3 spectra could be fitted simultaneously which provided a more accurate determination of $\vec{V}$ when the peaks were resolved and greatly reduced the uncertainties in the density determinations.

The method used to fit the parametric function I_j^P ($\vec{V}_i$, n_i, w_i) in

Table 9 Summary of conditions and free parameters included in different fit procedures

	Description	Free Parameters	Number of Parameters	Degrees of Freedom	Comments
	Independent velocity components, densities and thermal speeds.	V_{in}, n_i, ω_i for each species	$3N^+$	$M - 3N^+$	When each spectral peak is separate.
SINGLE SENSOR	Common velocity component, independent densities and thermal speeds.	V_n, n_i, ω_i	$2N + 1$	$M - 2(N+1)$	When the spectral peaks are well-resolved and a plausible choice of A/Z^* values suggest the different ionic species have the same bulk motion.
	Velocity component fixed, independent densities and common thermal speed.	n_i, ω	$N + 1$	$M - N + 2$	When spectral peaks strongly overlap, the bulk velocity of the plasma is assumed (e.g., rigid corotation) and the ionic species are assumed to have the same thermal speed.
	Velocity component fixed independent densities and common temperature	n_i, T	$N + 1$	$N - N + 2$	Same as above except the ionic species are assumed to have a common temperature.
	Independent velocity components, densities and thermal speeds	V_i, n_i, ω_i for each species and	$3N$ for each of 3 cups	$M - 3N$ for each of 3 cups	When there are well-resolved peaks in 3 cups and each spectrum is fitted separately.
THREE SENSORS	Common velocity vector independent densities and thermal speeds.	$\vec{V}$, n_i, ω_i	$2N + 3$	$3M - 2N + 4$	When there are well-resolved peaks in 3 cups and the 3 spectra are fitted simultaneously
	Velocity vector fixed, independent densities and common thermal speed	n_i, ω	$N + 1$	$3M - N + 2$	When there are strongly overlapping spectral peaks in 3 cups and the 3 spectra are fitted simultaneously.
	Velocity vector fixed, independent densites and common temperature	n_i, T	$N + 1$	$3M - N + 2$	Same as above

*N = number of ionic species

+M = number of data points in each spectrum

equation (9) to the measured currents I_j^m is a standard iterative linearized last squares procedure. The computer code used to analyze the data come from of Bevington (1969) but the method is essentially the same as methods generally applied to geophysical inverse boundary value problems. The following is a brief outline of the method in Bevington's nomenclature.

Let y be the fitting function so that the goodness of fit between the first guess values y_{oj} and the measurements y_j^m is given by the chi-square

$$\chi^2 = \sum_j \frac{1}{\sigma_j^2} \left(y_j^m - y_{oj} \right)^2 \tag{17}$$

where σ_j is the estimated error in the jth measurement.(The values of χ^2 in the tables above have been normalised by dividing χ^2 by the degrees of freedom ν = # of measurements - # of free parameters).

The first order expansion of y in parameters a_i gives

$$y_j = y_{oj} + \sum_i \frac{\partial y_{oj}}{\partial a_i} \delta a_i \tag{18}$$

To minimize χ^2, y_j above is substituted into equation (17) and $(\partial\chi^2/\partial\delta q_k)$ set to zero which yields a set of simultaneous equations:

$$\beta_k = \sum_i \left(\delta a_i \, \alpha_{ik} \right) \tag{19}$$

where

$$\beta_k = \sum_j \left\{ \frac{1}{\sigma_j^2} \left(y_j^m - y_{oj} \right) \frac{\partial y_{oj}}{\partial a_k} \right\} \tag{20}$$

$$\alpha_{ik} = \sum_j \left\{ \frac{1}{\sigma_j^2} \left(\frac{\partial y_{oj}}{\partial a_i} \quad \frac{\partial y_{oj}}{\partial a_k} \right) \right\} \tag{21}$$

which is solved

$$\delta a_i = \sum \beta_k \left(\alpha\right)^{-1}_{ik} \tag{22}$$

The gradient expansion algorithm of Marquardt hastens the convergence by directing the search for new parameters in the direction of steepest gradient on the χ^2 surface in parameter space. This is done by weighting the diagonal elements of the curvature matrix α:

$$\alpha'_{ik} = \alpha_{ik} \left(1 + \lambda \delta_{jk}\right) \tag{23}$$

The factor λ can be large to start with if the initial guess is crude or if there is little confidence in the appropriateness of the fitting function. If convergence is rapid then λ is subsequently reduced. Bevington's recommended starting value of 0.001 was used in this analysis.

c) Errors and resolution

The formal error σ_{ai}^2 in the determination of the parameter a_i is given by the diagonal elements of the matrix $(\alpha)^{-1}_{ii}$ so $a_i = a_i \pm \sigma_{ai}$. However, this formal error is only a true representation of the uncertainties in the derived parameters when χ^2 is close to unity and the off-diagonal elements of $(\alpha)^{-1}$ are small.

A better indication of the independence of the parameters and consequent uniqueness of the solution is given by the resolution matrix

$$R = (\tilde{A}A)^{-1}\,\tilde{A}A \qquad (24)$$

where $A_{ij} = \alpha'_{ij}$

If the diagonal elements of a row (or column) are close to unity and the off-diagonals close to zero then the corresponding parameter is well-resolved. If the off-diagonals are large then that parameter is not well-determined by the measurements or the model used to make the fit is inappropriate. If the elements of the nth row of R are consistently larger than other rows then the fit is particularly sensitive to the nth parameter. For example with well-resolved spectra such as the one shown in Figure 11 the resolution matrix showed that the fit is most sensitive to the velocity components. On the other hand when a spectrum with a single broad peak is fitted assuming co-rotation and a common temperature or thermal speed then the resolution matrix shows that the fit is far more sensitive to the value of the single thermal parameter than the densities of any of the ionic species.

APPENDIX II

Discussion of the assumptions made in the data analysis

There are several assumptions made in this analysis about the measurement technique as well as about the ambient plasma conditions during the measurements. Some of these assumptions need some discussion and justification. They will be treated as separate topics: (a) The sensor response function, (b) Spacecraft charging,

(a) Sensor response function

The attempt to make a detailed description of the motion of charged particles in the electric field between the grids and collector plate of each Faraday cup is an extensive and complex task. Considerable successes have been achieved firstly by V. Vasyliunas using numerical techniques and more recently S. Olbert has developed analytical expressions for the response function. However, both methods require very lengthy calculations so that the first analyses of the Voyager measurements have been restricted to sections of the data set where the response function can be assumed to be close to unity.

When the plasma has a large sonic Mach number (i.e., the bulk speed is much greater than the thermal speed) then the distribution function can be approximated by that of an infinitely cold beam (i.e. a delta function). This means that for cold plasma flowing at small angles of incidence to the sensor normal the response function can be calculated as the fraction of the aperture that is projected onto the collector plate along the flow direction. The response function then just depends on the bulk velocity vector $\vec{V}$ and the cup normal $\hat{n}$ so that $G(\vec{v},\hat{n})$ in equation (4) becomes $G'(\vec{V},\hat{n})$ which can be taken outside the integration. In fact,

the only parameters that are sensitive to the response function in this case are the densities n_i which can be corrected after the fitting procedure so

$$n_i(real) \cong \frac{n_i(fit)}{G'(\vec{V}, \hat{n})} \tag{1}$$

When the flow direction is far from the cup normal the effects of oblique incidence to the grid system become important connections to the geometrical response and the above approximation is no longer valid. In practice, S. Olbert's calculations suggest that for Mach numbers greater than ~3 the geometric response does not deviate from his "full" response by more than ~10% for angles of incidence up to ~60° from the cup normal.

(b) Spacecraft charging effects

As shown at the beginning of Appendix I the energy range of particles contributing to the measured AC current for a particular channel depends on the potential between the modulator grid and the collector plate. Although the width of the energy channel is strictly controlled by the voltage modulator the absolute value of the potential can only be determined if the collector plate is well "grounded". The question of what is "ground" potential for a spacecraft is an issue that has caused much controversy since probes were first sent into space plasmas. The ground potential is determined by the net electric charge on the surface of the spacecraft. A net charge will be accumulated if there is a difference in the total positive and negative charge fluxes impinging on (or leaving) the spacecraft. As the spacecraft is made

largely out of metal the net charge is spread fairly uniformly over the conducting surfaces and the resulting potential between the surrounding plasma and the surface is roughly the same all over the spacecraft. The charge fluxes probably do not vary over the period of a measurement (< 31 seconds) so that "ground" potential may be assumed to be a constant for each spectrum.

If the spacecraft acquires a small potential (ϕ_0) with respect to the surrounding plasma the positive ion measurements are affected as follows. The set of contiguous voltages (ϕ_j) discussed in the beginning of Appendix I will become ($\phi_j + \phi_0$) and the corresponding set of velocities (v_j) become

$$v_j = \left[\frac{2eZ^*}{m_p A} (\phi_j + \phi_0) \right]^{1/2} \qquad (2)$$

This means that the velocity corresponding to the center of a peak in the energy per charge spectrum is given by

$$V = \frac{2e}{m_p} \frac{Z_i^*}{A_i} (\phi_j + \phi_0) \qquad (3)$$

$$= V_n^2 + \frac{2e}{m_p} \frac{Z_i^*}{A_i} \phi_0$$

where V_n is the component of the plasma bulk velocity in the direction of

the cup normal. Therefore an estimate of the spacecraft "ground" potential ϕ_0 can be made if there is a linear variation of V^2 with Z^*/A. For the spectrum made at 1120 UT (Figure 11) in the cold torus separate determinations of the velocity components for three species with A/Z^* equal to 8, 16 and 32 suggested the spacecraft was slightly negatively charged with a potential of -0.8 (±0.5) volts. The corresponding shift of the peaks was less than 2%. Hence the effect of a spacecraft potential on the determination of plasma properties in the cold region of the torus was considered to be negligible.

In the warm torus where the spectral peaks overlapped a spacecraft potential cannot be determined directly from the positive ion measurements. If the spacecraft potential remains quite small (< 50 volts) then the bulk of the ion distribution function remains within the measurement range of the instrument. However most of the electrons not only have much less energy than the ions but they are also repelled by the negative charge on the spacecraft so that a significant proportion of the distribution function lies outside the measurement range. Therefore an estimate of the spacecraft potential can be obtained in the warm torus from the difference between the total positive charge density of the measured ions and the negative charge density of the measured electrons. Ed Sittler (private communication) has compared the positive and negative charge densities at various radial distances in the torus and determiend that the spacecraft potential is between -10 and -15 volts. Although small compared with the energy per charge of the peak of the distribution function (~125 volts), adding a spacecraft potential of -15 volts can have a significant effect on the determination of composition because the separation between neighboring A/Z^* peaks in the energy per charge

spectrum can be as small as ~50 volts in this region. Additional evidence of a spacecraft potential is shown by comparing spectra from the three cups of the main sensor. If the spacecraft is not charged the different positions (and shapes) of the broad spectral peak in the three spectra in Figure 14 would be rsolely due to the different components of the plasma bulk velocity (assumed to be rigid co-rotation) along the three cup normals. Adding a spacecraft potential has the effect of uniformly shifting the spectra in energy per charge by the same amount for all three cups. Comparing (a), (b) and (c) of Figure 14 shows that when the spectra are fitted simultaneously and assuming rigid co-rotation, a consistently better fit is obtained for all three cups when a -15 volt spacecraft potential is included.

Appendix III

The Distribution of Plasma along Magnetic Field Lines

To determine the variation of plasma density along a magnetic field line in the Io plasma torus several simplifying assumptions have been made. First of all, the system is taken to be in a steady state since the characteristic time-scale for diffusion is on the order of several days while typical bounce periods range from seconds for electrons to a few hours for cold, heavy ions. Forces due to coulomb collisions have also been ignored because except in the coldest and densest part of the torus collisions are relatively infrequent. The electron population has been split into two components: a predominant one of cold thermal electrons and the other a minor proportion of hot electrons. These two components are treated separately and any coupling that must occur between them is taken to be negligible. This steady state picture also ignores any loss of particles due to precipitation into the ionosphere of Jupiter. Such an assumption is probably reasonable in this case except for the hot electrons which may have a significant loss cone.

With the above assumptions, the variation of plasma density along a magnetic field line is determined by the equilibrium pressure gradient which balances the combined forces of gravitation, centrifugal acceleration and a polarization electric field for all electrons and ions. The equation for the balance of field-aligned forces for each electron component is

$$-\frac{dP_e}{ds} = -m_e n_e f + n_e qE \qquad (1)$$

and for each ionic species there is a similar equation,

$$-\frac{dP_i}{ds} = -m_i n_i f - Z_i^* n_i qE \qquad (2)$$

where P_e and P_i are the partial pressures of the electrons and each ionic species (i); m_e, m_i, n_e, n_i, Z_i^* correspond to mass, number density and charge state; s is the distance along the field line; f is the "gravitational" term which includes the effects of centrifugal acceleration and can be determined for the simple geometry of a dipole magnetic field.

These two sets of equations are coupled by the preservation of local charge neutrality

$$n_e^{hot} + n_e^{cold} = \sum_i Z_i^* n_i \qquad (3)$$

To discuss the properties of these expressions, it is helpful to consider the history of their application to magnetospheric studies. Angerami and Thomas (1964) took a single electron component, assumed the ideal gas law and set T_e/T_i to be constant along each field line so Eq. (3) became

$$\frac{dP_e}{T_e} = \sum_i \frac{Z_i^* dP_i}{T_i} \qquad (4)$$

They then used Eq. (4) to couple Eq. (1) and (2) and, hence, relate the parallel electric field E to the "gravitational" term.

$$qE = \left[\frac{\sum_i m_i n_i Z_i^* C_i - m_e n_e}{\sum_i n_i Z_i^{*2} C_i + n_e} \right] f \qquad (5)$$

$$= m^+ f$$

where $C_i = T_e/T_i$ and m^+ is the effective ("temperature-weighted") ion mass.

(For a single ion species and C_i=1, m^+ is simply $m_i/(Z_i^*+1)$). Substituting Eq. (5) back into Eq. (1) and (2) and integrating along the field line yields

$$\frac{n_e(s)\, T_e(s)}{n_i(s_o) T_i(s_o)} = \exp\left[-\int_{s_o}^{s} \frac{m^+}{kT_e}\, fds'\right] \qquad (6)$$

$$\frac{n_i(s)\, T_i(s)}{n_i(s_o) T_i(s_o)} = \exp\left[-\int_{s_o}^{s} \frac{(m_i - Z_i^* m^+)}{kT_i}\, fds'\right] \qquad (7)$$

Angerami and Thomas (1964) used various models of temperature to solve Eqs. (6) and (7) to determine the distribution of plasma from the Earth's ionosphere and away from the planet along dipolar magnetic field lines.

Gledhill (1967) was the first to apply these expressions to Jupiter's magnetosphere. He showed that because of Jupiter's rapid rotation, the centrifugal contribution will dominate the "gravitational" force so that a plasma with a single ionic species will find an equilibrium position at the furthest point along the field line from the rotational axis of the planet. Gledhill also noted that because of the 10° tilt of the magnetic axis with respect to the rotation axis, the equilibrium position is on a

surface between the magnetic and rotational equatorial planes. Hill et al. (1974) have called this plane the "centrifugal symmetry surface." As true gravitational forces can be neglected at distances greater than 2 R_J (Michel and Sturrock, 1974) the equilibrium position of the plasma is found where the sum of field-aligned components of the remaining forces become zero (Siscoe, 1977).

$$F = -\mu \frac{\partial B}{\partial s} - m\Omega^2 r \cos(\theta - \alpha) \cos\delta + Z^* qE \qquad (8)$$

The first term on the right hand side of (8) is the magnetic mirror force where the magnetic moment $\mu = (mV_g)^2/2B$ (V_g is the gyrospeed, Ω is the rotation rate of Jupiter, r the radial distance, δ the angle between the rotational equator and the tangent to the local magnetic field, and α is the angle between the rotational and magnetic equatorial planes, see figure 17). For a dipole geometry the magnetic mirror force can be approximated by

$$F_m = \frac{9}{2} \frac{mV_g^2 \sin\theta}{R_J L \cos^2\theta} \qquad (9)$$

for low magnetic latitudes ($\theta \lesssim 10°$) (Siscoe, 1977). Similarly, the centrifugal force becomes

$$F_c = 3 m\Omega^2 R_J L \cos^2\theta \cos(\alpha-\theta) \cos\delta \qquad (10)$$

The relative importance of these for ions is given by the ratio of the

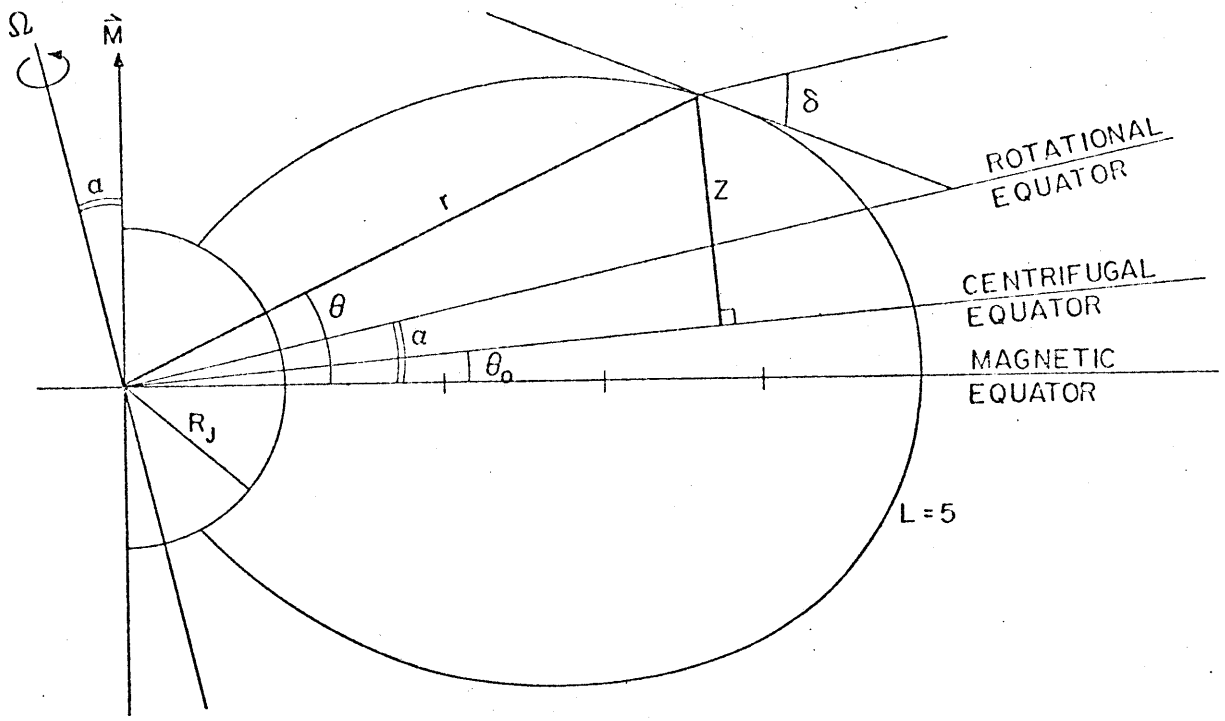

Figure 36. Geometry of a tilted dipole magnetic field in a meridional plane. The angle between the tangent to the local magnetic field line and the projection of the rotational axis onto the meridional plane is shown by δ.

gyro energy K_g to rotational energy, K.

$$\frac{F_m}{F_c} \sim \frac{3K_g}{2K} = \frac{3V_g^2}{2\Omega^2 L^2 R_J^2} \qquad (11)$$

(For full expression see Cummings et al. 1980). Therefore, if the plasma is "hot" and the gyroenergy $K_g = 1/2\ mV_g^2$ is large, then the equilibrium position will be where $\sin\theta = 0$, at the magnetic equator (Goertz, 1976). On the other hand, for cold plasma, the magnetic mirror force can be ignored and the equilibrium position is $\theta_o \simeq \alpha/3$ (Hill et al. 1974). For the Voyager plasma data analysed in this paper 3/2 Kg/K has a maximum value at 6.8-7.4 R_J of ~0.1 but is well below 0.05 in the rest of the torus. The magnetic mirror force is then negligible and the centrifugal symmetry surface may taken to be inclined at $\alpha/3$ from the magnetic equatorial plane. The magnetic mirror force can also be neglected for electrons because for small variations in latitude (±10°) the magnitude of the magnetic field does not change significantly compared with the electrostatic potential.

$$\frac{\Delta B}{B} << \frac{\Delta\Phi}{T_e} \sim \frac{m_i \Delta f}{2T_e} \qquad (12)$$

For the hot component of the electron population, the magnetic mirror force is more important. In fact, Scudder et al. (1981) show that in the middle magnetosphere, the local density maximum (of the hot component) is nearer the magnetic rather than centrifugal equator. However, it will be illustrated below that in the torus region, the hot electrons play a very minor role in the spatial distribution of plasma. Therefore, the

"gravitational" term f is just due to the centrifugal force F_c (Eq. 10) which can now be inserted into the exponent of equations (6) and (7). These two sets of equations can be solved if the temperatures T_e and T_i are known as a function of s. The simplest case is to arbitrarily assume the temperatures are constant along a field line. This is probably quite a reasonable assumption for a collisionless plasma dominated by the strong centrifugal forces on the heavy ions which vary quite rapidly with distance from the equator. If m^+, T_e, and T_i are constant along a field line, the exponents in (6) and (7) can be integrated along s. The result is an exponential scale height solution for the distribution of ions along a field line, in the region of small distance $z = r \sin\theta$ from the centrifugal symmetry surface.

$$\frac{n_i(z)}{n_o(z=0)} = \exp\left[-\frac{(m_i - Z_i^* m^+)}{kT_i}\,\frac{3\Omega^2 z}{2}\right] \qquad (13)$$

$$= \exp\left[-\left(\frac{z}{H}\right)^2\right]$$

(Hill and Michel, 1976), where the scale height is $H = (2kT_i/3m^*\Omega)^{1/2}$, $m_i^* = (m_i - Z_i^* m^+)$ is the effective mass for the ions (which becomes $m^* = m^+ = m_i/(Z_i^* + 1)$ a single ion species and $T_i = T_e$). The electrons have a similar distribution with $m^* = m^+$.

This exponential scale height distribution was used (with $T_e = T_i$) by Bagenal et al. (1980) to construct a preliminary model of electron density structure in the torus. However, the validity of the method hinges on the assumption that the effective mass is constant for a given

field line. The effective mass will not vary if the composition is constant; i.e., a single ionic species predominates or most of the ions have a similar scale height This assumption does not hold in the Io plasma torus where there are comparable proportions of S^+, S^{2+}, S^{3+}, O^+ and O^{2+} with different scale heights. Therefore, it was necessary to return to the original equations (1) and (2) to derive the expression for the plasma distribution along the field line without eliminating the electric field. Under the steady state condition, the parallel electric field can be expressed as a gradient of an electrostatic potential so that if the temperatures T_e and T_i are taken to be constant for a given field line then (1) and (2) can be integrated over s to give

$$\frac{n_e(s)}{n_e(s_o)} = \exp\left[-q \frac{(\phi(s) - \phi(s_o)}{kT_e}\right] \tag{14}$$

and

$$\frac{n_i(s)}{n_i(s_o)} = \exp\left[- \frac{m_i \Omega^2 r^2 \cos^2\theta}{kT_i^2} + Z^* q \frac{(\phi(s) - \phi(s_o)}{kT_i}\right] \tag{15}$$

$$\left(\int_{s_o}^{s} f \, ds = \int_{s_o}^{s} \Omega^2 r \cos(\theta-\alpha) \cos\delta \, ds \simeq \frac{\Omega^2 r^2}{2} \cos^2\theta\right)$$

As $m_e \ll m_i$ the centrifugal term is neglected for electrons.

In this paper, Eqs. (14) and (15) have been combined with the condition of charge neutrality; Eq. (3),

$$n_e^{hot} + n_e^{cold} = \sum_i Z_i^* n_i$$

in an iterative procedure to determine the densities of each ion species $n_i(s)$, and the electrons, $n_e(s)$ as well as the electrostatic potential $\phi(s)$, with respect to a reference point s_o, the spacecraft location where $n_i(s_o)$, $n_e(s_o)$, T_i, T_e are measured. The values of n_i, T_i and (n_e^{hot} + n_e^{cold}) are determined from fits to the positive ion spectral measurements while T_e^{hot}, T_e^{cold} and n_e^{hot}/n_e^{cold} are determined where possible from the electron measurements. Outside ~7 R_J, the electron parameters are well determined. Between 5.7 and 7 R_j, in the warm torus, the spacecraft probably became slightly negatively charged which at present introduces an uncertainty in the electron measurements (approximately a factor of 3 for T_e^{cold}). The uncertainties in the determination of T_e^{hot} and n_e^{hot}/n_e^{cold} are insignificant as the large value of T_e^{hot} makes n_e^{hot} almost constant along a field line (see Eq. (14)) and because n_e^{hot}/n_e^{cold} has a value of less than 1% in the torus. All of these uncertainties in the electron parameters have a smaller effect than the uncertainties in T_i due to the two different thermal models used in the fit procedure in the warm torus. In the cold torus, the electrons were not detected as they were below the energy per charge threshold of the instrument. Therefore, inside 5.7 R_J all the electrons were arbitrarily assumed to be at the same temperature as the ions.

References

Acuña, M.H., and N.F. Ness, The Main Magnetic Field of Jupiter, J. Geophys. Res. 81, 2917, 1976.

Acuña, M.H., F.M. Neubauer, N.F. Ness, Standing Alfvén Wave Current System at Io: Voyager 1 Observations, J. Geophys. Res. Voyager special issue, 1981.

Angerami, J.J., and J.O. Thomas, Studies of Planetary Atmospheres, J. Geophys. Res., 69, 4537, 1964.

Bagenal, F., J.D. Sullivan, and G.L. Siscoe, Spatial Distribution of Plasma in the Io Torus, Geophys. Res. Lett., 7, 41, 1980.

Bagenal, F. and J.D. Sullivan, J. Geophys. Res., Voyager special issue, 1981.

Belcher, J.W., C.K. Goertz, and H.S. Bridge, The Low Energy Plasma in the Jovian Magnetosphere, Geophys. Res. Lett., 7, 17, 1980.

Belcher, J.W., C.K. Goertz, J.D. Sullivan, and M.H. Acuña, Plasma Observations of the Alfvén Wave Generated by Io, J. Geophys. Res., Voyager special issue, 1981.

Berge, G.L., and S. Gulkis, Earth-based Radio Observations of Jupiter: Millimeter to meter wavelengths, in Jupiter (ed. T. Gehrels), U. of Arizona Press, 1976.

Bergstrahl, J.T., J.W. Young, D.L. Matson, and T.V. Johnson, Astrophys.J., 211, L51, 1977.

Bevington, P.R., Data reduction and error analysis for the physical sciences, McGraw-Hill, 1969.

Bigg, E.K., Influence of the Satellite Io on Jupiter's decametric emission, Nature, 203, 1008, 1964.

Birmingham, T.J., J.K. Alexander, M.D. Desch, R.F. Hubbard and B.M. Pedersen, Observations of electron gyroharmonic waves and the structure of the Io torus. J. Geophys. Res. Voyager special issue, 1981.

Brice, N.M., Bulk motion of the magnetosphere, J. Geophys. Res., 72, 5193, 1967.

Brice, N.M. and G.A. Ioannidis, The magntospheres of Jupiter and Earth, Icarus, 13, 173, 1970.

Bridge, H.S., J.W. Belcher, R.J. Butler, A.J. Lazarus, A.M. Marvetic, J.D. Sullivan, G.L. Siscoe, and V.M. Vasyliunas, The Plasma Experiment on the 1977 Voyager Mission, Space Sci. Rev., 21, 259, 1977.

Bridge, H.S., J.W. Belcher, A.J. Lazarus, J.D. Sullivan, R.L. McNutt, F. Bagenal, J.D. Scudder, E.C. Sittler, G.L. Siscoe, V.M. Vasyliunas, C.K. Goertz and C.M. Yeates, Plasma Observations Near Jupiter: Initial Results from Voyager 1, Science 204, 987, 1979.

Broadfoot, A.L., M.J.S. Belton, P.Z. Takacs, B.R. Sandel, D.E. Shemansky, J.B. Holberg, J.M. Ajello, S.K. Atreya, T.M. Donahue, H.W. Moos, J.L. Bertaux, J.E. Blamont, D.F. Strobel, J.C. McConnell, A. Dalgarno, R. Goody, and M.B. McElroy, Extreme Ultraviolet Observations from Voyager 1 Encounter with Jupiter, Science, 204, 979, 1979.

Broadfoot, A.L., B.R. Sandel, D.E. Shemansky, J.C. McConnell, G.R. Smith, J.B. Holberg, S.K. Atreya, T.M. Donahue, D.F. Strobel, and J.L. Bertaux, J. Geophys. Res., Voyager special issue, 1981.

Brown, R.A. I.A.U. Symposium No. 65, presented 1973, in Exploration of Planetary Systems, Woszczyk and Iwaniszewoka (eds.), I.A.U. Publication, p. 527, 1974.

Brown, R.A., A Model of Jupiter's Sulphur Nebula, Astrophs. J., 206, L179, 1976.

Brown, R.A. Measurements of SII optical emission from the thermal plasma of Jupiter, Astrophys.J., 224, L97, 1978.

Brown, R.A., The Jupiter Hot Plasma Torus: Observed Electron Temperature and Energy Flows, submitted to Astrophys. J., 1980.

Brown, R.A. and W.H. Ip, On atomic clouds as a distributed source for the Io plasma torus, Science, 1981.

Brown, R.A., C.B. Pilcher and D.F. Strobel, Photometric Study of the Io torus, in Physics of the Jovian Magnetosphere, (ed. A.J. Dessler), 1981.

Burke, B.F. and K.L. Franklin, Observations of a variable radio source associated with the planet Jupiter, J. Geophys. Res., 60, 213, 1955.

Carlson, R.W., D.L. Matson, and T.V. Johnson, Electron impact ionization of Io's sodium emission cloud, Geophys. Res. Lett., 2, 469, 1975.

Carlson, R.W., and D.L. Judge, pioneer 10 Ultraviolet Photometer Observations at Jupiter Encounter, J. Geophys. Res., 79, 3623, 1974.

Carr, T.D., and M.D. Desch, Recent decametric and hectometric observations of Jupiter, in Jupiter (ed. T. Gehrels), U. of Arizona Press, 1976.

Cheng, A.F., Effects of Io's volcanoes on the plasma torus and Jupiter's magnetosphere, Astrophys.J., 242, 812, 1980.

Cloutier, P.A., R.E. Daniell, A.J. Dessler, and T.W. Hill, A cometary ionosphere model for Io, Ap. Space Sci., 55, 93, 1978.

Cummings, W.D., A.J. Dessler, T.W. Hill, Latitudinal Oscillations of Plasma within the Io Torus, J. Geophys. Res., 85, 2108, 1980.

Dessler, A.J. and T.W. Hill, Jovian Longitudinal Control of Io-Related Radio Emission, Astrophys. J., 227, 664, 1979.

Dessler, A.J., Mass-injection note from Io into the Io plasma torus, Icarus, 1980.

Drell, S.D., H.M. Foley, and M.A. Ruderman, Drag and propulsion of large satellites in the ionosphere: Alfvén propulsion engine in space, J. Geophys. Res., 70, 3131.

Eviator, A., G.L. Siscoe and Y. Mekler, Temperature anisotropy of the Jovian sulphur nebula, Icarus, 39, 450, 1977.

Eviator, A., and G.L. Siscoe, Limit on rotational energy available to excite Jovian aurora, Geophys. Res. Lett, 7, 1085, 1980.

Fälthammer, C.G., On the transport of trapped particles in the outer magnetosphere, J. Geophys. Res., 71, 1487, 1966.

Fanale, F.P., R.H. Brown, D.P. Cruikshank, R.N. Clarke, Significance of Absorption Features on Io's IR Reflectance Spectrum, Nature, 280, 761, 1979.

Ferraro, V.C.A., Non-uniform rotation of the sun and its magnetic field, Mon. Notices Roy. Astron. Soc., 97, 458, 1937.

Frank, L.A., K.L. Ackerson, J.H. Wolfe and J.D. Mihalov, Observations of Plasmas in the Jovian Magnetosphere, J. Geophys. Res. 81, 457, 1976.

Gledhill, J.A., Magnetosphere of Jupiter, Nature 214, 155, 1967.

Goertz, C.K., and P.A. Deift, Io's interaction with the mangetosphere, Planet. Space Sic., 21, 1399, 1973.

Goertz, C.K., Jupiter's magnetosphere in Jupiter (ed. T. Gehrels), U. Arizona Press, 1976.

Goertz, C.K., Plasma in the Jovian Magnetosphere, J. Geophys. Res. 81, 2007, 1976.

Goertz, C.K., Io's Interaction with the Plasma Torus, J. Geophys. Res., 85, 2949, 1980.

Goertz, C.K. and M.F. Thompsen, Radial Diffusion of Io-injected Plasma, J. Geophys. Res. 84, 1499, 1979.

Gold, T., Motions in the magnetosphere of the Earth, J. Geophys. Res.,

64, 1219, 1959.

Goldberg, B.A., Y. Mekler, R.W. Carlson, T.V. Johnson, and D.L. Matson, Io's sodium emission cloud and the Voyager 1 encounter, Icarus, 1980.

Goldreich, P., and D. Lyden-Bell, Io, a Jovian unipolar inductor, Astrophys.J., 156, 59, 1969.

Goldstein, M.L., and J.R. Theiman, The formation of arcs in the dynamic spectra of Jovian decemeter bursts, J. Geophys. Res., Voyager special issue, 1981.

Gurnett, D.A., Sheath effects and related charged-particle acceleration by Jupiter's satellite Io, Astrophys.J., 175, 525, 1972.

Gurnett, D.A., R.R. Shaw, R.R. Anderson and W.S. Kurth, Whistlers Observed by Voyager 1: Detection of Lightening on Jupiter, Geophys. Res. Lett. 6, 511, 1979.

Gurnett, D.A., and C.K. Goertz, Multiple Alfvén Wave Reflections Excited by Io: Origin of the Jovian Decametric Arcs, J. Geophys. Res., 86, 717, 1981.

Gurnett, D.A., F.L. Scarf, W.S. Kurth, R.R. Shaw and R.L. Poynter, Determination of Jupiter's Electron Density Profile from Plasma Wave Observations, J. Geophys. Res., Voyager special issue, 1981.

Hill, T.W., A.J. Dessler, and F.C. Michel, Configuration of the Jovian Magnetosphere, Geophys. Res. Lett. 1, 19, 1974.

Hill, T.W. and F.C. Michel, Heavy ions from the Galilean satellites and the centrifugal distortion of the Jovian Magnetosphere, J. Geophys. Res., 81, 4561, 1976.

Hill, T.W., Corotation lag in Jupiter's magnetosphere, Science, 207, 301, 1979.

Kennel, C.F. and F.V. Coroniti, Jupiter's magnetosphere Ann. Rev. of Astron. Astrophys., 15, 389, 1977.

Kivelson, M.G., J.A. Slavin, and D.J. Southwood, Magnetospheres of the Galilean satellites, Science, 205, 491, 1979.

Klein, M.J., The variability of the total flux density and polarization of Jupiter's decimetric radio emission, J. Geophys. Res., 81, 3380, 1976.

Krimigis, S.M., T.P. Armstrong, W.I. Axford, C.O. Bostrom, C.Y. Fan, G. Gloeckler, L.J. Lanzerotti, E.P. Keath, R.D. Zwickl, J.F. Carbary, D.C. Hamilton, Low-Energy Charged Particle Environment at Jupiter: A First Look, Science, 204, 998, 1979.

Kumar, S., The Stability of an SO_2 Atmosphere on Io, Nature 280, 758,

1979.

Kumar, S. and D.M. Hunten, The Atmospheres of Io and Other Satellites, The Satellites of Jupiter, U. of Arizona Press, 1980.

Kupo, I., Yu Mekler and A. Eviatar, Detecton of Ionized Sulphur in the Jovian Magnetosphere, Astrophys. Space Sci. 40, 63, 1976.

Levy, G.S., D.W. Green, H.N. Royden, and G.E. Wood, Dispersive doppler measurement of the electron content of the torus of Io, J. Geophys. Res., Voyager special issue, 1981.

Masursky, H., G.G. Schaber, L.A. Soderblom and R.G. Strom, Preliminary Geological Mapping of Io, Nature 280, 725, 1979.

Matson, D.L., T.V. Johnson, and F.P. Fandle, Sodium D-line emission from Io, Astrophys.J., 192, L43, 1974.

McNutt, R.L., J.W. Belcher, J.D. Sullivan, F. Bagenal, and H.S. Bridge, Departure from Rigid Corotation of Plasma in Jupiter Dayside Magnetosphere, Nature 280, 803, 1979.

McNutt, R.L., J.W. Belcher, and H.S. Bridge, Properties of Low Energy Positive Ions in the Middle Magnetosphere of Jupiter, J. Geophys. Res., Voyager special issue, 1981.

Mekler, Y., A. Eviatar and I. Kupo, Jovian sulphur nebula, J. Geophys. Res., 82, 2809, 1977.

Mekler, Y., and A. Eviator, Thermal electron density in the Jovian magnetosphere, J. Geophys. Res., 83, 5679, 1978.

Mekler, Yu. and A. Eviatar, Time Analysis of Volcanic Activity on Io by Means of Plasma Observation, J. Geophys. Res., in press, 1980.

Melrose, D.B., Rotational effects on the distribution of thermal plasma in the magnetosphere of Jupiter, Planet. Space Sic., 15, 381, 1967.

Michel, F.C., and P.A. Sturrock, Centrifugal Instability of the Jovian Magnetosphere and its Interaction with the Solar Wind, Planet Space Sci. 22, 1501, 1974.

Moos, H.W. and J.T. Clarke, Ultraviolet observations of the Io torus from Earth orbit using the I.U.E. Observatory, Astrophys.J., 1981.

Morgan, J.S. and C.G. Pilcher, Plasma characteristics of the Io torus, Astrophys.J., 1981.

Murcray, F.T., and R. Goody, Pictures of the Io sodium cloud, Astrophys.J., 226, 327, 1978.

Nash, D.B., The Jupiter Sulphur Plasma Ring, EOS 60, 307, 1979.

Ness, N.F., M.H. Acuña, R.P. Lepping, L.F. Burlaga, K.W. Behannon, F.M. Neubauer, Magnetic field studies at Jupiter by Voyager 1, Science, 204, 982, 1979.

Neubauer, F.M., Nonlinear standing Alfvén wave current system at Io, J. Geophys. Res., 85, 1171, 1980.

Neugebauer, M. and A. Eviatar, An Alternative Interpretation of Jupiter's "plasmapause", Geophys. Res. Lett. 3, 708, 1976.

Oliversen, R., J. Lattis, F.L. Roesler, F. Scherb, J. Lawrance, D. York, P. Zuchina, and T. Williams, AGU Spring Meeting, Toronto, Ontario, May 1980.

Pearl, J., R. Hanel, V. Kunde, W. Maguire, K. Fox, S. Gupta, C. Ponnamperuma, and F. Raulin, Identification of Gaseous SO_2 and New Upper Limits on Other Gases on Io, Nature 280, 755, 1979.

Piddington, J.H. and J.F. Drake, Electrodynamic effects of Jupiter's satellite Io, Nature, 217, 935, 1968.

Pilcher, C.B. and J.S. Morgan, Detection of Singly Ionized Oxygen Around Jupiter, Science 205, 297, 1979.

Pilcher, C.B., and J.S. Morgan, The Distribution of [SII] Emission Around Jupiter, Astrophys. J., 238, 1980.

Pilcher, C.B., Images of Jupiter's Sulphur Ring, Science 207, 181, 1980.

Pilcher, C.B. and D.R. Strobel, Emissions from neutrals and ions in the Jovian magnetosphere, in The Satellites of Jupiter, (ed. D. Morrison), U. of Arizona Press, 1981.

Richardson, J.D., G.L. Siscoe, F. Bagenal and J.D. Sullivan, Time Dependent Plasma Injection by Io, Geophys. Res. Lett. 7, 37, 1980.

Richardson, J.D. and G.L. Siscoe, Factors Governing the Ratio of Inward to Outward Diffusion of Flux of Satellite Ions, J. Geophys. Res., Voyager special issue, 1981.

Sandel, B.R., D.E. Shemansky, A.L. Broadfoot, J.L. Bertaux, J.E. Blamont, M.J.S. Belton, J.M. Ajello, J.B. Holberg, S.K. Atreya, T.M. Donahue, H.W. Moos, D.F. Strobel, J.C. McConnell, A. Dalgarno, R. Goody, M.B. McElroy, and P.Z. Takacs, Extreme Ultraviolet Observations from Voyager 2 Encounters with Jupiter, Science 206, 962, 1979.

Scudder, J.D., E.C. Sittler, and H.S. Bridge, A Survey of the Plasma Electron Environment of Jupiter: Direct Measurements, J. Geophys. Res., Voyager special issue, 1981.

Shemansky, D.E., Mass loading and the diffusion loss rate of the Io plasma torus, Astrophys. J., 242, 1266, 1980.

Scarf, F.L., D.A. Gurnett, and W.S. Kurth, Jupiter Plasma Wave observations, Science, 204, 991, 1979.

Scarf, F.L., F.V. Coroniti, C.F. Kennel and D.A. Gurnett, Jupiter and Io: A binary magnetosphere, Vistas in Astronomy, special Jupiter issue, 1981.

Schemansky, D.E., and G.R.Smith, The Voyager EUV spectrum of the Io plasma torus, J. Geophys. Res., Voyager special issue, 1981.

Siscoe, G.L., On the Equatorial Confinement and Velocity Space Distribution of Satellite Ions in Jupiter's Magnetosphere, J. Geophys. Res. 82, 1641, 1977.

Siscoe, G.L. and D. Summers, Centrifugally Driven Diffusion of Iogenic Plasma, J. Geophys. Res., Voyager special issue, 1981.

Siscoe, G.L., A. Eviatar, R.M. Thorne, J.D. Richardson, F. Bagenal, and J.D. Sullivan, A dynamic coupling between the Io plasma formation and the ring current, J. Geophys. Res., Voyager special issue, 1981.

Smith, R.A., Models of Jovian decametric radiation, in Jupiter (ed. T. Gehrels), U. of Arizona Press, 1976.

Smythe, W.D., R.M. Nelson and D.B. Nash, Spectral Evidence for SO_2 Frost of Adsorbate on Io's Surface, Nature 280, 766, 1979.

Southwood, D.J., M.G. Kivelson, R.J. Walker, and J.A. Slavin, Io and its plasma environment, J. Geophys. Res., 85, 5959, 1980.

Strobel, D.F., and J. Davis, Properties of the Io plasma torus from Voayger EUV data, Astrophys.J., 238, L49, 1980.

Sullivan, J.D. and F. Bagenal, In Situ Identification of Various Ionic Species in Jupiter's Magnetosphere, Nature 280, 798, 1979.

Trafton, L., T. Parkinson, W. Macy, The spatial extent of sodium emission around Io, Astrophys.J., 190, L85, 1974.

Trafton, L. and W. Macy, Io's sodium emission profiles Astrophys.J., 215, 971, 1977.

Trafton, L., The Jovian SII Torus: Its Longitudinal Asymmetry, Icarus 42, 111, 1980.

Trauger, J.T., G. Munch, and F.L. Roesler, A study of the Jovian [SII] and [SIII] nebulae at high spectral resolution, Bull. Amer. Astron. Soc., 11, 591, 1979.

Trauger, J.T., G. MUnch and F.L. Roesler, A Study of the Jovian [SII] nebula at high spatial resolution, Astrophys. J., 236, 1035, 1980.

Vasyliunas, V.M., In Methods of Experimental Physics, Vol. 93 of Plasma

Physics, Edited by R.H. Lovbergs, p. 49, Academic Press, 1971.

Vogt, R.E., W.R. Cook, A.C. Cummings, T.L. Garrard, N. Gehrels, E.C. Stone, J.H. Trainor, A.W. Schardt, T. Conlon, N. Lal, F.B. McDonald, Voyager 1: Energetic Ions and Electrons in the Jovian Magnetosphere, Science, 204, 1003, 1979.

Warwick, J.W., Radiophysics of Jupiter, Space Sci. Rev., 6, 841, 1967.

Warwick, T.W., J.B. Pearce, A.C. Riddle, J.K. Alexander, M.D. Desch, M.L. Kaiser, J.R. Thieman, T.D. Carr, S. Gulkis, A. Boischot, C.C. Harvey and B.M. Pederson, Voyager 1 Planetary Radio Astronomy Observations near Jupiter, Science 204, 955, 1979.

Acknowledgements

I would like to express my gratitude first and foremost to Professor Herbert Bridge. Not only is the success of the Voyager plasma measurements at Jupiter attributable in many ways to his experimental expertise, but he has also paid detailed attention to the analysis and interpretation of the data. I am very grateful for the encouragement and guidance he has given to me in the past four years.

I would like to thank John Belcher for his advice and particularly his guidance in analysis of the data. I am grateful to Dr. Christoph Goertz, Dr. Alan Lazarus and Professor Stanislaw Olbert for helping me understand the physics behind the plasma processes that occur in Jupiter's magnetosphere. I would also like to thank my "comrades-in-arms", Ralph McNutt, Jr. and Alan Barnett for many discussions (even the ones about plasma physics).

For their assistance and support while I was completing the research for this thesis, I am grateful to the staff at both the Center for Space Research and the L.N.S. computer facility. I am especially indebted to the team of women who helped put the paper work together: Mary Terkoski, Anne Bowes, Maggie Carracino, Pamela Milligan, Joan Boughan and Patricia Welch.

Now for the other side of my split personality. I would like to express my gratitude to Professor Theodore Madden from whom I learnt, among other things, that geophysics is not a soft science. I also thank the many people from the Green Building who teased, cajoled, restrained and poured coffee or beer down me at appropriate moments.

Biography

Frances Bagenal, born 4th November, 1954 in Dorchester, England; educated at Huntingdon Grammer/Hinchingbrooke Comprehensive School, Huntingdon (1966-1973); obtained a joint B.Sc. degree in Physics and Environmental Sciences from the University of Lancaster (1976); studied geophysics and planetary physics at the Earth and Planetary Sciences Department, M.I.T. (1976-1981); research assistant for the Space Plasma Group at the Center for Space Research, M.I.T. (1977-1981).